Biophysical Investigation into the Protein Dynamics Governing the Allosteric Regulation of Plant and Animal 15-Lipoxygenases

by

Daniella Roberts

May 2022

Director of Thesis: Adam R. Offenbacher

Major Department: Chemistry

Lipoxygenases (LOXs) are a family of enzymes found in plants, animals, fungi, and bacteria that catalyze the per-oxidation of polyunsaturated fatty acids. In plants, LOXs are involved in growth, development, and defense against pathogenic attacks. There are also multiple isoforms present in humans, which have contradictory roles in the body. Specifically, human 15-LOX isoforms, 15-LOX-1 and 15-LOX-2, are involved in both homeostasis and pro-inflammatory pathways. In order to selectively target the activity of these enzymes, research has turned to allosteric regulation, which is the focus of this Thesis. Previously, the allosteric regulation of a model plant 15-LOX, soybean lipoxygenase-1 (SLO), has been characterized using hydrogen-deuterium exchange mass spectrometry (HDX-MS), revealing that the addition of the allosteric effector, oleyl sulfate (OS), alters a specific region of the enzyme. Herein, we used a combination of thermodynamic and biophysical techniques such as isothermal titration calorimetry and differential scanning calorimetry to investigate the allosteric regulation of SLO by OS. We present data which supports that the allosteric regulation of SLO by OS does not induce oligomerization or large-scale conformational changes and that the allostery is dynamically driven. We also employed HDX-MS to study the dynamics of 15-LOX-1 compared to previously collected data of 15-LOX-2 to reveal structural differences between the two isozymes that may explain their altered catalytic behavior.

Biophysical Investigation into the Protein Dynamics Governing the Allosteric Regulation of Plant and Animal 15-Lipoxygenases

A Thesis

Presented to the Faculty of the Department of Chemistry

East Carolina University

In Partial Fulfillment of the Requirements for the Degree

Master of Science in Chemistry

by

Daniella Roberts

May 2022

Biophysical Investigation into the Protein Dynamics Governing the Allosteric Regulation of Plant and Animal 15-Lipoxygenases

by

Daniella Roberts

APPROVED BY:

DIRECTOR OF THESIS: _____

Adam R. Offenbacher, Ph.D.

COMMITTEE MEMBER: _____

Shouquan Huo, Ph.D.

COMMITTEE MEMBER:_____

Sambuddah Banerjee, Ph.D.

COMMITTEE MEMBER:_____

John Latham, Ph.D.

CHAIR OF THE
DEPARTMENT OF CHEMISTRY:_____

Andrew T. Morehead, Jr., Ph.D.

DEAN OF THE
GRADUATE SCHOOL: _____

Paul Gemperline, Ph.D.

Acknowledgements

I would first like to thank my mentor, Dr. Adam Offenbacher, who has given me tremendous guidance these past four years. Thank you for taking a chance on a young sophomore, I would not have my passion for science if it were not for you. You have created a lab environment that pushes everyone to do their best and succeed, and I am all the better for it.

Thank you to everyone in the Offenbacher Lab for all the fun times we've had together and for making the group really feel like a family. A special thank you to my fellow graduate students, Amanda Ohler and Rachel Signorelli. Somehow, you two made waking up at 8 AM feel enjoyable. Thank you for making so many wonderful memories with me, I will cherish them always.

Finally, a huge thank you to my family, who have always been by my side. Especially my Mom and Dad, your support through everything means the world to me.

Table of Contents

List of Tables

Chapter 2

Chapter 3

Chapter 4

List of Figures

Chapter 1

Chapter 2

Chapter 3

Chapter 4

Chapter 1

Introduction

Enzymes and Catalysis

Enzymes are catalysts that accelerate the rate in which chemical reactions occur to a degree that allows the sustainability of life. Without enzymes, reactions that occur at room temperature as estimated to take anywhere from minutes to upwards of millions of years to proceed, while enzymatic reactions take 10^0 to 10^4 s^{-1}.[1] The ratio of the rates of catalyzed versus uncatalyzed reactions is called the rate enhancement. Many proficient enzymes that catalyze C-H, C-N, and C-C bond cleavage have a rate enhancement of 10^{12} - 10^{20}, with the gold standard being a 2×10^{26}-fold rate enhancement.[2] In 1913, the scientists Leonor Michaelis and Maud Menten developed a model to describe the effect of enzymes on the rate of the reaction. They postulated that the enzyme reversibly binds to the substrate, forming an enzyme-substrate complex, and then the enzyme irreversibly converts the substrate to the product. Using this theory, Michaelis and Menten studied steady-state kinetics and were able to create an equation that related the concentration of the substrate to the overall rate of the reaction, Eq. 1, in what is now known as the Michaelis-Menten equation.[3]

$$v = \frac{k_{cat} * s}{K_M + s} \qquad \textit{Eq. 1}$$

In this equation, the first-order rate constant, k_{cat}, which describes the rate of the reaction at saturating substrate levels, is directly correlated to the concentration of the substrate, s. The other relevant parameter in this equation is the Michaelis constant, K_M, which represents the substrate concentration at half of the k_{cat} value. The Michaelis-Menten equation can be plotted and is shown in graphical form in Figure 1 below. Using the Michaelis-Menten parameters, the specificity constant can be derived, k_{cat}/K_M. The specificity constant, also called the second-order

rate constant, measures the efficiency of the enzyme to discriminate between available substrates and this value is often used as a marker for the catalytic efficiency of the enzyme.

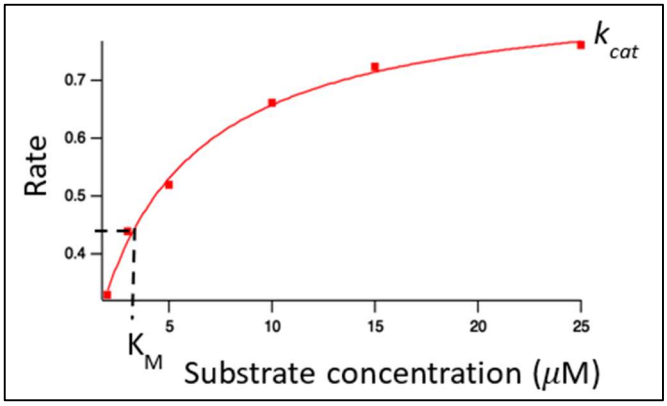

Figure 1.1 *Michaelis-Menten plot relating the rate of the reaction to the substrate concentration, μM, with the first order rate constant, $k_{cat,}$ and Michaelis constant, K_M, displayed on the plot.*

While the catalytic effect of enzymes on the rate of reactions is well studied, how that effect is achieved remains unsolved. Scientists have been studying enzymes for decades and no man-made catalyst has come close to matching the catalytic power of natural enzymes. In 1948, Linus Pauling theorized that enzymes lower the activation energy of the reaction by stabilizing the transition state.[4] Using the concept of electrostatic interactions to stabilize the transition state, man-made catalysts have only been able to enhance the rate by (at best) 10^9 over uncatalyzed reaction with assistance from directed evolution.[5] Despite modest advancements in the understanding of transition state catalysts, the discovery of quantum tunneling driven reactions such as enzymatic C-H activation requires new considerations for enzyme design.[6]

Protein Allostery

Allostery is defined as when an effector bound at a distal site alters the functional activity at the active site of a protein.[7] Allosteric effectors can affect the substrate binding affinity or catalytic efficiency of an enzyme in a positive or negative manner, Figure 1.2. Historically, these changes were considered to be caused by conformational changes occurring upon effector binding.

However, a later model was proposed where allostery could occur without a conformational change, and that allostery occurred via altered protein dynamics in response to shifts in entropy caused by effector binding.[8] This theory explained how some proteins could be allosterically regulated but no large-scale structural changes would occur. This model was further strengthened by the identification of evolutionarily conserved residues that form an allosteric network, which is theorized to allow for communication to occur between the allosteric and active sites.[9]

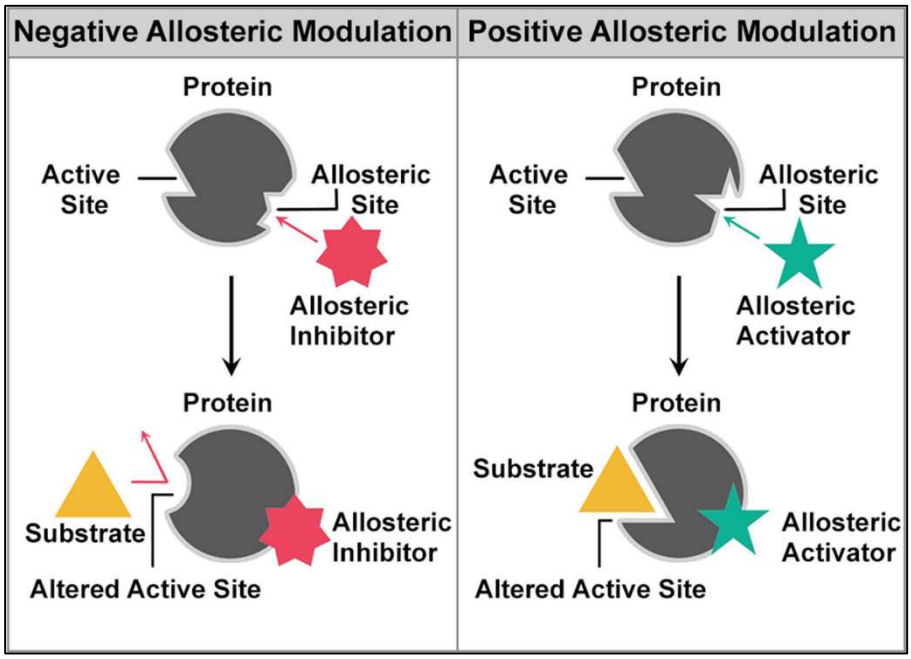

Figure 1.2 *Graphical representation of negative and positive allosteric regulation of an enzyme. Reproduced from reference.*[10]

Lipoxygenases

Lipoxygenases (LOXs) are a class of enzymes that are found in plants, animals, fungi, and bacteria. LOXs are known to regio- and stereo-specifically catalyze the peroxidation reaction of poly-unsaturated fatty acids (PUFAs).[11] This reaction is a form of C-H activation that is catalyzed using a non-heme metal center. C-H activation, also called C-H bond cleavage, is the process of an sp^3 hybridized C-H bond being cleaved, forming a carbon radical, and then subsequently being replaced with a C-X bond, where X is oxygen, nitrogen, or carbon.[12] In LOXs, the cofactor

abstracts the hydrogen using proton-coupled electron transfer (PCET), forming a carbon radical on the PUFA chain. The radical then reacts with molecular oxygen, forming a hydroperoxide product. A proposed mechanism of this reaction in soybean lipoxygenase-1 is shown in Figure 1.3 with linoleic acid as the substrate.[13] The hydroperoxide products formed by LOXs act as key signaling molecules in the organism.

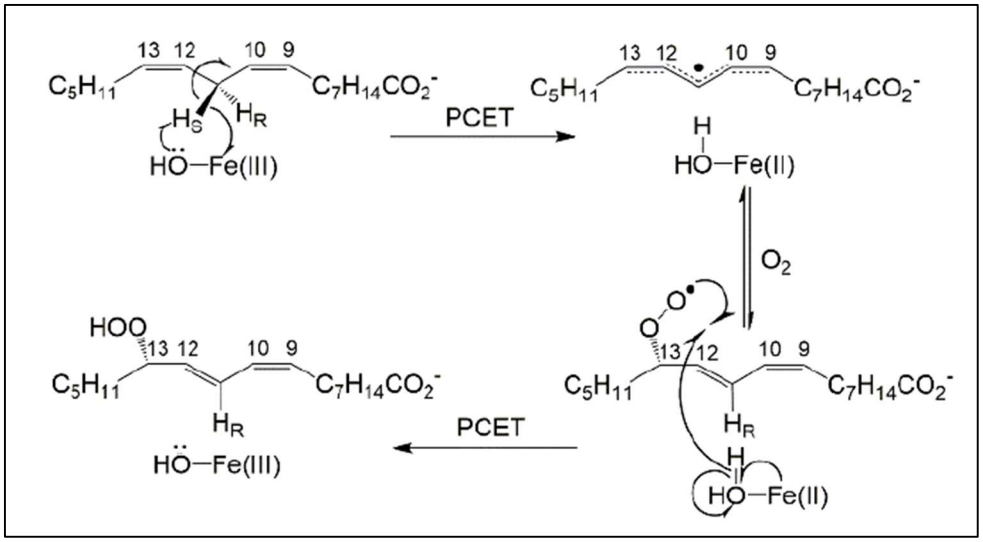

Figure 1.3 *C-H bond cleavage mechanism done by soybean lipoxygenase-1 on linoleic acid.*

The mechanism of this process can be examined by switching the hydrogen in the C-H bond to deuterium and measuring the kinetic isotope effects (KIEs).[6] Following classical transition state theory (TST), the deuterium KIE of the first-order rate constant, ${}^{D}k_{cat}$, has an upper limit of 7. The limit of this KIE is dominated by the difference in the ground state zero-point energies between hydrogen and deuterium. However, enzymes that catalyze C-H bond cleavage have documented ${}^{D}k_{cat}$ of over 100. This large ${}^{D}k_{cat}$ value can implicate quantum tunneling.[12]

While there is low sequence homology between the LOXs from the different kingdoms, they all maintain certain structural similarities. Highlighted in Figure 1.4, LOXs all maintain a predominantly alpha-helical catalytic domain with a metal catalytic center. Additionally, plant and animal LOXs also have a second domain composed primarily of beta-sheets located at the N

terminus called the Polycystin-1, Lipoxygenase, α-Toxin (PLAT) domain.[14] humans, there are multiple isoforms present that are involved in maintaining homeostasis. Human LOXs are involved in both pro- and anti-inflammatory responses and have been implicated in inflammatory diseases such as atherosclerosis and arthritis. In plants, LOXs are involved in the growth and development of the plant as well as the defense against pathogenic attacks.[15]

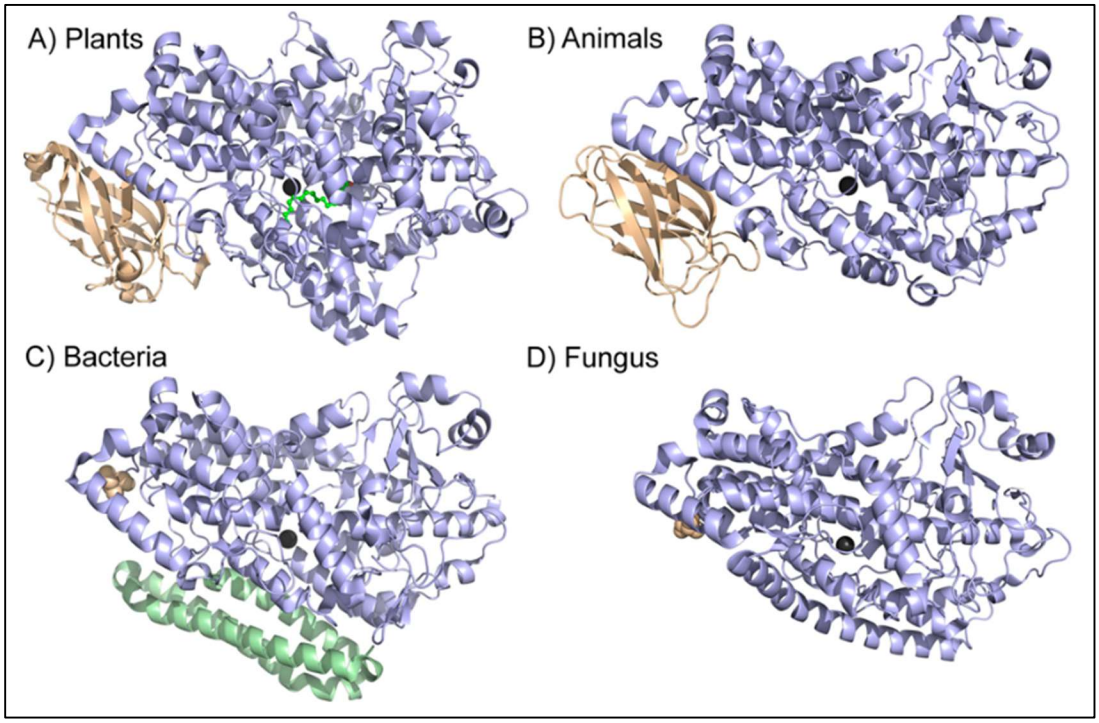

Figure 1.4 *Structural comparison of lipoxygenases from different kingdoms. The catalytic domains are colored light blue, and the catalytic metal center is colored dark gray. For A and B, the PLAT domain is colored wheat, for C and D, the N-terminal amino acid is shown using wheat-colored spheres. Bacteria have extra alpha helices, shown in green in C. (PDBs: (A) 3PZW, (B) 3O8Y, (C) 4G32, (D) 5FNO). Reproduced from reference.*[15]

Quantum Tunneling

Quantum tunneling is a phenomenon where the hydrogen atom, instead of going over the activation barrier, shown in Figure 1.5A, acts as a wave and proceeds through the barrier, as shown in Figure 1.5B. For quantum tunneling to occur the hydrogen donor, carbon, and the hydrogen acceptor, which is often oxygen or nitrogen, must come close together, typically within 2.7 to 2.8

Å. The transfer will occur when the wave functions overlap at the tunneling-ready state. Hydrogen tunneling is difficult to identify, with the key factors that implicate hydrogen tunneling being an abnormally large KIE and a lack of temperature dependence. For classical TST, the presence of hydrogen versus deuterium will result in different activation energies due to their different zero-point energies.[12]

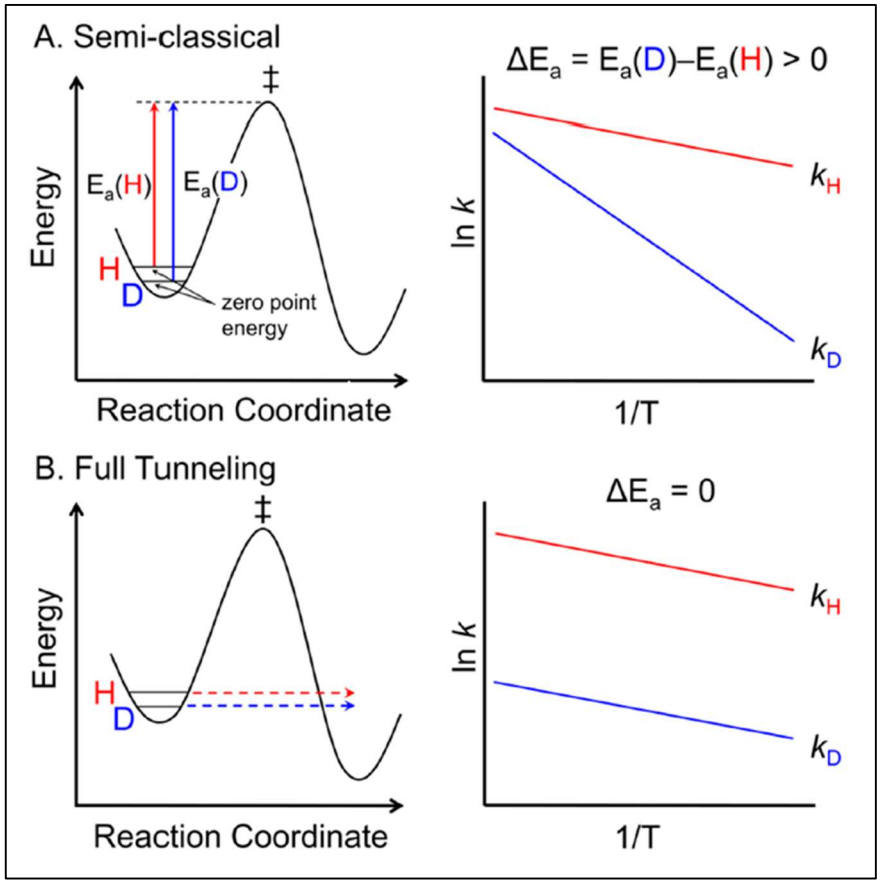

Figure 1.5 *Comparison of the reaction coordinate diagrams and Arrhenius plots for C-H activation with the transition state marked with '‡'. A shows a representation of the classical transition state theory model while B shows the quantum tunneling model. Reproduced from reference.*[16]

The activation energy, and therefore the temperature dependence, of the reaction can be determined using the Arrhenius equation, Eq. 2, which can be redefined to a linear form, Eq. 3, where k is the rate constant, A is the Arrhenius factor, E_a is the activation energy, R is the ideal gas constant, and T is the temperature in Kelvin.

$$k = A * e^{-E_a/RT} \qquad \textit{Eq. 2}$$

$$\ln(k) = -\frac{E_a}{R(1/T)} + \ln(A) \qquad \textit{Eq. 3}$$

Arrhenius plots representative of classical TST and quantum tunneling are shown on the right side of Figure 1.5. The slope of the line on the Arrhenius plots equals the activation energy divided by the ideal gas constant. Temperature dependence can be measured by comparing the activation energies between the different isotopes. Under classical TST, there is an observed KIE that is temperature dependent, resulting in a ΔE_a larger than zero. However, under the quantum tunneling model, there is no temperature dependence and the observed ΔE_a is close to zero. This indicates that there is no significant difference in the activation energies of the isotopes, something that does not follow classical TST, implicating quantum tunneling.[12]

Soybean Lipoxygenase-1

Soybeans have emerged as the ideal organism to study plant LOXs due to the abundance of enzyme that they produce and decades of foundational research. Specifically, most studies use soybean lipoxygenase-1 (SLO) due to the ease of purification and structural stability. SLO is also considered a paradigm for the study of C-H activation and has become a prime model for the investigation of hydrogen tunneling. SLO has an observed ${}^{D}k_{cat}$ value of over 80, well above the classical TST limit of 7.[17] Additionally, SLO has a ΔE_a of 0.9 kcal/mol, which is also non-classical. These two factors combined implicate that SLO has extensive hydrogen tunneling.[18] While the

isotope effect on the first order rate constant, $^{D}k_{cat}$, is large, under select conditions, the isotope effect on the second-order rate constant, $^{D}k_{cat}/K_M$, is much smaller than $^{D}k_{cat}$, implicating a rate-determining step preceding the C-H cleavage step of catalysis.

Allosteric Regulation of Soybean Lipoxygenase-1

Scientists have discovered that soybean lipoxygenase-1 (SLO) is one of the enzymes that can be regulated through allostery. Oleic acid (OA) was thought to be a simple competitive inhibitor for SLO, however the hyperbolic rise in $^{D}k_{cat}/K_M$, shown in Figure 1.6A, indicated that the molecule was forming a ternary complex with the enzyme. Meaning that the instead of the enzyme being bound to either the substrate, linoleic acid/deuterated linoleic acid, or OA, it was instead bound to both of them at the same time. Indicating that there is either a secondary binding site other than the active site or that OA was aggregating with the substrate. To determine which was the cause, a new compound was synthesized that was based on OA, only being more soluble, called oleyl sulfate (OS). After testing the kinetics of OS, it was revealed that the addition of OS to SLO also caused a hyperbolic increase in the KIE (Figure 1.6B), and that OS had a 60-fold increase in binding affinity compared to OA. OS was also shown to cause a hyperbolic decrease in the k_{cat}/K_M of SLO (Figure 1.7), k_{cat}/K_M is the second order rate constant that acts as a marker of the catalytic efficiency of the enzyme. This hyperbolic increase in $^{D}k_{cat}/K_M$ and hyperbolic decrease in catalytic efficiency could not be attributed to aggregation, as the concentration of the OS used was lower than the aggregation point. Therefore, these results supported the conclusion that OS was altering the kinetics of SLO through the formation of a ternary complex with the enzyme and substrate by binding at an alternate binding site, implicating OS as an allosteric inhibitor of SLO.[19]

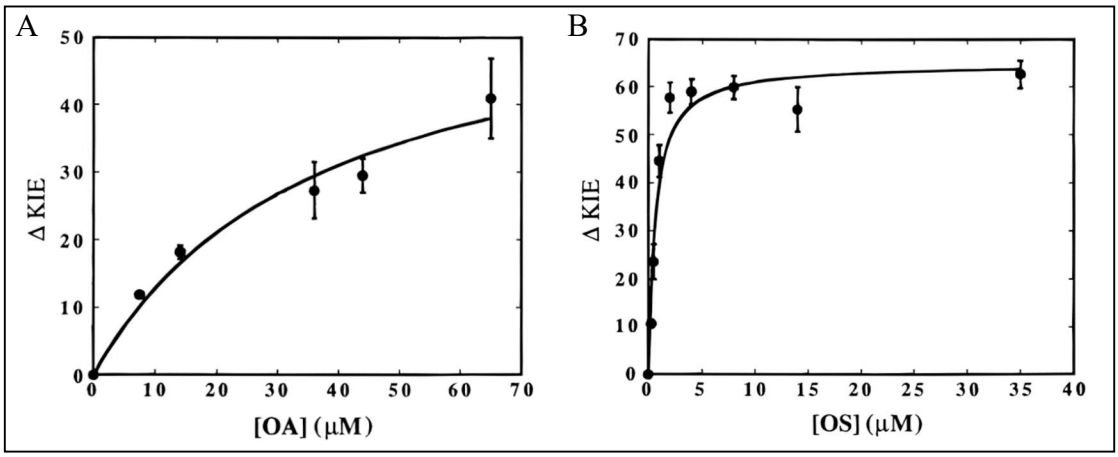

Figure 1.6 *Effect of oleic acid (A) and oleyl sulfate (B) on the ΔKIE* (i.e. $^{D}k_{cat}/K_M$) *for SLO. Reproduced from reference.*[19]

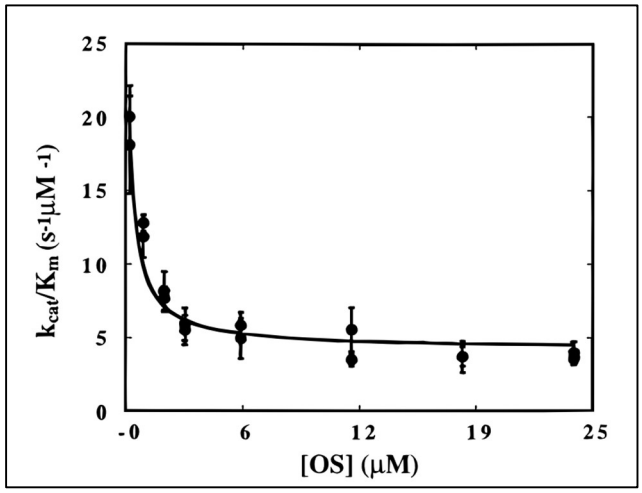

7

Figure 1.7 *Effect of oleyl sulfate on the k_{cat}/K_M for SLO. Reproduced from reference.*[19]

While the kinetics support that, upon binding to SLO at an allosteric site, OS inhibited the activity at the substrate binding site, how this effect was achieved within SLO was unknown. To shed light on this topic, hydrogen-deuterium exchange mass spectrometry (HDX-MS) was employed to determine the change in protein dynamics that occur in SLO upon OS binding.[15] HDX-MS is a bioanalytical technique where the protein is incubated in deuterated buffer for set amounts of time. During this incubation, any exposed hydrogens on the amide backbone of the protein will be exchanged for deuterium. At each timepoint, the reaction is both cold and acid

quenched, the protein is digested, the peptides are separated using liquid chromatography (LC), and then the peptides are analyzed using mass spectrometry, this process is shown in Figure 1.8.[20]

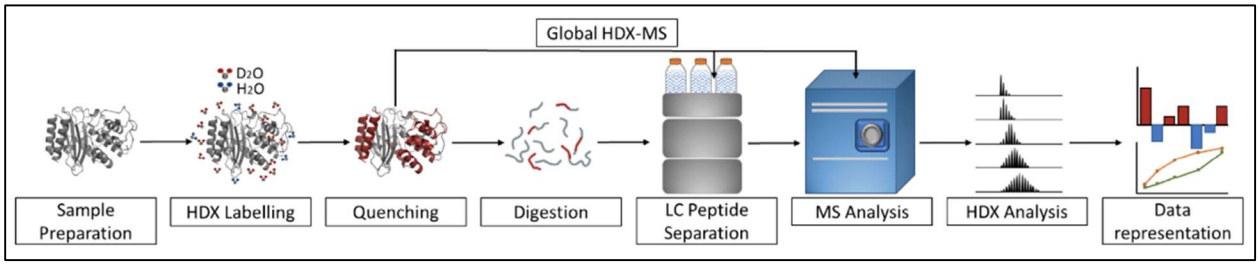

Figure 1.8 *Outline of global or local bottom-up protein analysis. Local bottom-up analysis digests the protein into peptides before separating them using LC while global analysis goes straight from quenching to MS analysis. Reproduced from reference.*[20]

HDX-MS is a useful technique as it can not only show which areas of the protein are solvent exposed or hydrophobic, but it also can reveal which areas of the protein are the most dynamic. The exchange process relies on the transient "opening" and "closing" motions of the backbone amide bonds. Once exposed, the amides can exchange with deuterium when proteins are incubated in D_2O, "heavy water". Regions of the protein that have quicker "breathing" rates will display an increase of H/D exchange over time. This technique can be used to investigate how dynamic regions of the protein are altered by interactions with small molecules, other proteins, or even parts of a membrane by incubating them together in the deuterated buffer.[20]

In this study, researchers incubated OS with SLO for 14 different timepoints (0, 10, 30, 45, 60, 180, 600, 1200, 1800, 2700, 3600, 7200, 10800, and 14400 seconds) at 10, 20, 30, and 40 °C. The results revealed that the peptide containing residues 1-14 of the protein had a significant increase in the extent of H/D exchange, particularly at 30 and 40 °C (Figure 1.9). This suggests that OS likely binds to SLO within or near that region of the protein and causes a conformational change. This region is located within the N-terminal, PLAT domain of SLO.[15]

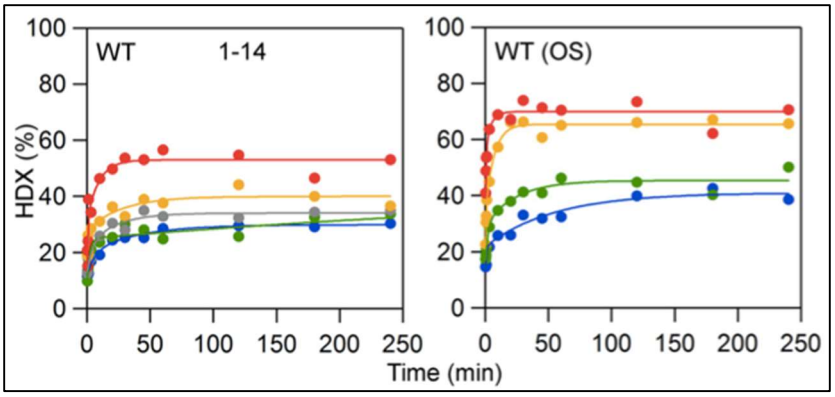

Figure 1.9 *HDX traces of SLO in the absence (left) and presence (right) of OS at 10 (blue), 20 (green), 30 (yellow) and 40 °C (red). The gray line on the left represents peptides that are adjacent to residues 1-14 that were not present in the HDX analysis done with OS. Reproduced from reference.*[15]

In addition to the increased extent of exchange at the N-terminal, HDX analysis of OS bound to SLO revealed destabilization of peptides making up C-terminal α-helices. Six non-overlapping peptides were shown to have increased rates of exchange in the presence of OS (Figure 1.10). Particularly, the peptide comprised of residues 257-273 was the most impacted by the addition of OS. This region comprises the majority of helix α2 in SLO, which acts as a gate to the substrate binding pocket within SLO. So, in summary, while a conformational change is likely occurring at the N-terminal in residues 1-14 in the presence of OS, α-helices within the C-terminal of SLO are also displaying increased flexibility upon OS binding, indicating that the secondary structure of this region is being destabilized. This result was interpreted that OS is inducing long-range dynamic changes to SLO upon binding.[15] The HDX behavior provided structural explanation for how the substrate binding commitment factor (i.e. increased $^{D}k_{cat}/K_M$) is achieved in the presence of OA and OS.

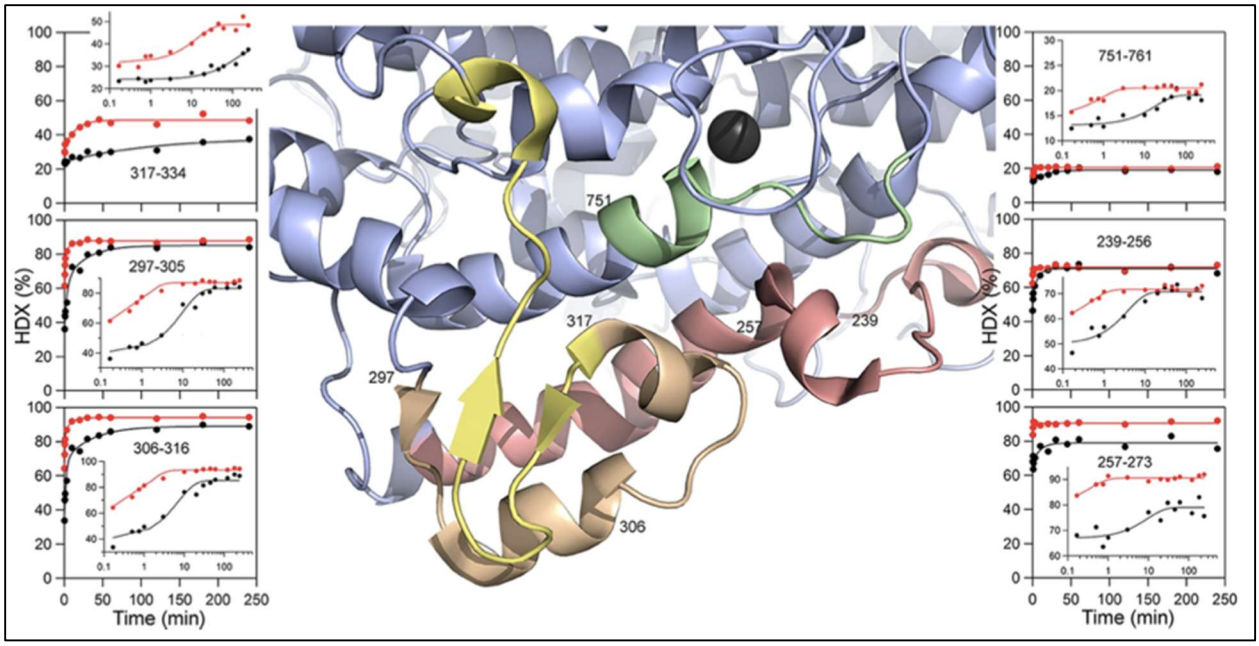

Figure 1.10 *HDX traces of the peptides most affected by the presence of OS (red) compared to the absence of OS (black). Reproduced from reference.*[15]

Human 15-Lipoxygenases

Within humans, there are 6 isoforms of lipoxygenase to be found, and they are named based on the carbon number on arachidonic acid where the oxygenation is catalyzed, e.g., 5-LOX catalyzes the oxidation at 5th carbon. Each LOX found in humans produces an array of products, shown in Figure 1.11, and they are tissue specific: 5-LOX is mainly expressed in leukocytes, 12-LOX can be found in platelets, the first isoform of 15-LOX, 15-LOX-1, is expressed in reticulocytes, eosinophils, and macrophages, while 15-LOX-2 is found in skin, cornea, prostate, lung, and esophageal cells. The second isoform of 15-LOX was discovered in 1997, and the two share only a 37% sequence homology.[21]

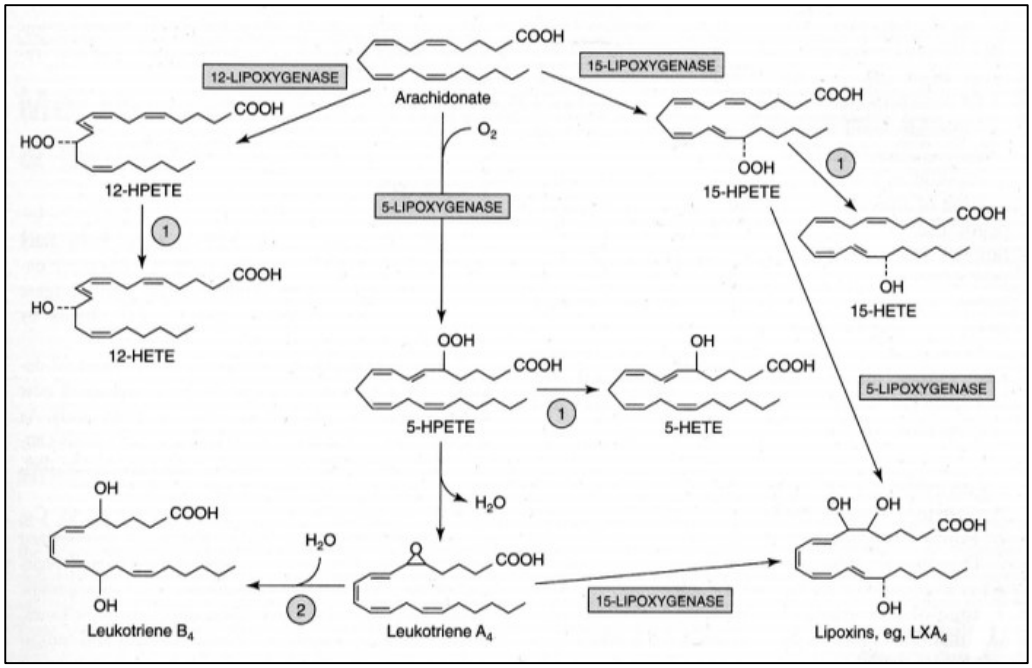

Figure 1.11 *Map of the reactions done by human LOXs on arachidonic acid within the human body, and their resulting products.*

One thing that the two isoforms have in common, however, is that they are both are key targets for drug design and development due to their involvement in disease. 15-LOX-1 produces 15-HpETE, which is converted to lipoxins, shown in Figure 1.11. Lipoxins are anti-inflammatory as well as having inflammation resolving capabilities. It has also been reported that 15-LOX-1 is involved in tumor suppression, but also that 15-LOX-1 acts as a carcinogen.[22] Meanwhile, 15-LOX-2 has been found to be highly expressed in atherosclerotic lesions, implicating its involvement in the pathogenesis of atherosclerosis. However, 15-LOX-2 also has anti-inflammatory properties, as they produce resolvins, which act as pro-resolving mediators that activate anti-inflammatory pathways.[23] Since 15-LOXs have neither a wholly positive nor negative role in humans, simply down or upregulating its expression will not be beneficial as a treatment. Therefore, an alternate approach is necessary for targeting this enzyme, so researchers have turned to allosteric regulation.

There has been evidence to support that 15-LOXs have an allosteric binding site, much like SLO. SLO is considered a model for 15-LOX since the enzymes all target the ω-6 carbon on their respective PUFAs, this is the 13th carbon on linoleic acid for SLO and the 15th carbon on arachidonic acid for 15-LOXs.[16] The first implication of allosteric regulation of a 15-LOX, was the allosteric inhibition of 15-LOX-1 by oleyl sulfate, OS. Similar to SLO, 15-LOX-1 also displayed both a hyperbolic increase in ${}^{D}k_{cat}/K_M$, also called ΔKIE, (Figure 1.12A) and a hyperbolic decrease in k_{cat}/K_M (Figure 1.12B) when in the presence of OS. Since these results were observed at OS concentration levels that were below the aggregation point, this indicates that 15-LOX-1 is regulated by OS through the formation of a ternary complex with OS and the substrate. This implicates OS as an allosteric inhibitor of 15-LOX-1, and displays the first observed form of allsoteric regulation of a human 15-LOX.

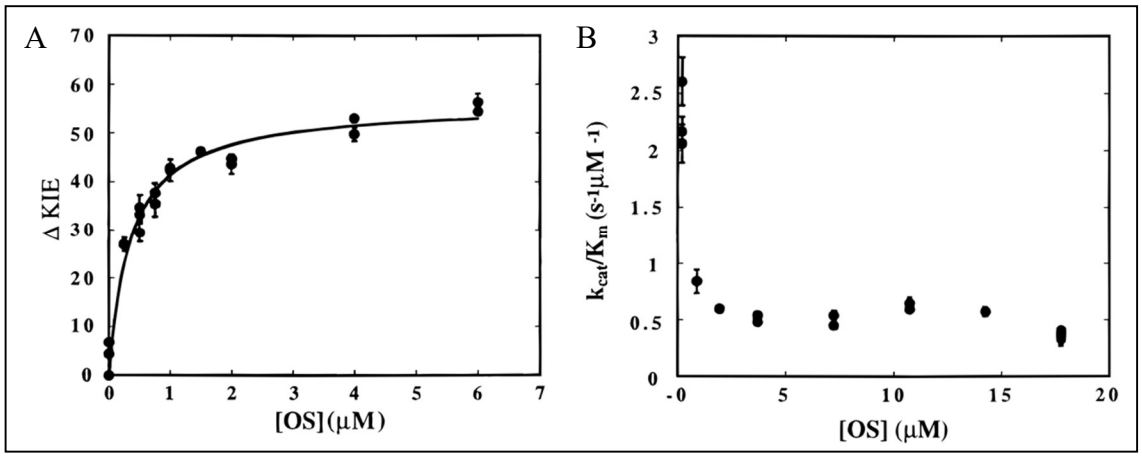

Figure 1.12 *Effect of oleyl sulfate on the ΔKIE (A) and on the k_{cat}/K_M (B) for 15-LOX-1. Reproduced from reference.*[19]

Scope of Thesis

The overall scope of the Thesis is centered on understanding how the myeloperoxidase family of enzymes (lipoxygenases, α-dioxygenases, and cyclooxygenases), which catalyze the C-H activation (or C-H cleavage) of fatty acids, are regulated through their structure and dynamic

allostery. In Chapter 2, the role of the sidechain bulk at a large hydrophobic residue, F552, on the efficiency of substrate C-H activation is investigated for the *Oryza sativa* α-Dioxygenase (αDOX) enzyme. Herein, I will present results from my efforts to express and purify the rice αDOX enzyme from bacterial cultures and the subsequent protein characterization by SDS-PAGE and enzyme kinetics using an O2 electrode. In Chapter 3, I will present direct evidence of OS binding to SLO through the use of isothermal titration calorimetry (ITC). Additionally, biophysical techniques, such as dynamic light scattering (DLS) and differential scanning calorimetry (DSC), were used to provide experimental support for the fact that OS does not induce any large-scale conformational changes in SLO upon binding this effector. Thus, the combined data support that SLO is allosterically regulated through dynamically driven allostery. I will also present HDX-MS data of SLO performed under elevated ionic strength conditions to investigate the effects of salt on the dynamics of SLO and how those effects alter the allosteric regulation of SLO by OS. In Chapter 4, I will present HDX-MS data collected on human 15-LOX-1 and compare the observed enzyme dynamics to the previously observed results from human 15-LOX-2.

References

(1) Radzicka, A.; Wolfenden, R. A Proficient Enzyme. *Science.* **1995**, *267* (5194), 90–93.

(2) Wolfenden, R.; Snider, M. J. The Depth of Chemical Time and the Power of Enzymes as Catalysts. *Acc. Chem. Res.* **2001**, *34* (12), 938–945.

(3) Cornish-Bowden, A. One Hundred Years of Michaelis–Menten Kinetics. *Perspect. Sci.* **2015**, *4*, 3–9.

(4) Pauling, L. Nature of Forces between Large Molecules of Biological Interest. *Nature* **1948**, *161* (4097), 707–709.

(5) Röthlisberger, D.; Khersonsky, O.; Wollacott, A. M.; Jiang, L.; DeChancie, J.; Betker, J.; Gallaher, J. L.; Althoff, E. A.; Zanghellini, A.; Dym, O.; Albeck, S.; Houk, K. N.; Tawfik, D. S.; Baker, D. Kemp Elimination Catalysts by Computational Enzyme Design. *Nat. 2008 4537192* **2008**, *453* (7192), 190–195.

(6) Cha, Y.; Murray, C. J.; Klinman, J. P. Hydrogen Tunneling in Enzyme Reactions. *Science.* **1989**, *243*, 1325–1330.

(7) Guo, J.; Zhou, H. X. Protein Allostery and Conformational Dynamics. *Chem. Rev.* **2016**, *116* (11), 6503–6515.

(8) Liu, J.; Nussinov, R. Allostery: An Overview of Its History, Concepts, Methods, and Applications. *PLOS Comput. Biol.* **2016**, *12* (6), e1004966.

(9) Süel, G. M.; Lockless, S. W.; Wall, M. A.; Ranganathan, R. Evolutionarily Conserved Networks of Residues Mediate Allosteric Communication in Proteins. *Nat. Struct. Biol. 2002 101* **2002**, *10* (1), 59–69.

(10) Cheng, X.; Jiang, H. Allostery in Drug Development. *Adv. Exp. Med. Biol.* **2019**, *1163*, 1–23.

(11) Brash, A. R. Lipoxygenases: Occurrence, Functions, Catalysis, and Acquisition of Substrate. *J. Biol. Chem.* **1999**, *274* (34), 23679–23682.

(12) Whittington, C.; Latham, J.; Offenbacher, A. R. Tunneling through the Barriers: Resolving the Origins of the Activation of C-H Bonds Catalyzed by Enzymes. In *ACS Symposium Series*; 2020; Vol. 1357.

(13) Hatcher, E.; Soudackov, A. V.; Hammes-Schiffer, S. Proton-Coupled Electron Transfer in Soybean Lipoxygenase. *J. Am. Chem. Soc.* **2004**, *126* (18), 5763–5775.

(14) Newcomer, M. E.; Brash, A. R. The Structural Basis for Specificity in Lipoxygenase Catalysis. *Protein Sci.* **2015**, *24* (3), 298–309.

(15) Offenbacher, A. R.; Iavarone, A. T.; Klinman, J. P. Hydrogen-Deuterium Exchange Reveals Long-Range Dynamical Allostery in Soybean Lipoxygenase. *J. Biol. Chem.* **2018**, *293* (4), 1138–1148.

(16) Offenbacher, A. R.; Holman, T. R. Fatty Acid Allosteric Regulation of C-H Activation in Plant and Animal Lipoxygenases. *Molecules* **2020**, *25* (15), 3374.

(17) Glickman, M. H.; Klinman, J. P. *Nature of Rate-Limiting Steps in the Soybean Lipoxygenase-1 Reaction?*; 1995; Vol. 34.

(18) Knapp, M. J.; Rickert, K.; Klinman, J. P. Temperature-Dependent Isotope Effects in Soybean Lipoxygenase-1: Correlating Hydrogen Tunneling with Protein Dynamics. *J. Am. Chem. Soc.* **2002**, *124* (15), 3865–3874.

(19) Mogul, R.; Johansen, E.; Holman, T. R. Oleyl Sulfate Reveals Allosteric Inhibition of Soybean Lipoxygenase-1 and Human 15-Lipoxygenase. *Biochemistry* **2000**, *39* (16), 4801–4807.

(20) Oganesyan, I.; Lento, C.; Wilson, D. J. Contemporary Hydrogen Deuterium Exchange

Mass Spectrometry. *Methods* **2018**, *144*, 27–42.

(21) Klil-Drori, A. J.; Ariel, A. 15-Lipoxygenases in Cancer: A Double-Edged Sword? *Prostaglandins Other Lipid Mediat.* **2013**, *106*, 16–22.

(22) Meng, H.; Dai, Z.; Zhang, W.; Liu, Y.; Lai, L. Molecular Mechanism of 15-Lipoxygenase Allosteric Activation and Inhibition. *Phys. Chem. Chem. Phys.* **2018**, *20* (21), 14785–14795.

(23) Kuhn, H.; Banthiya, S.; Van Leyen, K. Mammalian Lipoxygenases and Their Biological Relevance. *Biochim. Biophys. Acta - Mol. Cell Biol. Lipids* **2015**, *1851* (4), 308–330.

Chapter 2

Expression and purification of αDOX

Introduction

Enzymes are catalysts that accelerate chemical reactions to take place at rates that allows for the sustainability of life. There are billions of chemical reactions that occur within the body and are necessary for the functionality of cells. Without enzymes, uncatalyzed reactions at room temperature are estimated to require anywhere from hours to decades and upwards of millions of years to proceed, while the rate of reactions that take place in the presence of enzymes take 10^0 to 10^4 s^{-1}.[1] The ratio of the rates of catalyzed versus uncatalyzed reactions is called the rate enhancement. Many proficient enzymes that catalyze C-H, C-N, and C-C bond cleavage exhibit rate enhancement of $10^{12} – 10^{20}$, with the gold standard being a rate enhancement of 2×10^{26}-fold.[2] The catalytic effect that enzymes have on the rate of reactions is evident, however how the effect is achieved remains largely unresolved. Scientists have been studying enzymes for decades and no man-made catalyst has come close to matching the catalytic power of natural enzymes. In 1948, Linus Pauling theorized that enzymes lower the activation energy of the reaction by stabilizing the transition state.[3] Using the concept of electrostatic interactions to stabilize the transition state, man-made catalysts have only been able to enhance the rate by (at best) 10^9 over uncatalyzed reaction with assistance from directed evolution.[4] Despite modest advancements in the understanding of transition state catalysts, the discovery of quantum tunneling driven reactions such as enzyme C-H activation requires new considerations for enzyme design.[5]

C-H activation, also called C-H bond cleavage, is the process of a sp^3 hybridized C-H bond being cleaved, shown in Figure 2.1, and replaced with a C-X bond, where X is oxygen, nitrogen, or carbon. An estimated one-third of biological chemical transformations occur by C-H bond

activation. Because C-H bonds can be stably labeled with deuterium, the mechanism of this process can be examined by switching the hydrogen out for deuterium to measure the kinetic isotope effects (KIEs).[6]

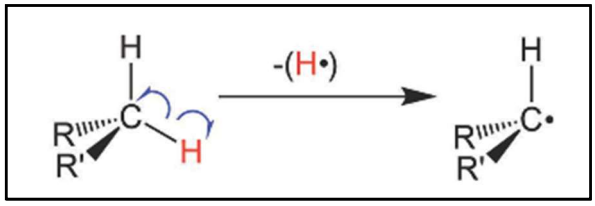

Figure 2.1 *Homolytic C-H activation that results in the transfer of a hydrogen atom. Reproduced from reference.*[6]

Following the classical transition state theory, the deuterium KIE on the first order rate constant, $^{D}k_{cat}$, has an upper limit of 7. The limit of this KIE is dominated by the difference in the ground state zero-point energies between H and D. However, enzymes that catalyze C-H bond cleavage have documented $^{D}k_{cat}$ of over 100. This large $^{D}k_{cat}$ value can implicate quantum tunneling. Quantum tunneling is when the hydrogen atom, instead of going over the activation barrier, acts as a wave and proceeds through the barrier, thus surpassing the classical transition state. In this case, the hydrogen donor, carbon, and the hydrogen atom acceptor (often O or N atom) must come very close together to facilitate wave function overlap.[6] Importantly from the study of enzymatic C-H activation, especially from the model lipoxygenase family, four keys to the origins of catalysis have been proposed: proximity, hierarchy of protein motions, the role of large hydrophobic resides, and the involvement of evolved protein networks.[7]

Lipoxygenases (LOX) are a class of enzymes that catalyze the peroxidation of polyunsaturated fatty acids using C-H activation.[8] LOXs can be found in plants, animals, fungi, and bacteria. In humans, there are multiple isoforms of LOX that have been implicated in various inflammatory diseases such as arthritis. LOXs have served as the paradigm for studying mechanisms of the C-H activation.[7] C-H activation is well studied in LOX, and so for this proposal,

I want to expand the mechanistic studies of C-H activation to α-Dioxygenase (α-DOX). I am choosing to study α-DOX because it reacts to the same fatty acid substrates as LOX, however it catalyzes a different reaction and has a different structure. The goal with α-DOX is to determine how ubiquitous the rules for the origins of C-H activation are. The central focus of this thesis will be to determine the role of volume-filling aliphatic residues, namely phenylalanine at position 552 in *Oryza sativa* α-DOX, on the proficiency of C-H bond cleavage.

α-DOXs are heme-containing enzymes that generate oxylipins in defense against pathogen attack.[9] It has been suggested that α-DOXs are a part of a plant's defense system that prevents it from excessive necrosis and oxidative stress in the event of an infection.[9]

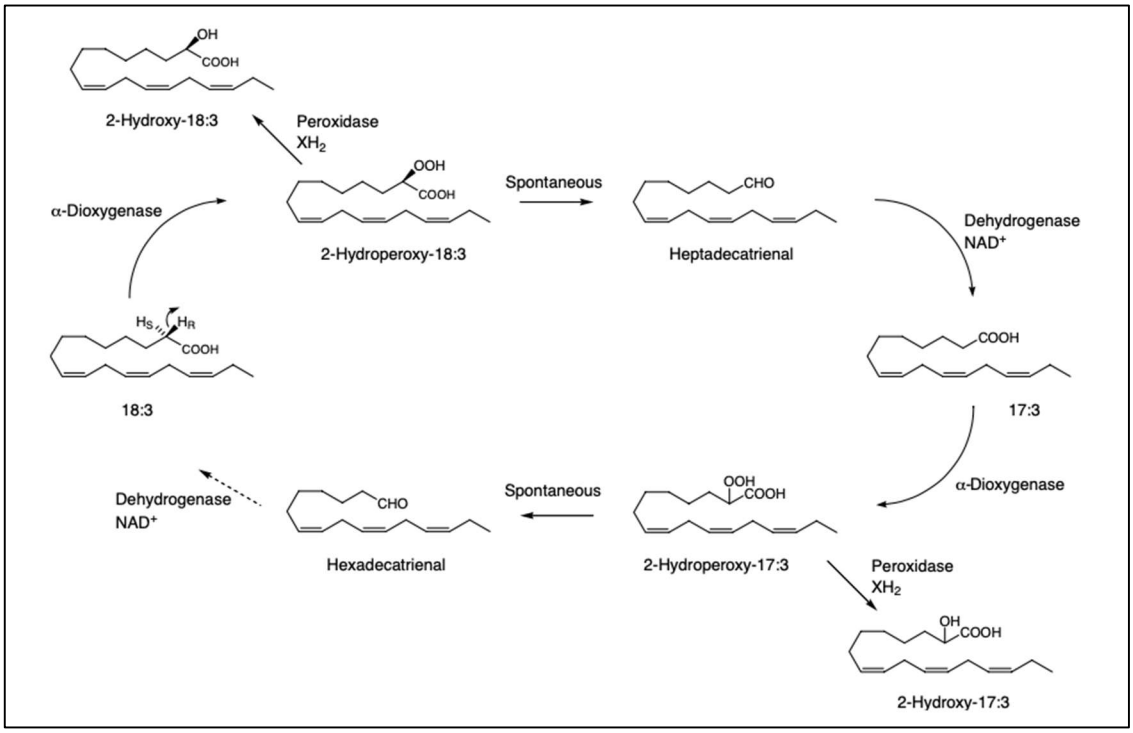

Figure 2.2 *α-Oxidation of linoleic acid (18:3) in plants. α-DOX oxidizes the α-carbon to make 2-hydroperoxidases. Reproduced from reference.*[9]

α-DOXs are present in plants and fungi and constitute a subfamily within the cyclooxygenase-peroxidase superfamily. α-DOX is distinct from LOXs and cyclooxygenases as it oxidates the α-carbon of the fatty acid chain rather than the allylic or bis-allylic carbon

positions.[10] α-DOXs are the enzymes that initialize the stereospecific α-oxidation of carbon fatty acid substrates, such as linoleic acid (LA), to make 2-hydroperoxy fatty acids. These 2-hydroperoxy fatty acids are then spontaneously converted into oxylipins like heptadectrienal, shown in Figure 2.2 above.[9] One of the more prevalent models used to learn more about α-DOXs and the underlying mechanism is the enzyme from rice, *Oryza sativa.*

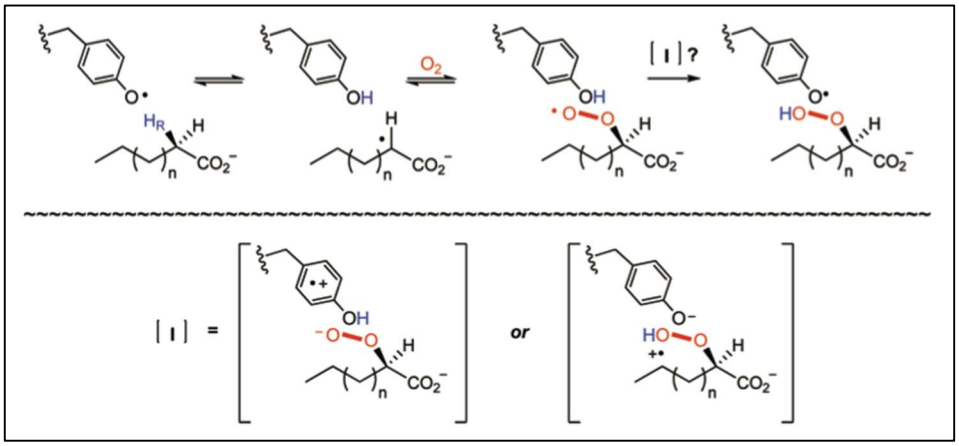

Figure 2.3 *Proposed mechanism of oxidation on a fatty acid by Oryza sativa α-DOX. Reproduced from reference.*[11]

α-DOX catalyzes the α-oxidation of fatty acids through a tyrosyl mediated reaction mechanism, shown in Figure 2.3. The tyrosyl radical uses C-H activation to abstract a hydrogen from the α-carbon on the fatty acid chain and initiate the reaction. Specifically, it has been determined that the tyrosine (Y) that proceeds the reaction in rice α-DOX is Y379. This was confirmed by analyzing the reactivity of enzymes with Y379 mutated to a phenylalanine (F). The Y379F mutants were found to be catalytically inactive. The proposed mechanism in Figure 2.3 depicts both the concerted and sequential proton-coupled electron transfer (PCET) possibilities. The sequential PCET mechanism is less thermodynamically favorable compared to the concerted mechanism due to the high-energy intermediates necessary in the sequential mechanism. These intermediates are depicted in the brackets in the lower half of Figure 2.3.[11]

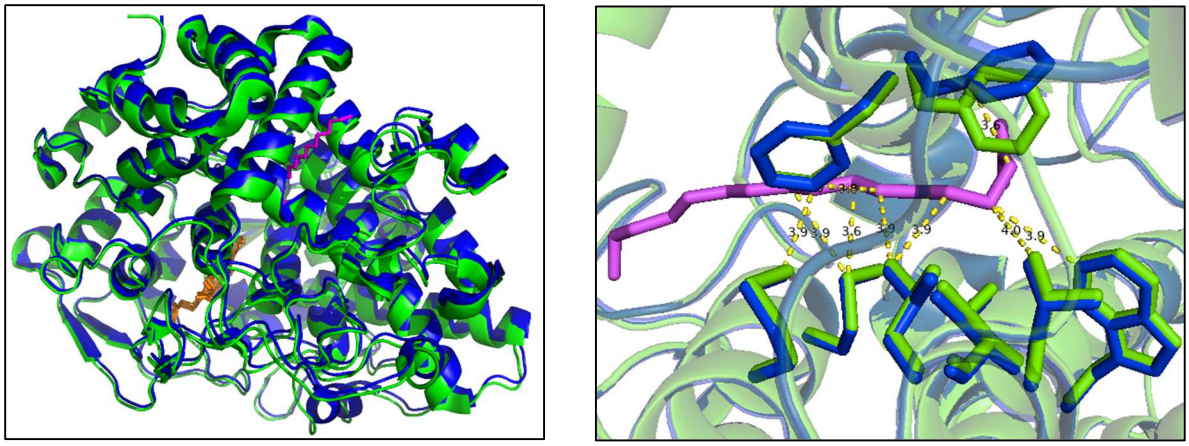

Figure 2.4 *X-ray crystal structure of α-DOX. The green molecule represents α-DOX (PDB: 4KVK) and the blue molecule represents catalytically inactive α-DOX with bound substrate, palmitic acid (PDB: 4KVL). The pink structure is PA bound to α-DOX. Modified from reference.*[10]

The x-ray crystal structures of rice α-DOXs have been solved in absence and presence of the substrate, palmitic acid. The α-DOX structure in the presence of palmitic acid was a catalytically inactive α-DOX mutant, Y379F.[10] In Figure 2.4, it is noted that for most of the amino acids closest to the binding site there is no conformational change in the presence of palmitic acid (PA). There is one aliphatic residue, however, phenylalanine (F) 552 that rotates approximately 90 degrees when the substrate is bound to the enzyme. This is the first example of this type of movement that has been identified in a C-H activation enzyme. We believe that the bulk of F552 is critical for enzyme proficiency and planned to show this using two aims:

Aim 1: Optimization of expression and purification of α-DOX and characterization of kinetics

Aim 2: Mutagenesis study of F552 in α-DOX

For this aim, four mutants will be synthesized and tested. F552 will be mutated to other similar non-polar amino acids, a mutational study of F552 has not yet been conducted. We planned to mutate F552 into a Leucine (L), Valine (V), Alanine (A), and Glycine (G). These amino acids were chosen because the side chains are all comprised of just carbon and hydrogen. Additionally, from F to L to V to A to G, the side chain volume becomes increasingly smaller so that the effect

of the bulk of F552 can be properly analyzed. As the side chain gets smaller, the distance between the substrate and tyrosyl radical cofactor is expected to increase. The distance between these molecules is expected to play a key role in tunneling because the donor and acceptor need to be very close for the particle to efficiently proceed through the barrier.[7]

Methods and Results

Transformation, Expression, and Purification

Starting this project, *Oryza Sativa* alpha dioxygenase (αDOX) was transformed using a pQE-30 expression vector into *E. coli* NEBExpress® I^q competent cells. The protein was expressed, and the cells were lysed, sonicated, and centrifuged as previously described.[12] The supernatant was recentrifuged at 180,000 g for one hour. The resulting cell pellet was solubilized with 8mL/g of wet cell weight in 20 mM sodium phosphate buffer (pH 7) with 300 mM NaCl, and 0.1% Nonidet P-40 substitute, buffer A. The cell suspension was recentrifuged at 180,000 g for one hour. The supernatant was applied to a Ni-NTA column and eluted with 20 mM sodium phosphate buffer (pH 7) with 300 mM NaCl, 0.1% Nonidet P-40 substitute, and 200 mM imidazole, buffer B. As shown in Figure 2.5, lanes 6 and 7 lack any significant band at 70 kDa, showing that this method did not yield any protein.

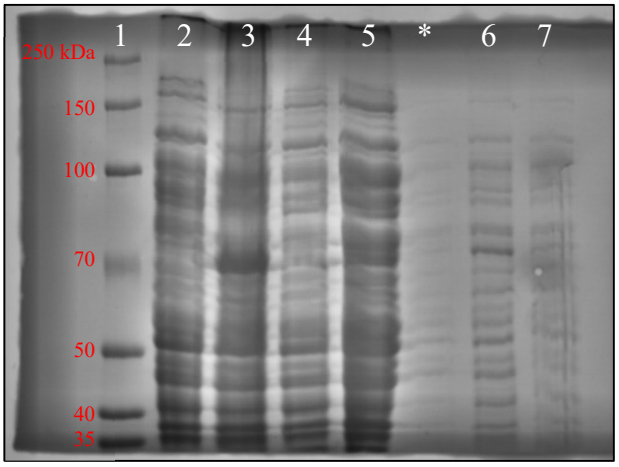

Figure 2.5 *SDS-PAGE results from the initial expression and purification method. Lanes are as follows: 1 is the ladder; 2 and 3 are previously discarded cell pellets that have been re-lysed and sonicated to check for protein, their specific identity is unknown; 4 and 5 are WT and F552A αDOX after the 1st centrifugation at 180,000 g; * is overflow from 5; 6 and 7 are WT and F552A αDOX samples after the 2nd centrifugation at 180,000 g.*

Going forward, the protein expression procedure was altered and instead of inducing at an OD_{600} = 0.9 to a final concentration of 1 mM IPTG and reducing the temperature to 20 ℃ to shake overnight,[1] when the OD_{600} = 1.1, IPTG was added to a final concentration of 1 μM and the temperature was reduced to 18 ℃. Also, for the *Arabidopsis thaliana* αDOX, 5-aminolevulinic acid hydrochloride was added to a final concentration of 250 μM during expression.[12] Additionally, instead of sonicating the lysate for five 15-second pulses,[13] the lysate was sonicated for three 5-minute pulses before centrifugation. For the solubilization during the purification procedure, instead of stirring the cell suspension on ice for one hour, the cells were homogenized first before stirring for an hour.

As shown in Figure 2.6, this method yielded some *Oryza Sativa* αDOX, which is evident by the dark band in lane 8, but no *Arabidopsis thaliana* αDOX. However, upon further investigation, the *Oryza Sativa* αDOX was shown to be kinetically inactive.

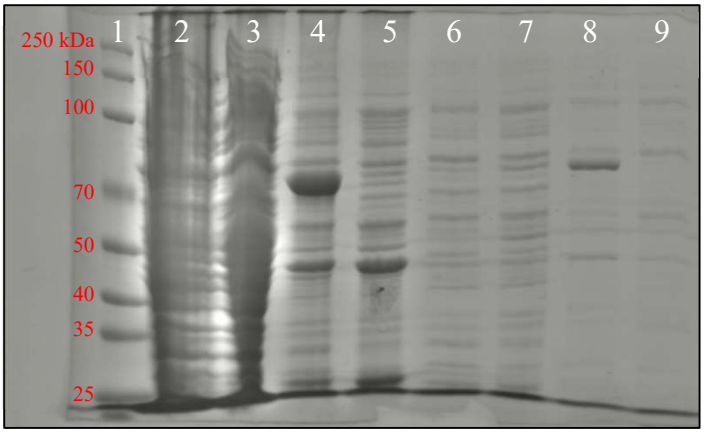

Figure 2.6 *SDS-PAGE results from the first adjusted method of expression and purification for αDOX. The lanes are as followed: 1 is the ladder; 2 and 3 are the lysates of WT Oryza sativa (R) and WT Arabidopsis thaliana (A) αDOX respectively; 4 and 5 are post solubilizations from R and A; 6 and 7 the flow through from R and A; 8 and 9 are the elutions from R and A.*

Moving forward, the purification procedure was altered for the *Oryza Sativa* αDOX. After the lysate was sonicated and centrifuged for ten minutes, 5 mL of 700 μM *n*-Dodecyl β-D maltoside was slowly added to the supernatant over the course of ten minutes and then was left to stir for one hour. The resulting suspension was centrifuged at 100,000 g for one hour. The supernatant was applied to a Ni-NTA column and instead of being eluted with buffer B, it was eluted with a variant of buffer A that had a pH of 5 instead of 7.

There was no yield from this altered method. Additionally, a protein that was applied to that same Ni-NTA column later revealed some impurities that could have been from αDOX, implying that the protein may not have eluted from the column.

Since none of alterations to the method yielded any viable protein, it was decided to clone αDOX into a different expression vector. An alternate wild-type *Oryza Sativa* αDOX was obtained that was within the 2CT plasmid, and it was expressed into BL21 Codon Plus *E. Coli* cells. During expression, once the OD_{600} = 1, the cells were induced using a final concentration of 1 mM IPTG and the temperature was reduced to 18 ℃ and the cells were left to shake overnight. Following the harvesting, the cells were lysed using a lysis buffer containing 52 mL of 18 MΩ water, 16 mL of

50% glycerol, 4 mL 20 mM $MgSO_4$, 8 mL 0.5 M sodium phosphate (pH 8) with 0.5 M NaCl, 800 µL 10% tween-20, 19 mg AEBSF, 5 mg DNAse, and 10-15 mg of lysozyme. The suspension was sonicated using three cycles of 5-minute pulses then centrifuged for twenty minutes at 18,000 g. The supernatant was applied to the Ni-NTA column that was pre-equilibrated with 20 mM Tris-HCl (pH 8) containing 500 mM NaCl, and 20 mM imidazole. The flow through was collected, then the column was washed with more of the same buffer and that was collected. Then the column was washed with 20 mm Tris-HCl (pH 8) that contained 500 mM NaCl, and 200 mM imidazole and the following elution was collected.

An SDS-PAGE of samples taken from various points in the purification process was conducted. The resulting gel, shown in Figure 2.7, shows that there was no αDOX yield after the purification process.

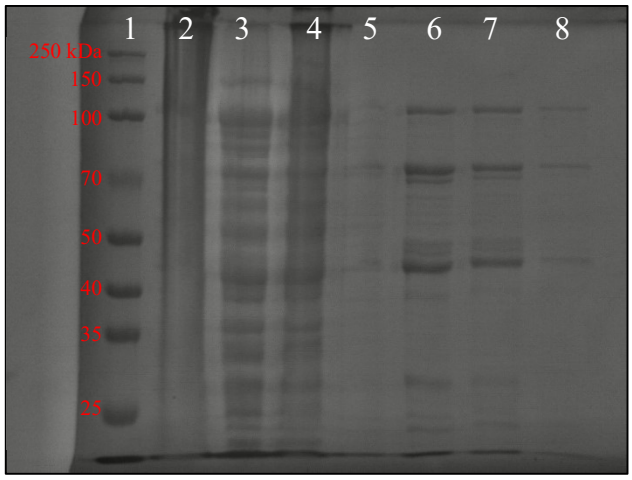

Figure 2.7 *SDS-PAGE from wild type αDOX expressed using 2CT expression vector. The lanes are as follows: 1 is the ladder; 2 is the lysate after sonication; 3 is the supernatant before loading onto the column, 4 is the flow through from the column; 5 is the column wash; 6, 7, and 8 are the elutions from the column.*

Kinetic Analysis via O_2 electrode

The concentration of *Oryza Sativa* αDOX had was measured using a UV/Vis spectrophotometer, and the absorbance was measured at $\varepsilon_{411\ nm}$. To check the activity of the enzyme, an O_2 electrode was used to observe the oxygen consumption at 25 ℃. The rate of oxygen consumption was measured for the enzyme using linoleic acid (LA), oleic acid (OA), and with and without the addition of 100 equivalents of H_2O_2 to the enzyme.[13]

The data for all of the above conditions are displayed in Table 2.1. The oxygraph traces for αDOX reacting with OA and LA in the presence of H_2O_2 are shown in Figure 2.8. In addition to αDOX, a trial run was performed with SLO reacting with LA, to determine if the oxygen electrode was reading properly. As shown in Table 1.A and in Figure 2.8, the SLO reaction with LA had a large rate and proceeded in under 3 minutes. This is a contrast to the results from αDOX kinetic trials, which display little-to-no oxygen consumption and the reaction did not reach completion within 93 minutes. Therefore, it was determined that the αDOX that was collected was kinetically inactive.

Table 2.1 *Kinetic Data from O_2 Electrode*[a]

Enzyme	Substrate	With H_2O_2[b]		Without H_2O_2	
		[enzyme] (mM)	Rate (1/s)	[enzyme] (mM)	Rate (1/s)
SLO	LA	N/A	N/A	0.008700	300.575
αDOX	LA	0.3185	0.064	0.756	0.026146
		0.1334	0.482		
		0.2548	0.233		
	OA	0.1334	0.161		
		0.2548	0.034		

[a]*Collected at 25 ℃ in 25 mM HEPES (pH 7.2)* [b]*100 equivalents of H_2O_2 incubated with the enzyme for 5 mins. prior to reaction.*

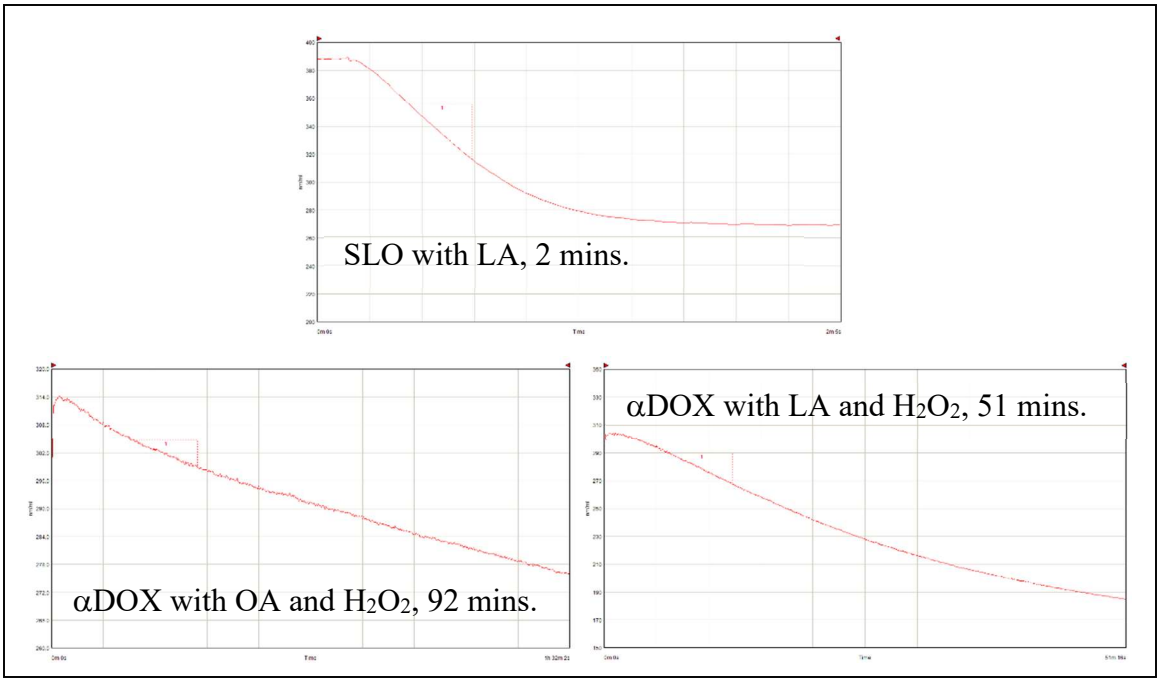

Figure 2.8 *Oxygraph traces of SLO reacting with LA and αDOX reacting with OA and LA, in the presence fo 100 equivalents of H_2O_2.*

Conclusion

In conclusion, we have pursued several methods of expression and purification, initially focusing on the procedures described in previous literature sources,[12] but with no success. We altered the buffer used to lyse the cells, the sonication procedure, the method of solubilization, and the expression vector – to include a solubility tag (*e.g.* MBP), all to no avail. Our only success at isolating what we belive to be our protein displayed virtually no activity. However, we have not confirmed the presence using Western blot or mass spectrometry analysis. These data suggest that we were not successful at isolating the desired protein. Therefore, it was decided to switch the focus of this Thesis from αDOX and instead direct our efforts to a diffferent project, focuses on plant and animal lipoxygenase enzymes. Future studies using folding chaperones, other solubilizing agents, cell lines (*e.g. E. coli* M15), or softer cell lysis methods could be pursued to help isolate αDOX.

References

(1) Radzicka, A.; Wolfenden, R. A Proficient Enzyme. *Science.* **1995**, *267* (5194), 90–93.

(2) Wolfenden, R.; Snider, M. J. The Depth of Chemical Time and the Power of Enzymes as Catalysts. *Acc. Chem. Res.* **2001**, *34* (12), 938–945.

(3) Pauling, L. Nature of Forces between Large Molecules of Biological Interest. *Nature* **1948**, *161* (4097), 707–709.

(4) Röthlisberger, D.; Khersonsky, O.; Wollacott, A. M.; Jiang, L.; DeChancie, J.; Betker, J.; Gallaher, J. L.; Althoff, E. A.; Zanghellini, A.; Dym, O.; Albeck, S.; Houk, K. N.; Tawfik, D. S.; Baker, D. Kemp Elimination Catalysts by Computational Enzyme Design. *Nat. 2008 4537192* **2008**, *453* (7192), 190–195.

(5) Cha, Y.; Murray, C. J.; Klinman, J. P. Hydrogen Tunneling in Enzyme Reactions. *Science.* **1989**, *243*, 1325–1330.

(6) Whittington, C.; Latham, J.; Offenbacher, A. R. Tunneling through the Barriers: Resolving the Origins of the Activation of C-H Bonds Catalyzed by Enzymes. In *ACS Symposium Series*; 2020; Vol. 1357.

(7) Klinman, J. P.; Offenbacher, A. R.; Hu, S. Origins of Enzyme Catalysis: Experimental Findings for C-H Activation, New Models, and Their Relevance to Prevailing Theoretical Constructs. *J. Am. Chem. Soc.* **2017**, *139* (51).

(8) Brash, A. R. Lipoxygenases: Occurrence, Functions, Catalysis, and Acquisition of Substrate. *J. Biol. Chem.* **1999**, *274* (34), 23679–23682.

(9) Hamberg, M.; De Leon, I. P.; Rodriguez, M. J.; Castresana, C. α-Dioxygenases. *Biochem. Biophys. Res. Commun.* **2005**, *338* (1), 169–174.

(10) Zhu, G.; Koszelak-Rosenblum, M.; Malkowski, M. G. Crystal Structures of α-

Dioxygenase from Oryza Sativa: Insights into Substrate Binding and Activation by Hydrogen Peroxide. *Protein Sci.* **2013**, *22* (10).

(11) Mukherjee, A.; Angeles-Boza, A. M.; Huff, G. S.; Roth, J. P. Catalytic Mechanism of a Heme and Tyrosyl Radical-Containing Fatty Acid α-(Di)Oxygenase. *J. Am. Chem. Soc.* **2011**, *133* (2).

(12) Goulah, C. C.; Zhu, G.; Koszelak-Rosenblum, M.; Malkowski, M. G. The Crystal Structure of α-Dioxygenase Provides Insight into Diversity in the Cyclooxygenase-Peroxidase Superfamily. *Biochemistry* **2013**, *52* (8).

(13) Koeduka, T.; Matsui, K.; Akakabe, Y.; Kajiwara, T. Catalytic Properties of Rice α-Oxygenase. A Comparison with Mammalian Prostaglandin H Synthases. *J. Biol. Chem.* **2002**, *277* (25), 22648–22655.

Chapter 3

Thermodynamic and biophysical study of allosteric effector binding to soybean lipoxygenase-1

Reproduced from FEBS Letters
Manuscript ID: FEB214275
Title: "Thermodynamic and biophysical study of fatty acid effector binding to soybean lipoxygenase: implications for allostery driven by helix α2 dynamics"
Authors: Daniella E. Roberts, Amy M. Benton, Claire Fabian-Bayola, Anne M. Spuches, and Adam R. Offenbacher

Introduction

Lipoxygenases (LOXs) are widely represented in plants, animals, fungi, and some prokaryotes. These enzymes oxidize polyunsaturated fatty acids to produce functionally diverse cell signaling hydroperoxides (Figure 3.1A).[1] Despite low sequence homology for LOXs within (and across) kingdoms,[2] crystal structures of representatives highlight a structurally conserved catalytic core that harbors the metallocofactor responsible for catalysis (Figure 3.1B).[3] LOXs from higher eukaryotes have a second domain at the N terminus and are referred to as the Polycystin-1, Lipoxygenase, α-Toxin (PLAT) domain.[3] In select LOXs, including human 5-LOX and coral 11R-LOX, Ca^{2+} binding at the PLAT domain induces membrane association that is required for full activity. This putative allosteric control is considered to be facilitated through a cation-π interaction involving a conserved Trp in the PLAT domain.[4,5] In addition to membrane binding, the PLAT domain has been implicated in regulating 15-LOX substrate specificity, through fatty acid allostery.[6] For example, human epithelial 15-LOX-2 oxidation of arachidonic acid (AA) to 15-HpETE has been shown to be modulated in vitro by the 15-LOX-1 product, 13-(*S*)-hydroxy-(9Z,11E)-octadecadienoic acid (13*S*-HODE).[7] This is expected to have important relevance in human health as 15-HpETE production in macrophages has been linked to the progression of

atherosclerosis,[8,9] a common form of cardiovascular disease. Conversely, the pro-resolution molecule, resolvin-D5 (7*S*,17*S*-diHDHA; RvD5), has been suggested to play a role in the mitigation of this inflammation and atherosclerotic plaques.[10] Recently, 15-LOX-2 has been shown to synthesize RvD5 from the oxidation of docosahexaenoic acid (DHA),[11] although the interplay of LOX isozyme metabolism of DHA is complex.[12–14] Thus, resolving the allosteric mechanisms and interactions from these fatty acid effectors is expected to expound our understanding of 15-LOX biochemistry.

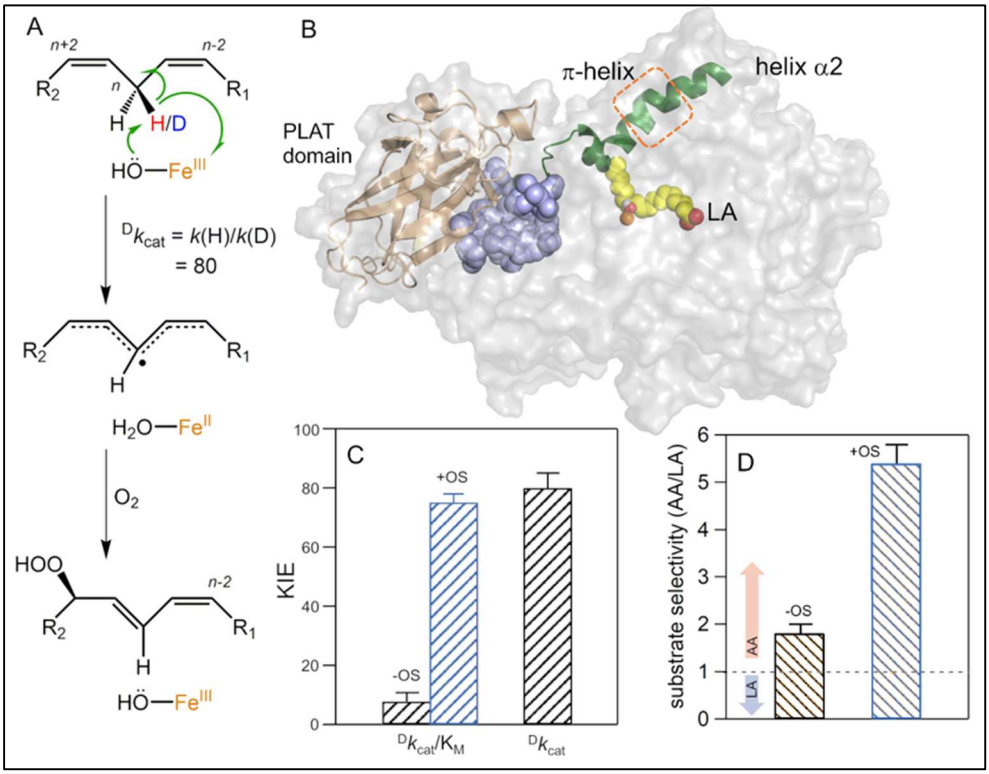

Figure 3.1 *Reaction mechanism and structure of SLO. (A) Mechanism of LA peroxidation catalyzed by SLO. (B) X-ray surface structure of SLO with the PLAT regulatory shown in wheat cartoon for reference. Note that helix α2, as discussed in text, lines the substrate entrance portal and is colored in green. The blue spheres represent the predicted pocket for the fatty acid allosteric site, based on previous in silico docking studies.*[6] *LA is modelled as yellow spheres into the active site, adjacent to the catalytic iron (orange sphere). (C) The experimentally observed kinetic isotope effects (KIEs) reported*[15] *for the first-order ($^{D}k_{cat}$) and second-order ($^{D}k_{cat}/K_M$) rate constants for the reaction of SLO with substrate LA, in the absence (black) and presence (grey) of allosteric effector, oleyl sulfate (OS) at 5 °C. (D) The reported impact of OS on SLO's substrate selectivity, $(k_{cat}/K_M)^{AA}/(k_{cat}/K_M)^{LA}$.*[16]

Soybean lipoxygenase-1 (SLO) has emerged as a robust model plant 15-LOX that has been studied for the origins of enzyme catalysis and LOX allostery.[6,17] There is kinetic evidence that the fatty acid derivative, oleyl sulfate (OS), acts as an allosteric inhibitor and changes the substrate preference for both SLO and human 15-LOX-1, with modest-to-no effect on the first-order rate constants.[6,16] The allosteric regulation of both SLO and human 15-LOX-1 by the fatty acid derivative, oleyl sulfate (OS), was initially inferred from comparative kinetic isotope effects (KIEs) (Figure 3.1C).[15,18] The initial step in LOX chemistry is an irreversible C-H bond cleavage (i.e. C-H activation) step at the bis-allylic carbon (Figure 3.1A), generating a delocalized pentadienyl radical that is subsequently quenched by molecular oxygen to form a specific (13*S*) hydroperoxide product. In the absence of OS, the steady-state reaction of SLO with natural substrate, linoleic acid (LA), is associated with a large, nearly temperature-independent, primary deuterium KIE of the first-order rate constant, $^{D}k_{cat} = 80$.[19] This value is an order of magnitude larger than the classical limit imposed by transition state theory and consistent with hydrogen tunneling.[20] At low temperatures (5-10 °C), the KIE on the second-order rate constant, $^{D}k_{cat}/K_M$, is small (*ca.* 5-15), such that $^{D}k_{cat}/K_M << {}^{D}k_{cat}$ for SLO (Figure 3.1C).[21] Under these conditions, substrate capture dominates the rate-limiting step of catalysis. Importantly, the addition of OS, which does not bind to the active site,[18] leads to a significant increase in the $^{D}k_{cat}/K_M$ to match $^{D}k_{cat}$ at 5–10 °C, corresponding to a change in the rate-limiting step of catalysis (Figure 3.1C).[15] In addition, OS has been shown to alter the preference of fatty acid substrates for SLO, with an enhanced substrate preference for arachidonic acid over LA in the presence of OS (Figure 3.1D).[16] Note that natural fatty acids, such as oleic acid (OA), have also been shown to act as allosteric effectors; however, OA is associated with mixed-type inhibition that competes with substrate binding at the active site.[16,22] For the current study, we used OS as a model allosteric effector to

investigate the mechanism(s) of the allosteric effects in SLO. While the kinetic data have inferred allosteric binding site for OS and other natural fatty acids, direct detection for effector binding to SLO (or other 15-LOXs) has not been previously demonstrated.

The application of temperature-dependent hydrogen-deuterium exchange mass spectrometry (HDX-MS) previously identified regional protein flexibility to SLO that was sensitive to the presence of OS.[23] The most notable effect was an increased apparent rate of H/D exchange along helix α2 that gates the substrate entrance channel (Figure 3.1B). We have recently reported similarly altered HDX properties linked to dimerization of the human 12-LOX, when the native dimeric and mutant monomeric forms of the isozyme were compared.[24] These oligomerization changes in human 12-LOX also influence substrate binding and reactivity, and the affinity for an isozyme selective inhibitor. One of the most compelling examples of protein controlling substrate selectivity is highlighted by the enzyme ribonucleotide reductase (RNR). This system exploits two levels of allostery with on/off 'activity' regulation that is facilitated by functionally linked oligomerization changes of the RNR subunit through ATP/dATP binding and with 'specificity' regulation which involves intricate structural changes of a protein loop adjacent to the active site elicited by the binding of defined substrate/effector cognate pairs.[25,26] In contrast to this classic view of protein allostery,[27] an alternative model of allostery was posited by Cooper in 1984, in which enzyme function could be modulated in the absence of a conformational change.[28] In this case, allostery is governed by protein dynamics.[29] Several examples with differing degrees of dynamically driven protein allostery have been reported in the literature.[30–32] Thus, the previously reported, regional altered HDX properties of SLO appearing in the presence of OS could be attributed to a change in oligomerization, structure and/or protein dynamics.

In this study, we employed a combination of biophysical tools including dynamic light scattering and differential scanning calorimetry to further elucidate the mechanistic features of SLO allostery. The results presented herein provide evidence that SLO is a monomer and does not undergo oligomerization or a structural transition upon OS binding. We also demonstrate OS binding to SLO using isothermal titration calorimetry. The mounting biophysical and kinetic data strongly support effector binding and a role for dynamically driven allostery for the regulation of SLO catalysis by fatty acids.

Methods

Expression and Purification of SLO

Wild type (WT) SLO was expressed using the T7-7 expression plasmid in *E. coli* BL21(DE3) codon plus RIL cells and purified as previously described, using cation exchange chromatography.[33] The presence and purity of SLO in the fractions were confirmed via sodium dodecyl sulfate-polyacrylamide gel electrophoresis (SDS-PAGE). Fractions containing SLO were dialyzed overnight in 0.1 M borate (pH 9). SLO was concentrated to 0.1 mM, frozen in liquid N_2, and stored in aliquots at -80 °C. Iron content was determined using ferrozine as a colorimetric iron chelator.[34] WT had 0.65-0.75 Fe atoms per SLO monomer. SLO concentration was determined using ε_{280} = 131 mM^{-1} cm^{-1}.[35]

Steady-state Kinetics

Steady-state kinetic assays of SLO were performed at 10 and 30 °C on a Shimadzu UV-1800 spectrophotometer. The spectrophotometer was equipped with a water jacketed cell holder and a Julabo 600F circulating water bath. Product (13*S*-HpODE) formation was monitored in single wavelength mode at 234 nm with an ε_{234} = 23.6 mM^{-1} cm^{-1}. LA (H_{31}-LA) and deuterated

LA (11,11-D_2-LA) were varied in six concentrations from 1 to 130 μM. D_2-LA was synthesized previously.[36] Stock LA concentrations were determined enzymatically. Kinetic parameters (k_{cat} and k_{cat}/K_M) were determined from Michaelis-Menten fits ($v_{initial} = (k_{cat}[S])/(K_M + [S])$) to the data using Igor Pro (v 5.0) software. All reported rate constants are presented as the mean ± s.e.m. from at least three independent measurements and corrected for iron content. When appropriate, buffers were supplemented with 15 μM OS. OS was synthesized as previously described.[23] As an important control, steady-state kinetics were also collected for SLO in 50 mM borate pH 9 in which a 1 μM SLO stock solution was pre-incubated with 15 μM OS and at a designated time (0-2 h), the relative maximal rate was measured with 100 μM LA concentration. The enzyme maintained high activity (≥ 82%) in the presence of saturating OS up to 2 h. These data demonstrate that the enzyme remains stable and active in the prolonged presence of saturating OS.

Isothermal Titration Calorimetry (ITC)

Thermodynamic analyses of the binding between SLO and OS were performed using TA Instruments Nano-ITC. OS working solution was prepared fresh daily by diluting OS stock solutions (80 mM in 100% dimethyl sulfoxide, DMSO) to 250 μM in 50 mM sodium pyrophosphate, 50 mM sodium borate, and 50 mM CHES buffers for pH 9 studies or 50 mM sodium phosphate for pH 7.5 studies. At this working concentration, the OS sample contained 0.3% DMSO. Prior to use, a 350 μL aliquot of SLO (55-65 μM) was thawed and 1.05 μL of DMSO was added to match the percentage of DMSO present in the OS working solution. During a typical experiment, 50 μL of OS was injected (1 injection of 1.01 μL and 24 injections of 2.02 μL) into SLO solution in the reaction cell that was stirred at a rate of 320 rpm.

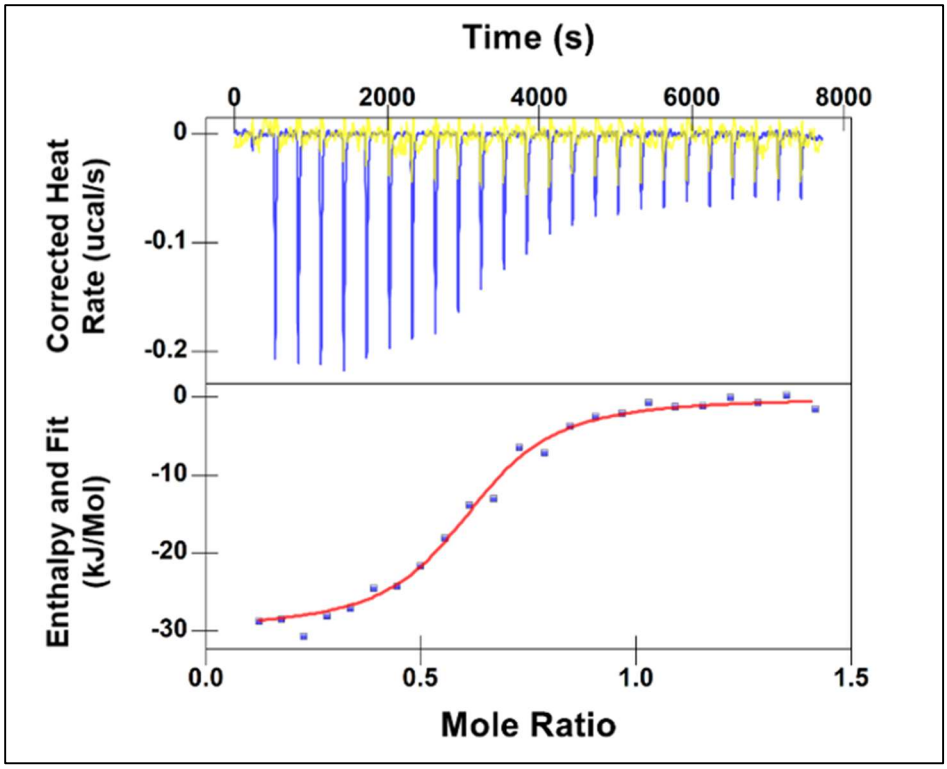

Figure 3.2 *Representative ITC thermogram of OS (250 μM) titrated into WT SLO (60 μM). The example is for 50 mM pyrophosphate buffer (pH 9.0) with 0.3% DMSO at 20 °C (blue trace). The yellow trace represents OS titration into buffer. The corrected, integrated data were fit to an independent model (red trace).*

As an important control, OS was titrated into pyrophosphate buffer without protein (Figure 3.2, yellow trace). The heats of dilution observed in this ligand-buffer titration accounted for the heat of dilution observed at the end of the OS-SLO titration (Figure 3.2, blue trace after 6000 s). This heat is larger than what is usually expected due to a slight mismatch in the DMSO concentration in both the ligand and protein/buffer solutions. Note that DMSO is required to initially dissolve the effector. The integrated heats from the last five injections from the experiment were averaged and this value was subtracted from each data point in the experimental titration prior to data fitting, in accordance with common practice.[37] Experiments were conducted at 10, 20, and 30 ºC for pH 9.0 and at 20 ºC for pH 7.5. An additional experiment at 20 ºC and pH 9.0 was collected in which the buffer for the syringe and ITC sample cell were supplemented with

0.15 M NaCl. The thermodynamic parameters (n, K_d, ΔH, and ΔS) were obtained from best fit to the ITC raw data (*cf.* Figure 3.2) using an independent binding model (Nano Analyze Software). Each ITC experiment was replicated 3-5 times and all thermodynamic parameters represent the mean ± S.D.

Dynamic Light Scattering (DLS)

DLS measurements were performed at room temperature using a DynaPro NanoStar instrument to study the impact of OS addition on the oligomerization state of WT SLO. An average of 10 scans was recorded per sample with an acquisition time of 3 seconds for each scan. The kinetic experiments were carried out in triplicate using three different protein concentrations (5, 2.5, and 1.25 mg/mL). When included, OS was added in a 1:1 molar ratio to SLO. Four different conditions were collected: 50 mM borate (pH 9), 50 mM borate (pH 9) with 0.15 M NaCl, 50 mM pyrophosphate (pH 9), and 50 mM pyrophosphate (pH 9) with 0.15 M NaCl.

Size Exclusion Chromatography (SEC)

The protein oligomerization state was tested using SEC with a Superdex^{TM} 200 increase 10/300 GL column on an ÄKTA^{TM} Prime FPLC. The buffer used for SEC-fast protein liquid chromatography (FPLC) was 50 mM HEPES (pH 7.5), 0.15 M NaCl, or 50 mM borate (pH 9) with or without 0.15 M NaCl. When appropriate, the column was pre-equilibrated in buffer supplemented with 15 μM OS. The elution volume was monitored by a change in absorbance at 280 nm. A calibration curve was constructed from a set of gel filtration standards (Sigma, St. Louis, MO, USA): cytochrome *c* from horse heart (12.4 kDa), carbonic anhydrase, bovine erythrocyte (29 kDa), albumin, bovine serum (66 kDa), alcohol dehydrogenase, yeast (150 kDa), and β-amylase, sweet potato (200 kDa). The dead volume was determined by blue dextran.

Differential Scanning Calorimetry (DSC)

DSC experiments were conducted on a TA-instruments Nano-DSC microcalorimeter. The SLO samples were prepared at 20 μM concentration in 50 mM borate (pH 9) or 50 mM borate (pH 9) with 0.15 M NaCl. When present, OS was added at equal molar concentration. The DSC experiments were carried out in heat-only mode, from 30 – 90 °C at a rate of 1 °C min^{-1}. The pressure was kept at 3 atm during the course of the experiment. These experiments were performed in triplicate.

Hydrogen-Deuterium Exchange Mass Spectrometry (HDX-MS)

Aliquots of SLO (100 μM) were thawed and were diluted 10-fold (5 μL into 45 μL) in 10 mM HEPES, 0.15 M NaCl, pD 7.4 D_2O (99% D) buffer (corrected; $pD = pH_{read} + 0.4$). Samples were incubated randomly at 8 time points (0, 10, 30, 60, 180, 600, 2700, and 7200 seconds) at 10 °C using a water bath. The HDX samples were prepared over the course of three days and the time points were randomized to reduce systematic error. Each time point was prepared and processed once. At the designated incubation time, all samples were then treated identically; the samples were rapidly cooled (5-6 seconds in a -20 °C bath) and acid quenched (to pH 2.4, confirmed with pH electrode, with 0.32 M citric acid stock solution to 90 mM final concentration). The acid solution was supplemented with 20 mM DTT to maintain reducing conditions for reducing disulfide bonds. Procedures from this point were conducted near 4 °C. Prior to pepsin digestion, guanidine HCl (in citric acid, pH 2.4) was mixed with the samples to a final concentration of *ca.* 0.5 M. HDX samples of SLO were digested with pre-equilibrated (10 mM citrate buffer, pH 2.4), immobilized pepsin for 2.5 min. The peptide fragments were filtered, removing the pepsin, using spin cups (cellulose acetate) and by centrifugation for 10 seconds at 4 °C. Samples were flash frozen immediately in liquid N_2 and stored at -80 °C until data collection.

Deuterated, pepsin-digested SLO samples of were analyzed using an Agilent 1200 LC (Santa Clara, CA) that was connected in-line with the LTQ Orbitrap XL mass spectrometer (Thermo). The LC was equipped with a reversed-phase analytical column (Viva C8, 30 mm length × 1.0 mm inner diameter, 5 μm particles, Restek, Bellefonte, PA) and guard pre-column (C8, Restek). Solvent A was 99.9% water/0.1% formic acid and solvent B was 99.9% acetonitrile/0.1% formic acid (v/v). Each sample was thawed immediately prior to injection onto the column. The elution program consisted of a linear gradient from 5% to 10% B over 1 min, a linear gradient to 40% B over 5 min, a linear gradient to 100% B over 4 min, isocratic conditions at 100% B for 3 min, a linear gradient to 5% B over 0.5 min, and isocratic conditions at 5% B for 5.5 min, at a flow rate of 300 μL/min. The column compartment was maintained at 4 °C and lined with towels to absorb atmospheric moisture condensation. The column exit was connected to the ESI source of the mass spectrometer using PEEK tubing (0.005" inner diameter × 1/16" outer diameter, Agilent). Mass spectra were acquired in the positive ion mode over the range m/z = 350 to 1800 using the Orbitrap mass analyzer, in profile format, with a mass resolution setting of 100,000 (at m/z = 400). Data acquisition was controlled using Xcalibur software (version 2.0.7, Thermo).

Mass spectral data acquired for HDX measurements were analyzed using the software, HDX Workbench.[38] The percent deuterium incorporation was calculated for each of these peptides, taking into account the number of amide linkages (excluding proline residues) and the calculated number of deuterons incorporated. The values were normalized for 100% D_2O and corrected for peptide-specific back-exchange, HDX% = (observed, normalized extent of deuterium incorporation {in percent})/(1-{BE/100}). Peptide-specific back-exchange was determined and reported previously.[39] Back-exchange values ranged from 2 to 50%, for an average value of 20%.

The resulting data were plotted as deuterium exchange versus time using Igor Pro software (See Appendix A).

Results and Discussion

Binding Thermodynamics of Effector OS to SLO

To provide direct evidence for binding of allosteric effectors to SLO, we first performed isothermal titration calorimetry (ITC) experiments to assess the thermodynamics for OS interactions with wild-type (WT) SLO protein at 20 °C and pH 9, under which conditions SLO allosteric effects from OS have been previously characterized.[15,16] Figure 3.2 displays a representative raw data set and thermogram for the titration of OS into SLO. From four independent data sets, the K_d for OS titration into SLO was found to be 1.0 ± 0.1 μM (Table 3.1), which is within uncertainty to the K_i value of 0.7 ± 0.3 μM determined from the competitive KIE measurements reported previously at 5 °C.[15] From our ITC analysis, the enthalpic contribution for OS binding to SLO, ΔH = -30 ± 5 kJ/mol, was found to be more favorable than the entropic contribution, $T\Delta S$ = 7.9 ± 2 kJ/mol (Table 3.1). ITC measurements for OS binding to SLO were also conducted at 10 and 30 °C (Figure 3.3A-C). At 10 °C, the K_d value was comparable to that for 20 °C, though the ΔH had become significantly more negative, from -30 ± 5 kJ/mol to -41.7 ± 2 kJ/mol, as the temperature was reduced (Table 3.1). This temperature dependent ITC behavior is consistent with the trends in the OS-induced changes in the temperature dependent HDX properties of SLO, in which the difference in protein flexibility in the presence of OS were more pronounced at 10 °C.[23] The large background heats from later injections at 30 °C prevented accurate thermodynamic analysis (Figure 3.3D). Under these buffer conditions, the ITC data support that OS binding to SLO is dominated by enthalpic contribution(s).

Table 3.1 *Thermodynamics of OS binding to SLO by ITC*[a]

Condition	K_d (μM)	*n*	ΔH (kJ/mol)	TΔS (kJ/mol)
Pyrophosphate, pH 9	1.0 ± 0.1	0.46 ± 0.1	-30 ± 5	7.9 ± 2
Pyrophosphate, pH 9 (10 °C)	0.73 ± 0.2	0.48 ± 0.1	-41.7 ± 2	9.5 ± 3
Pyrophosphate, pH 9 + 0.15 M NaCl	0.78 ± 0.4	0.87 ± 0.06	-15.6 ± 2	18 ± 2
Phosphate, pH 7.5	9 ± 5	0.42 ± 0.1	-7.3 ± 1	15 ± 3

[a]*See Methods for details. Unless otherwise stated, the temperature was maintained at 20 °C. The data are averages from 3-5 experiments and reported as mean ± S.D. Buffers at pH 9 were prepared with 50 mM pyrophosphate ($\Delta_r H°$ = 1.4 kJ/mol) while buffers at pH 7.5 were prepared with 50 mM phosphate ($\Delta_r H°$ = 3.6 kJ/mol).*[40] *All buffers are supplemented with 0.3% DMSO.*

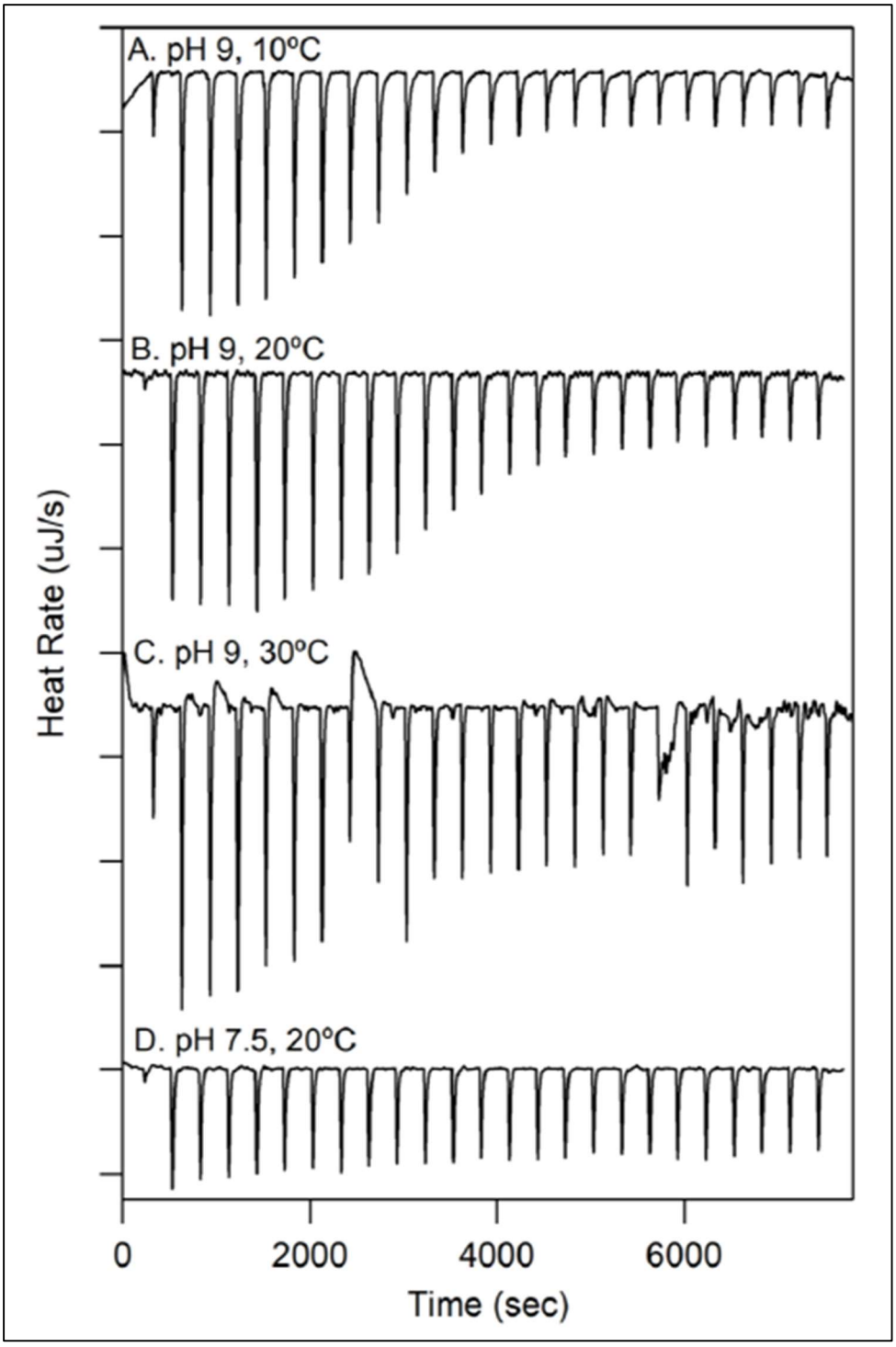

Figure 3.3 *Representative ITC thermograms of OS (250 μM) titrated into SLO (60 μM). The buffer conditions were (A-C) 50 mM pyrophosphate, pH 9 and (D) 50 mM phosphate, pH 7.5; each buffer was supplemented with 0.3% DMSO to help with OS solubility. (B) was reproduced from Figure 3.2. The y-axis tick marks represent 0.4 μJ/s.*

Borate buffers are typically used to characterize the kinetics of SLO at pH 9; however, pyrophosphate buffer was chosen herein for ITC experiments due to its low molar enthalpy for ionization ($\Delta_rH°$ = 1.4 kJ/mol) compared to borate ($\Delta_rH°$ = 14 kJ/mol).[40] To reveal the effect of buffer on the thermodynamic properties of OS binding to SLO, ITC experiments were also performed using two additional buffers, borate and CHES, which have comparable pKa values (9.2–9.5) and differing ionization enthalpies relative to pyrophosphate (Table 3.2). The resulting ITC data collected using identical buffer concentration, pH, temperature, and ionic strength (Figure 3.4) revealed similar K_d (0.8–1.2 μM) and *n* (0.4–0.6) values. Thus, the binding affinity and mole ratio of OS binding to SLO are independent of buffer used. A notable difference among these buffers was the observed increase in ΔH_{ITC} that tracked the magnitude of the buffer ionization enthalpies (Table 3.2 and Figure 3.4). Because of the near zero $\Delta_rH°$ value for pyrophosphate, we focused our ITC study using this buffer system at pH 9. Compared to steady-state kinetic parameters collected in borate the first-order rate constants in pyrophosphate are slightly elevated; however, the trends are comparable (Table 3.3). Note that the KIEs used to describe the OS allosteric effects in SLO (*eg*. Figure 3.1C) were found to be nearly identical for pyrophosphate and borate buffers (Table 3.5), supporting that pyrophosphate does not influence the OS-induced allosteric effects in SLO and validating the utility of pyrophosphate buffer in the ITC experiments.

Table 3.2 *Buffer properties and ITC enthalpies for OS titration into SLO.*

Buffer	Log K[a]	$\Delta_rH°$ (kJ/mol)[a]	ΔH (kJ/mol)[b]
Pyrophosphate	9.46	1.4	-30 ± 5
Borate	9.24	13.8	-49 ± 2
CHES	9.39	39.6	-65 ± 6

[a]Values are reported in reference.[40] [b]ITC-derived enthalpies were extracted from the fits to ITC data (Figure 3.4). The data are averages of 3-4 experiments and reported as the mean ± S.D.

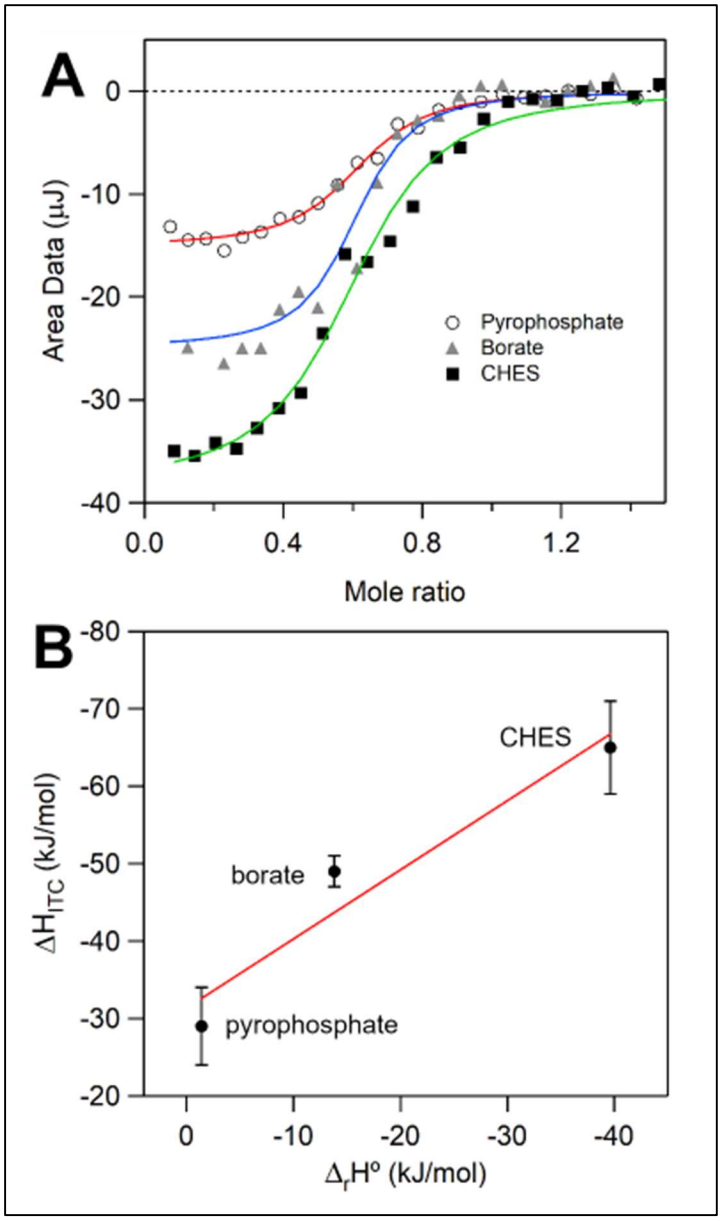

Figure 3.4 *Representative ITC data of OS (250 µM) titrated into SLO (60 µM) in pyrophosphate (open circles), borate (gray triangles), and CHES (black squares) buffers (A). All solution conditions were 50 mM buffer concentrations (no supplemented salt), pH 9.0, and 20 °C. All buffers are supplemented with 0.3% DMSO. (B) Proton displacement plot for OS binding to SLO using the three buffers in (A). $\Delta_r H°$ values are literature reported values.*[40] *The error bars represent S.D. of the mean from the fits in (A) from at least three independent experiments. The slope (0.89) of the linear regression represents the number of protons displaced from SLO upon binding OS (R2 = 0.93). This analysis has been previously described in detail for assessing metal-protein interactions by ITC.*[41]

To probe the electrostatic contributions on OS binding to SLO, 0.15 M NaCl was supplemented in the ITC experiment. In the presence of this added salt, the resulting ITC-derived K_d value of OS binding to SLO was within error to that in the absence of salt (Table 3.1). However, both the enthalpy (-30 ± 5 to -16 ± 2 kJ/mol) and entropy (8 ± 2 to 18 ± 2 kJ/mol) became increasingly positive with elevated salt concentration (Table 3.1), revealing a more significant entropic contribution to OS binding. Thus, these ITC experiments support that the increased ionic strength influences the binding of OS to SLO through the conformational entropy (i.e. dynamics) of the protein and/or by solvent effects.[42,43] This influence of salt on the structural dynamics of SLO is corroborated by kinetics isotope effects (Table 3.3).

KIEs Reveal Influence of SLO Chemistry from OS and Supplemented NaCl

Steady-state kinetics were conducted on SLO at 10 °C, at which the allosteric effects on the KIEs are more pronounced. First-order rate constants, k_{cat}, of SLO in the absence of OS was 225 ± 12 s^{-1}, comparable to 220-230 s^{-1} reported previously.[23,44] In the presence of saturating OS concentration (15 μM), k_{cat} is reduced by *ca.* 35%. Conversely, there is little effect on the second-order rate constant in the presence of OS at 10 °C (Table 3.3). Steady-state kinetics of SLO were also carried out in the presence of 0.15 M NaCl (Table 3.3). The resulting first- and second-order rate constants were comparable to the same buffer with no salt supplemented (Table 3.3). Addition of saturating OS (15 μM) to the reaction with elevated ionic strength buffer led to a modest reduction in k_{cat} and a modestly enhanced k_{cat}/K_M. Under these conditions, the supplementation of salt had no significant effects on the SLO reactivity. As an important control, steady-state kinetics were also collected for SLO in 50 mM borate pH 9 in which a 1 μM SLO stock solution was pre-incubated with 15 μM OS and at a designated time (0-2 h), the relative maximal rate was measured with 100 μM LA concentration (Table 3.4). The enzyme maintained high activity (≥ 82%) in the

presence of saturating OS up to 2 h. These data demonstrate that the enzyme remains stable and active in the prolonged presence of saturating OS.

Table 3.3 *Kinetics of SLO in the presence and absence of saturating OS at 10 °C.*[a]

SLO	k_{cat} (s^{-1})			k_{cat}/K_M ($\mu M^{-1}s^{-1}$)		
	-OS	+OS[b]	OS:apo[c]	-OS	+OS[b]	OS:apo[c]
Borate, pH 9	225 ± 12 (220-230)[d]	146 ± 9 N.R.[e]	0.65 ± 0.05	4.8 ± 0.8	5.7 ± 1.3	1.2 ± 0.3
Borate, pH 9 + 0.15 M NaCl	228 ± 15	202 ± 18	0.88 ± 0.09	5.8 ± 0.9	9.2 ± 2.1	1.6 ± 0.4
Pyrophosphate, pH 9	330 ± 45	321 ± 15	0.97 ± 0.14	4.4 ± 1.1	12 ± 3	2.7 ± 0.9

[a]*Values were corrected for Fe content.* [b]*In the presence of 15 μM OS.* [c]*Rate constant ratio for the presence of OS relative to the reaction without OS (i.e. 'apo').* [d]*From references.*[39,44] [e]*Not reported at 10 °C. The previous KIE study of SLO with OS was conducted using a competitive HPLC method that did not enable direct detection of OS effects on k_{cat} at 5-10 °C. Note that a reduction in k_{cat} was reported upon addition of OS using steady-state kinetics at 25 °C,*[15] *yielding a similar trend to our results, though the magnitude was slightly different at the elevated temperature.*

Table 3.4 *Relative maximal rate constant of SLO reaction with LA at 10 °C and in presence of OS.*

Incubation time (h)	Relative rate (%)[a]
0	100
0.5	95 ± 5
1	91 ± 7
1.5	92 ±12
2	82 ± 8

[a]*Relative rate at 100 μM LA concentration. The initial time point (0 h) was collected with the enzyme stock prepared in 50 mM borate pH 9 (no OS) and added to reaction buffer containing 15 μM OS in the cuvette immediately prior to data collection. The values represent mean ± S.D. from triplicate measurements.*

The kinetics were extended to study the impact of OS and elevated salt on the KIEs. In low ionic strength buffer, the first- and second-order KIEs for the SLO reaction with protium linoleic acid followed the comparable trends in the presence and absence of OS, as previously reported[15] (*cf.* Table 3.5 and Figure 3.1C). Most notable is the substantial increase in the second-order isotope

effect, $^{D}k_{cat}/K_M$, that, in our hands using steady-state non-competitive assays, is seen to increase from about 5 to 78 upon addition of saturating OS. Note that the previous second-order KIEs were determined using a competitive HPLC assay[45] that could account for differences in the *absolute* values of the $^{D}k_{cat}/K_M$, though the trends are the same as the results presented in Table 3.5. The addition of salt had a significant effect on the observed kinetic isotope effect for the second-order rate constant, $^{D}k_{cat}/K_M$. From Table 3.5, the $^{D}k_{cat}/K_M$ value in the presence of OS and salt was found to be only 21, compared to 78 in absence of salt.

Table 3.5 *KIEs for the reaction of SLO with LA in the absence and presence of OS at 10 °C.*

SLO	$^{D}k_{cat}$[a]	$^{D}k_{cat}/K_M$[a]	
Buffer	-OS	-OS	+15 μM OS
Borate, pH 9	77 ± 9 (80)[b]	5.1 ± 1.5 (15)[c]	78 ± 12 (70)[c]
Borate, pH 9 + 0.15 M NaCl	89 ± 10	4.7 ± 1.2	21 ± 8
Pyrophosphate, pH 9	93 ± 18	6.2 ± 2.1	88 ± 23

[a]Kinetic isotope effects, $^{D}k_{cat} = k_{cat}(H)/k_{cat}(D)$ and $^{D}k_{cat}/K_M = (k_{cat}/K_M)^{H}/(k_{cat}/K_M)^{D}$. [b]From references.[39,44] *[c]From reference.*[15] *The kinetics for the protio substrate are presented in Table 3.3.*

These KIE results have functional relevance to the SLO reaction coordinate. At reduced temperatures and in the absence of effector, the $^{D}k_{cat}/K_M$ value (~5) is much lower than the $^{D}k_{cat}$ of 80 (Table 3.5). Because $^{D}k_{cat}/K_M << {}^{D}k_{cat}$, substrate binding emerges as the rate limiting step of SLO catalysis at 10 °C. Upon addition of allosteric effector, OS, in low ionic strength buffer, the $^{D}k_{cat}/K_M$ approximates $^{D}k_{cat}$, which indicates a decrease in the commitment factor for catalysis (i.e. lowers the energetic barrier for substrate binding) and thereby indicates a change in the rate-limiting step from substrate binding to C-H cleavage. As shown in Table 3.5, the supplementation of 0.15 M NaCl led to only a slight increase in $^{D}k_{cat}/K_M$ in the presence of OS, from 5 to 20, such that $^{D}k_{cat}/K_M$ remains considerably smaller than $^{D}k_{cat}$ (*ca.* 80) In the presence of elevated NaCl, the

energetic barrier for substrate binding is lowered, but still large enough that it contributes significantly to the commitment factor for catalysis. Thus, these kinetic data suggest that the allosteric effects on the control of the rate-limiting steps of SLO catalysis are influenced by elevated salt concentrations.

DLS Measurements Indicate no Effector-Induced Oligomerization Change in SLO

The ITC thermograms for OS titration into SLO were fit with $n = 0.5 \pm 0.1$ (Table 3.1). This binding stoichiometry value could originate from a few factors, including OS-induced dimerization. In this study, dynamic light scattering (DLS) was employed to examine the possibility of SLO dimerization in the presence of effector OS. In the absence of OS, the hydrodynamic radius, R_h, of SLO collected from DLS was determined to be 3.89 nm (Figure 3.5 and 3.6). This size is comparable to that determined previously by small-angle X-ray scattering (SAXS).[46] The conversion for the DSC R_h value to SAXS radius of gyration, R_g, is a factor of 0.774 (i.e. $R_g = 0.774 \times R_h$).[47] The reported R_g from SAXS experiments was 3.00 ± 0.05 nm,[46] which translates to a predicted R_h value of 3.88 ± 0.06 nm, consistent with our current DLS results (Figure 3.5). These data support that SLO exists as a monomer in solution and are validated by SEC experiments (Figure 3.7). DLS experiments of SLO were then carried out in the presence of OS and/or elevated NaCl concentration. Only a 3.89-nm peak was observed under all conditions, suggesting no OS-induced change in oligomerization (Figure 3.6). These DLS data are further supported by SEC conducted using 50 mM borate (pH 9), 50 mM borate (pH 9) with 0.15 M NaCl, 50 mM pyrophosphate (pH 9), or 50 mM HEPES (pH 7.5) with 0.15 M NaCl. These SEC data show no shift in elution volume when the column was pre-equilibrated with OS (Figure 3.8). While there is evidence for dimerization in mammalian LOXs,[48–50] the biophysical data presented in this study rule out the possibility of oligomerization as the origin of the allosteric effects in SLO.

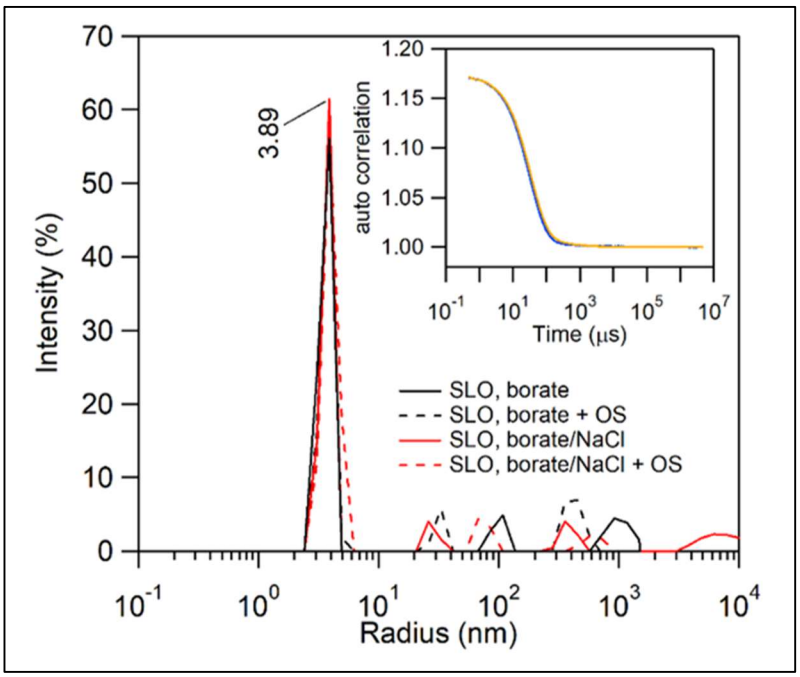

Figure 3.5 *Representative DLS intensity particle size distribution plots of SLO. The principle hydrodynamic radius, R_h, of 3.89 nm is labeled. The concentration of SLO was 5 mg/mL, with the intensity particle size distribution plots as a function of SLO concentration (5, 2.5, and 1.25 mg/mL) presented in Figure 3.7. Representative regularization fits of SLO in the absence (blue) and presence (gold) of OS are shown in the inset for reference.*

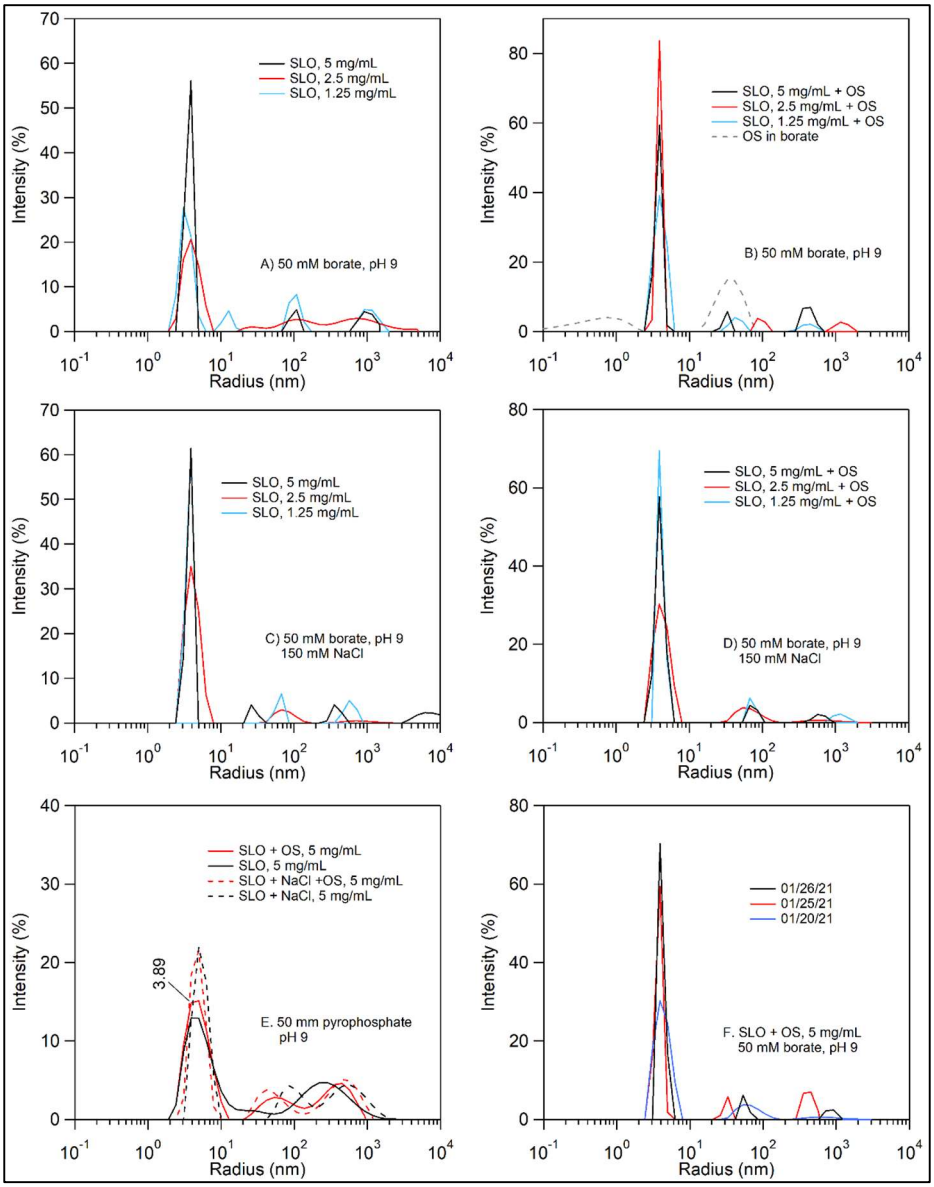

Figure 3.6 *SLO concentration and buffer dependence on the hydrodynamic radii (R_h) measured with DLS. (A) and (B) show SLO in 50 mM borate, pH 9 while (C) and (D) show SLO in 50 mM borate, pH 9 supplemented with 0.15 M NaCl. DLS data in (B) and (D) were collected in the presence of equal molar OS. (E) represents the particle size distribution plot of SLO prepared in 50 mM pyrophosphate, pH 9. (F) shows the reproducibility of the SLO particle size distribution collected in triplicate over three different days. The sample volume was 100 µL for each experiment.*

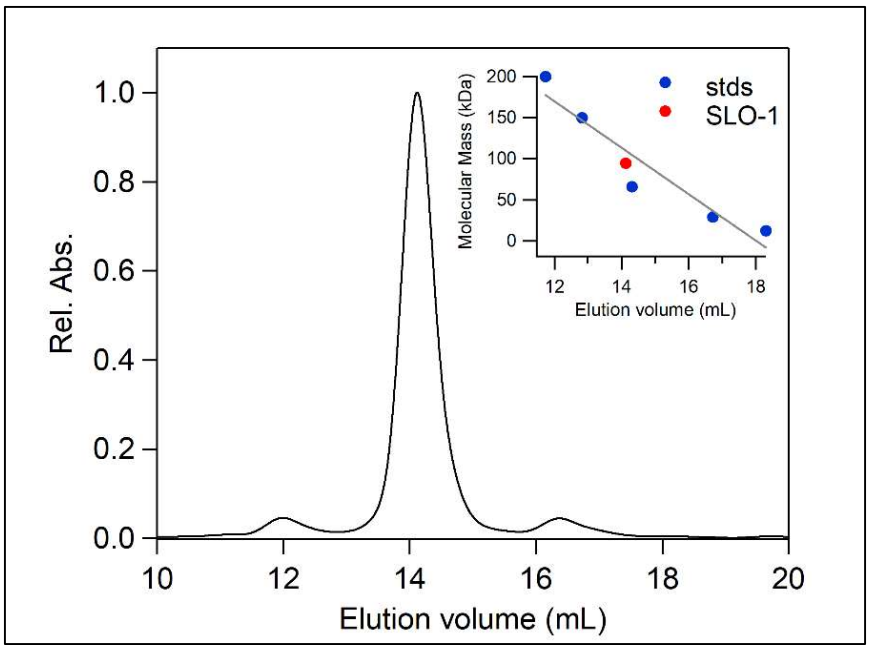

Figure 3.7 *Analytical size exclusion chromatogram of purified SLO, monitoring tryptophan absorbance at 280 nm. The peak elution volume of SLO occurs at 14.12 mL, which is consistent with a monomeric form of SLO based on the standard curve (inset) of molecular weight standards (blue dots). The buffer conditions were 50 mM HEPES, 150 mM NaCl, pH 7.4.*

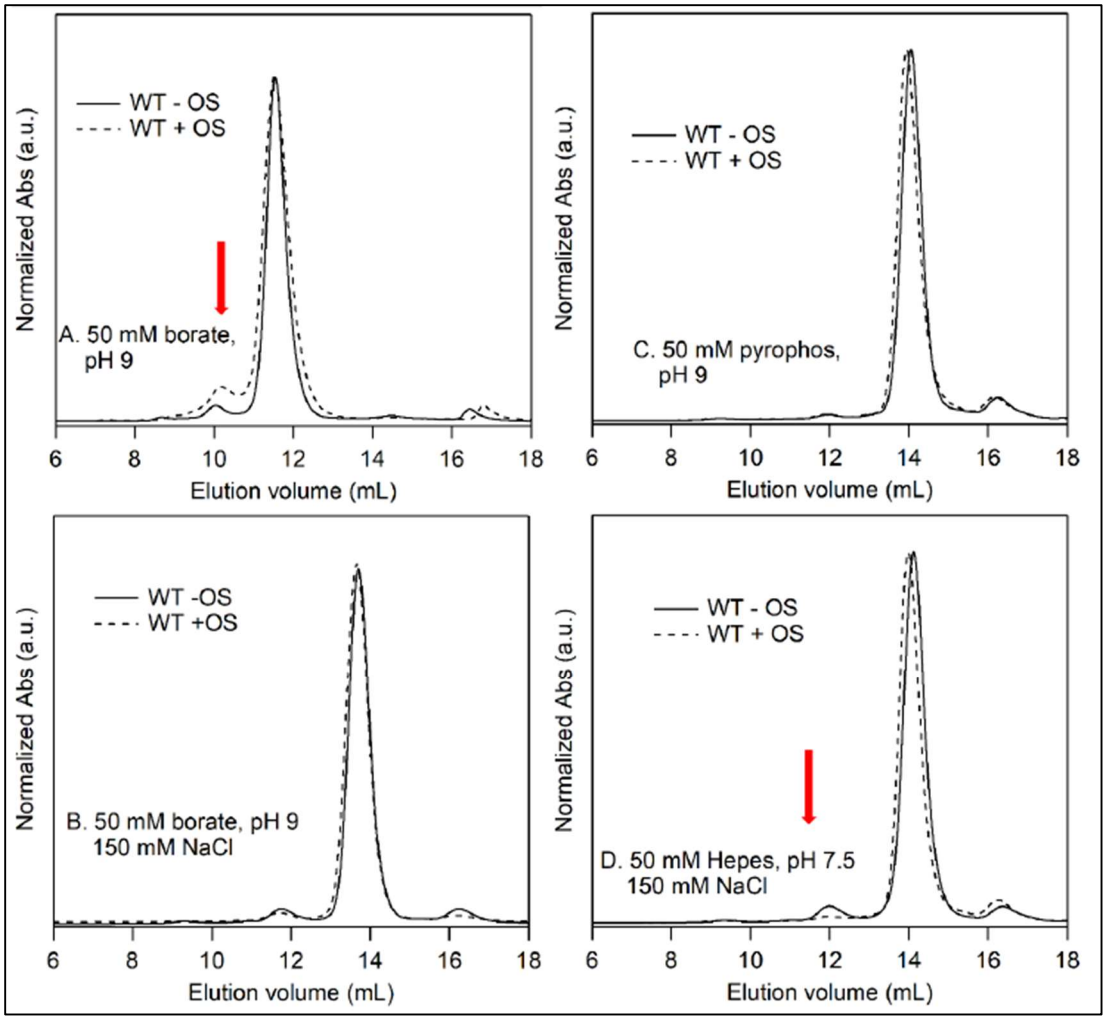

Figure 3.8 *SEC-FPLC of WT SLO various buffers. The dashed lines represent SLO experiments in which the column was equilibrated and run in the presence of 15 μM OS. Note that blue dextran, an SEC-FPLC marker used to estimate the column void volume elutes at 8 mL. Because there are no contributions in this elution range in (A-D), these SEC-FPLC data support that SLO does not aggregate in the presence or absence of OS and/or 0.15 M NaCl. Note that the elution volume is early for the SLO sample in 50 mM borate pH 9 (ca. 11.5 min). The borate buffer also changes the elution volume to shorter time for the gel standards. For reference, a red arrow in panels A and D represents the migration of β-amylase (200 kDa) that serves as the expected migration of an SLO dimer. This elution behavior is not expected to arise from a change in oligomerization as the DLS data provide support for SLO as a monomer in 50 mM borate, pH 9 (Figure 3.6A). Importantly, the addition of OS in 50 mM borate buffer (A) does not change the oligomerization of SLO.*

The data emerging from the DLS and SEC experiments raise the question into the origins of the observed less-than-unity ITC stoichiometry (i.e. $n \sim 0.5$) for OS binding to SLO in the low ionic strength buffer (Table 3.1). Previous ITC studies of fatty acid binding to fatty acid-binding

proteins (FABPs), especially in the case of heart FABP or β-lactoglobin, have also reported similar range of non-unity stoichiometry values (n = 0.3-0.9).[51–54] While these non-unity stoichiometries can be explained by either one ligand binding to two proteins, as in the case of dimerization, or *ca.* 50% occupancy of the monomer, no evidence was found for dimerization for either the heart FABP or β-lactoglobin systems. Furthermore, X-ray crystallographic studies of lactoglobulin have shown partial occupancy of fatty acids in the protein structure, verifying the ITC analyses.[54] Consistent with this, our DLS (Figure 3.5) and SEC (Figure 3.7) data also support a monomeric form of SLO with no evidence of protein aggregation or degradation. An alternative suggestion is that the less-than-unity ITC stoichiometries, especially for binding of long-chain fatty acids (e.g. C18), arise from their poor water solubility influencing the effective ligand concentrations and/or protein occupancy.[54]

OS Imparts no Large Structural Change in SLO

DSC experiments were conducted to provide thermodynamic information for the impact of effector, OS, on the structure and folding stability of SLO. DSC has been used previously to characterize ligand binding parameters to proteins.[55–57] Changes in the melting temperature, T_m, by 2–5 °C are often reported for 1:1 ligand:protein concentration ratios and accompanied by increases in the enthalpy of unfolding. In these cases, ligand binding is almost always associated with well-documented conformational change(s). The baseline corrected DSC thermograms of SLO presented a single asymmetric melting peak that could be modeled with two Gaussians with T_ms of 62 and 65 °C (Figure 3.9). Contrary to the examples presented above, DSC data of SLO collected in the presence of equal molar OS showed no significant gain in folding stability compared to the apo protein (Figure 3.9 and Table 3.6). Additionally, further addition of OS (2:1 OS:SLO) did not result in further shifted T_m. Consistent with the SEC and DLS results, the

thermodynamic parameters of SLO from DSC support the conclusion that SLO is a monomer and that there are no large protein structural transitions such as oligomerization, aggregation or large-scale conformational changes, occurring in the presence of OS.

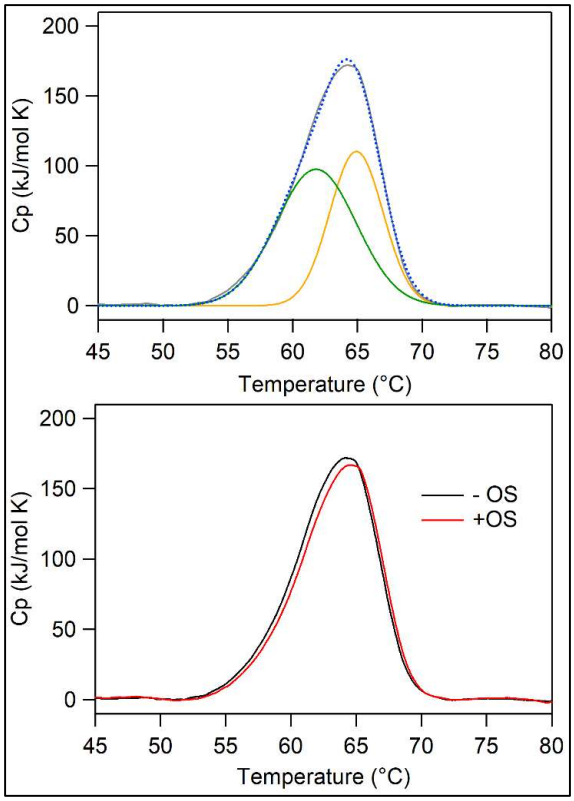

Figure 3.9 *Representative DSC thermograms for SLO. Top panel: SLO was prepared at 20 μM concentrations in 50 mM borate pH 9 buffer. The solid gray line represents the raw melting data, the dashed blue line represents the model sum obtained by fitting that raw data using two Gaussian models; the two Gaussians are represented by green and orange lines. Bottom panel: DSC overlays for SLO DSC thermograms collected in the absence (black; repeated from top panel) and presence (red) equal molar OS. The scans were collected from 30-90°C under 3 atm pressure, with scan rates of 1°C/min.*

Table 3.6 *DSC thermodynamics of SLO unfolding in the presence and absence of OS.*[a]

	OS	T_m (°C)	ΔH_m (kJ/mol)
Borate, pH 9	-	64.19 + 0.04	1300 + 38
	+	64.44 + 0.02	1293 + 13
Borate, pH 9 + 0.15 M NaCl	-	61.72 + 0.03	1276 + 10
	+	61.95 + 0.02	1271 + 14

[a]*When present, OS was added at equal molar concentrations to SLO.*

DSC experiments were also conducted in the presence of OS and/or elevated NaCl concentration. From these traces, the melting temperatures for WT were found to be responsive to the ionic strength, in which the samples collected in elevated salt concentration produced a lower melting temperature with a modest impact on the enthalpy of unfolding, ΔH_m (Table 3.6), indicating the addition of NaCl destabilized the structure of SLO.

HDX Analysis of SLO at Elevated Ionic Strength

To probe the effects of salt on the structure and dynamics of SLO, we conducted HDX-MS experiments with 0.15 M NaCl in the exchange buffer. HDX-MS has been previously characterized for SLO in low ionic strength buffers (Figure 3.10A).[39] There are examples in the literature that highlight the sensitivity of HDX-MS to investigate salt effects on protein structure and dynamics.[58,59] HDX-MS experiments on SLO resolved OS-induced enhanced flexibility of helix α2 (Figure 3.10A, box),[39] stemming from the PLAT:catalytic domain interface through helix α2, which has been proposed to regulate substrate binding.[6] While the previous work included temperature-dependent HDX-MS analysis at 5 temperatures, the altered exchange behavior from OS interactions with SLO was most notable at 10 °C.

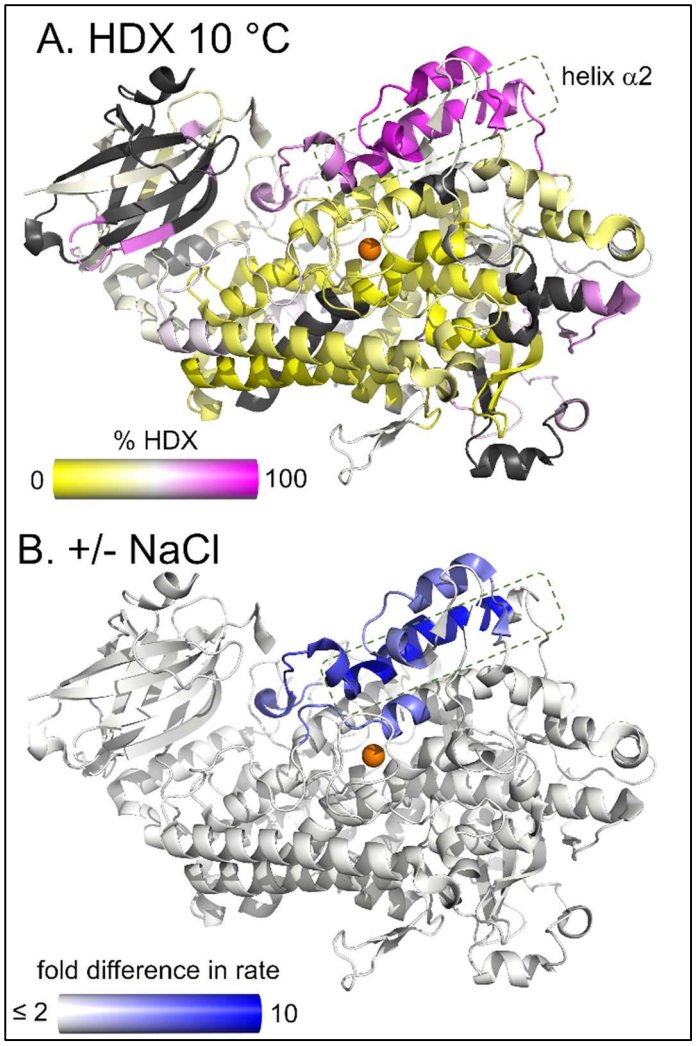

Figure 3.10 *HDX-MS properties of WT SLO and differences induced by NaCl and allosteric effector OS. In (A), the extent of exchange at 10 °C and 2 h for WT SLO in low ionic strength deuterated buffer (10 mM HEPES, pD 7.4). The color coding is defined by the spectrum bar; black represents uncovered regions of the protein. (B) shows the fractional differences in rate constant when the D_2O buffer is supplemented with 0.15 M NaCl; the elevation in exchange rate from salt is colored according to the spectrum bar. The apparent exchange rates for affected peptides are listed in Table 3.7. Helix α2 is designated by a dashed box in A-B.*

Herein, HDX-MS analysis was performed on SLO at 10 °C using a D_2O buffer supplemented with 0.15 M NaCl. With a few exceptions, many of the 44 previously characterized, non-overlapping peptides characterized in low ionic strength D_2O buffer exhibited nearly identical HDX-MS behavior with supplemented NaCl reported herein (See Appendix A). The overall HDX behavior at 10 °C in the absence of OS and salt is plotted onto the X-ray structural model in Figure

3.10A. The color coding is determined by the extent of H/D exchange at 2 hours and 10 °C and defined by the color bar. Peptides that exhibited differences in weighted average rate of exchange in the presence of 0.15 M NaCl are highlighted in varying shades of blue in Figure 3.10B. Among these peptides, helix α2 (dotted outline) is impacted by the greatest extent (Figure 3.11). Helix α2 lines the substrate entrance portal and is expected to regulate substrate access to the binding pocket for catalysis.[60] The addition of 0.15 M NaCl is seen to enhance the rate of exchange of these peptides at 10 °C (Figure 3.11 and Table 3.7). This increase in exchange rate is consistent with a destabilizing behavior introduced in the presence of elevated salt concentration.

Table 3.7 *Weighted average rate constants (min^{-1}) of exchange from HDX-MS fits*[a]

	0 M NaCl		0.15 M NaCl	
Peptide	-OS	+OS	-OS	+ OS
239-256	0.27 ± 0.09	2.1 ± 0.9	1.8 ± 1.0	2.2 ± 1.9
257-273	0.11 ± 0.07	2.8+ 0.9	1.14 ± 0.7	≥ 3[b]
297-305	0.10 ± 0.02	1.0 ± 0.2	0.45 + 0.17	1.4 ± 0.2
306-316	0.14 ± 0.04	0.9 ± 0.1	0.56 ± 0.2	1.4 ± 0.2
751-761	0.06 ± 0.02	1.1 ± 0.4	0.3 ± 0.2	2.1 ± 0.9

[a]*Apparent weighted average rate constants (± represents S.D.) were determined from one- or two-exponential fits to the data. Representative traces are displayed in Figure 3.11.* [b]*Exchange was too rapid to quantitate accurately within the dynamic range of the experiment.*

With the addition of OS to the elevated ionic strength buffer used for the exchange, only five select non-overlapping peptides exhibited altered HDX behavior in the form of increased weighted average rates of exchange (Figure 3.11 and Table 3.7). The OS-induced effects on SLO exchange using D_2O buffer supplemented with 0.15 M NaCl are similar to the OS differences in HDX with low ionic strength buffer. One notable exception is that the supplementation of salt

suppresses the previously characterized OS-induced conformational change at the N-terminal peptide (1-20) of the PLAT domain.

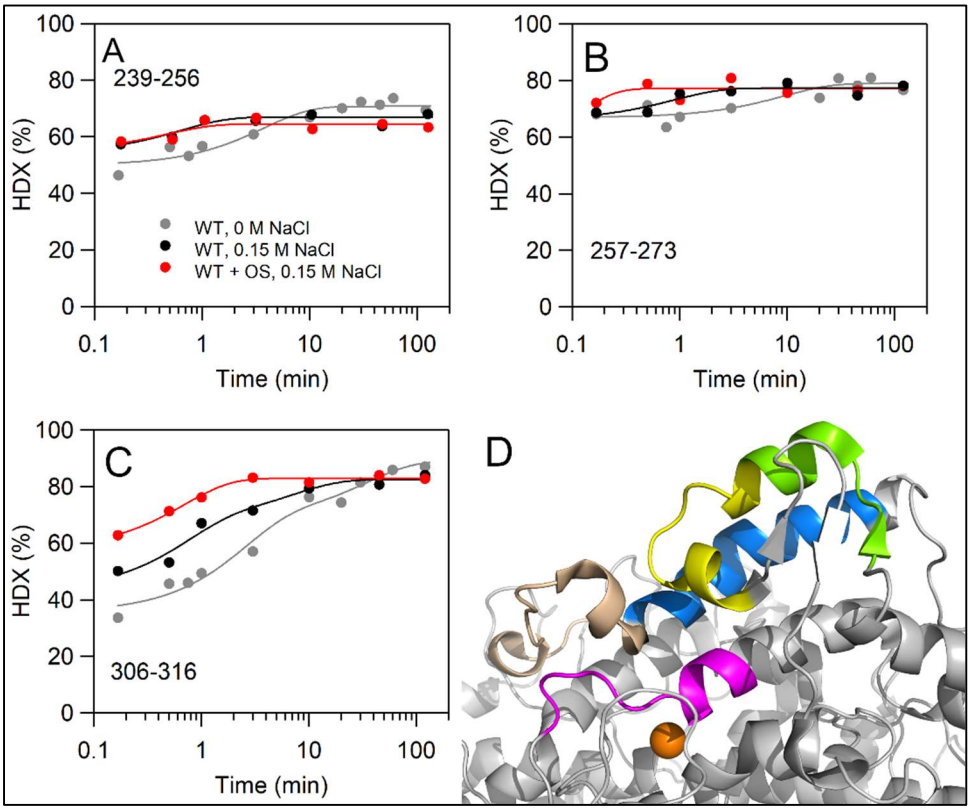

Figure 3.11 *Representative HDX-MS traces of SLO (A-C) that show differences in exchange rates between the absence (gray traces) and presence (black, red traces) of 0.15 M NaCl. Red traces represent SLO samples prepared with 15 μM OS in the D_2O buffer. (D) displays color coding of peptides whose rates are discussed in Table 3.7; the color coding represents: wheat, 239-256; marine, 257-273; chartreuse, 297-305; yellow, 306-316; and magenta, 751-761.*

From the comparative rates of exchange (Table 3.7), the most affected peptide is 257-273 (Figure 3.11D, marine), which comprises the majority of helix α2. This result is significant as the entrance portal for substrate is gated by helix α2.[60] In the middle of helix α2 of SLO lies a π-helix, residues 261-267 adjacent to the substrate portal.[61] π-helices are structural features comprised of an additional amino acid residue inserted into a canonical α-helix. As such, these features introduce a bend in the helical segment that causes local distortions and destabilizes α-helices. This property encodes enhanced functionality into the protein structure, including metal ion coordination,

regional protein flexibility, and enzyme-substrate binding interactions.[62] Consistent with our HDX-MS results, previous pulsed EPR experiments detected nanosecond dynamics for residues 260 and 264 are sensitive to substrate binding.[61]

Further, these HDX data, presented herein, show that the same regional peptide dynamics that might control the rate-determining step and substrate selectivity of SLO catalysis from OS effector binding are also influenced in the presence of elevated salt concentrations. These data provide an important structural basis and validation of the impact of NaCl on protein structure and dynamics, linked to catalysis.

Conclusion

In summary, we have provided direct experimental evidence, using ITC, for the binding of allosteric effector OS to SLO, a model plant 15-lipoxygenase. In addition, DLS and SEC, presented herein, reveal that SLO exists exclusively as a monomer, even in the presence of OS. These biophysical data rule out oligomerization as the mechanism for allosteric modulation of SLO catalysis. This finding for the model plant 15-LOX contrasts the studies of mammalian 12/15-LOXs that have implicated dimerization for allosteric regulation.[24,63] Further, thermodynamic analysis of SLO from DSC experiments also exclude the possibility of a large conformational transition to SLO upon OS binding. Taken together with the previous HDX results, the regulation of SLO by fatty acid effectors is facilitated by a dynamically driven process.

Supplementation of 0.15 M NaCl into the ITC experiment resulted in a change in the thermodynamics of effector binding, implicating a change in the SLO structure and/or electrostatic interaction with OS. HDX-MS results support that elevated NaCl concentration induces enhanced, regional peptide fluctuations in SLO, most significantly at helix α2 that lines the substrate entrance portal. This salt effect raises the question about its potential biological relevance. However, note

that all experiments were performed at pH 9, rather than physiological pH, because above pH 8 the kinetic parameters are pH independent. At near-physiological pH, the second-order rate constants become sensitive to pH, and the first- and second-order KIEs converge,[21] masking the allosteric effects from OS binding. Structural and kinetic studies at pH 9 provide a window into the mechanism of LOX allostery. Thus, we propose that the use of varying NaCl concentrations might serve as a perturbant to reveal insight into the LOX structure and function, complementary to the applications of site-directed mutagenesis, temperature and pressure.[24,39,64,65] The observation that elevated ionic strength buffers affect the regional protein flexibility of helix α2 and correlated with altered OS-induced $^{D}k_{cat}/K_M$ values and substrate selectivity further underscores the importance of the flexibility of this helix in governing the allosteric effects on SLO reactivity.

References

(1) Brash, A. R. Lipoxygenases: Occurrence, Functions, Catalysis, and Acquisition of Substrate. *J. Biol. Chem.* **1999**, *274* (34), 23679–23682.

(2) Prigge, S. T.; Boyington, J. C.; Gaffney, B. J.; Amzel, L. M. Structure Conservation in Lipoxygenases: Structural Analysis of Soybean Lipoxygenase-1 and Modeling of Human Lipoxygenases. *Proteins Struct. Funct. Genet.* **1996**, *24* (3), 275–291.

(3) Newcomer, M. E.; Brash, A. R. The Structural Basis for Specificity in Lipoxygenase Catalysis. *Protein Sci.* **2015**, *24* (3), 298–309.

(4) Hammarberg, T.; Provost, P.; Persson, B.; Rådmark, O. The N-Terminal Domain of 5-Lipoxygenase Binds Calcium and Mediates Calcium Stimulation of Enzyme Activity. *J. Biol. Chem.* **2000**, *275* (49), 38787–38793.

(5) Eek, P.; Järving, R.; Järving, I.; Gilbert, N. C.; Newcomer, M. E.; Samel, N. Structure of a Calcium-Dependent 11R-Lipoxygenase Suggests a Mechanism for Ca2+ Regulation. *J. Biol. Chem.* **2012**, *287* (26), 22377–22386.

(6) Offenbacher, A. R.; Holman, T. R. Fatty Acid Allosteric Regulation of C-H Activation in Plant and Animal Lipoxygenases. *Molecules* **2020**, *25* (15), 3374.

(7) Wecksler, A. T.; Kenyon, V.; Garcia, N. K.; Deschamps, J. D.; Van Der Donk, W. A.; Holman, T. R. Kinetic and Structural Investigations of the Allosteric Site in Human Epithelial 15-Lipoxygenase-2. *Biochemistry* **2009**, *48* (36), 8721–8730.

(8) Wuest, S. J. A.; Crucet, M.; Gemperle, C.; Loretz, C.; Hersberger, M. Expression and Regulation of 12/15-Lipoxygenases in Human Primary Macrophages. *Atherosclerosis* **2012**, *225* (1), 121–127.

(9) Kotla, S.; Singh, N. K.; Heckle, M. R.; Tigyi, G. J.; Rao, G. N. The Transcription Factor

CREB Enhances Interleukin-17A Production and Inflammation in a Mouse Model of Atherosclerosis. *Sci. Signal.* **2013**, *6* (293), 1–14.

(10) Serhan, C. N.; Petasis, N. A. Resolvins and Protectins in Inflammation Resolution. *Chem. Rev.* **2011**, *111* (10), 5922–5943.

(11) Perry, S. C.; Kalyanaraman, C.; Tourdot, B. E.; Conrad, W. S.; Akinkugbe, O.; Freedman, J. C.; Holinstat, M.; Jacobson, M. P.; Holman, T. R. 15-Lipoxygenase-1 Biosynthesis of 7S,14S-DiHDHA Implicates 15-Lipoxygenase-2 in Biosynthesis of Resolvin D5. *J. Lipid Res.* **2020**, *61* (7), 1087–1103.

(12) Freedman, C.; Tran, A.; Tourdot, B. E.; Kalyanaraman, C.; Perry, S.; Holinstat, M.; Jacobson, M. P.; Holman, T. R. Biosynthesis of the Maresin Intermediate, 13S,14S-Epoxy-DHA, by Human 15-Lipoxygenase and 12-Lipoxygenase and Its Regulation through Negative Allosteric Modulators. *Biochemistry* **2020**, *59* (19), 1832–1844.

(13) Jin, J.; Boeglin, W. E.; Brash, A. R. Analysis of 12/15-Lipoxygenase Metabolism of EPA and DHA with Special Attention to Authentication of Docosatrienes. *J. Lipid Res.* **2021**, *62*, 100088–100089.

(14) Tsai, W. C.; Kalyanaraman, C.; Yamaguchi, A.; Holinstat, M.; Jacobson, M. P.; Holman, T. R. In Vitro Biosynthetic Pathway Investigations of Neuroprotectin D1 (NPD1) and Protectin DX (PDX) by Human 12-Lipoxygenase, 15-Lipoxygenase-1, and 15-Lipoxygenase-2. *Biochemistry* **2021**, *60* (22), 1741–1754.

(15) Mogul, R.; Johansen, E.; Holman, T. R. Oleyl Sulfate Reveals Allosteric Inhibition of Soybean Lipoxygenase-1 and Human 15-Lipoxygenase. *Biochemistry* **2000**, *39* (16), 4801–4807.

(16) Wecksler, A. T.; Garcia, N. K.; Holman, T. R. Substrate Specificity Effects of Lipoxygenase

Products and Inhibitors on Soybean Lipoxygenase-1. *Bioorg. Med. Chem.* **2009**, *17* (18), 6534–6539.

(17) Klinman, J. P.; Offenbacher, A. R.; Hu, S. Origins of Enzyme Catalysis: Experimental Findings for C-H Activation, New Models, and Their Relevance to Prevailing Theoretical Constructs. *J. Am. Chem. Soc.* **2017**, *139* (51).

(18) Ruddat, V. C.; Whitman, S.; Holman, T. R.; Bernasconi, C. F. Stopped-Flow Kinetic Investigations of the Activation of Soybean Lipoxygenase-1 and the Influence of Inhibitors on the Allosteric Site. *Biochemistry* **2003**, *42* (14), 4172–4178.

(19) Glickman, M. H.; Wiseman, J. S.; Klinman, J. P. Extremely Large Isotope Effects in the Soybean Lipoxygenase-Linoleic Acid Reaction. *J. Am. Chem. Soc.* **1994**, *116*, 793–794.

(20) Klinman, J. P. An Integrated Model for Enzyme Catalysis Emerges from Studies of Hydrogen Tunneling. *Chem. Phys. Lett.* **2009**, *471* (4–6), 179–193.

(21) Glickman, M. H.; Klinman, J. P. *Nature of Rate-Limiting Steps in the Soybean Lipoxygenase-1 Reaction?*; 1995; Vol. 34.

(22) Mogul, R.; Holman, T. R. Inhibition Studies of Soybean and Human 15-Lipoxygenases with Long-Chain Alkenyl Sulfate Substrates†. *Biochemistry* **2001**, *40* (14), 4391–4397.

(23) Offenbacher, A. R.; Iavarone, A. T.; Klinman, J. P. Hydrogen-Deuterium Exchange Reveals Long-Range Dynamical Allostery in Soybean Lipoxygenase. *J. Biol. Chem.* **2018**, *293* (4), 1138–1148.

(24) Tsai, W. C.; Aleem, A. M.; Whittington, C.; Cortopassi, W. A.; Kalyanaraman, C.; Baroz, A.; Iavarone, A. T.; Skrzypczak-Jankun, E.; Jacobson, M. P.; Offenbacher, A. R.; Holman, T. Mutagenesis, Hydrogen-Deuterium Exchange, and Molecular Docking Investigations Establish the Dimeric Interface of Human Platelet-Type 12-Lipoxygenase. *Biochemistry*

2021, *60* (10), 802–812.

(25) Reichard, P. Ribonucleotide Reductases: The Evolution of Allosteric Regulation. *Arch. Biochem. Biophys.* **2002**, *397* (2), 149–155.

(26) Zimanyi, C. M.; Chen, P. Y. T.; Kang, G.; Funk, M. A.; Drennan, C. L. Molecular Basis for Allosteric Specificity Regulation in Class Ia Ribonucleotide Reductase from Escherichia Coli. *Elife* **2016**, *5* (JANUARY2016).

(27) Changeux, J. P.; Edelstein, S. J. Allosteric Mechanisms of Signal Transduction. *Science.* **2005**, *308* (5727), 1424–1428.

(28) Cooper, A.; Dryden, D. T. F. Allostery without Conformational Change. *Eur. Biophys. J. 1984 112* **1984**, *11* (2), 103–109.

(29) Nussinov, R.; Tsai, C. J. Allostery without a Conformational Change? Revisiting the Paradigm. *Curr. Opin. Struct. Biol.* **2015**, *30*, 17–24.

(30) Popovych, N.; Sun, S.; Ebright, R. H.; Kalodimos, C. G. Dynamically Driven Protein Allostery. *Nat. Struct. Mol. Biol. 2006 139* **2006**, *13* (9), 831–838.

(31) Guo, J.; Zhou, H. X. Protein Allostery and Conformational Dynamics. *Chem. Rev.* **2016**, *116* (11), 6503–6515.

(32) Motlagh, H. N.; Wrabl, J. O.; Li, J.; Hilser, V. J. The Ensemble Nature of Allostery. *Nat. 2014 5087496* **2014**, *508* (7496), 331–339.

(33) Hu, S.; Sharma, S. C.; Scouras, A. D.; Soudackov, A. V.; Carr, C. A. M.; Hammes-Schiffer, S.; Alber, T.; Klinman, J. P. Extremely Elevated Room-Temperature Kinetic Isotope Effects Quantify the Critical Role of Barrier Width in Enzymatic C-H Activation. *J. Am. Chem. Soc.* **2014**, *136* (23), 8157–8160.

(34) Riemer, J.; Hoepken, H. H.; Czerwinska, H.; Robinson, S. R.; Dringen, R. Colorimetric

Ferrozine-Based Assay for the Quantitation of Iron in Cultured Cells. *Anal. Biochem.* **2004**, *331* (2), 370–375.

(35) Zaragoza, J. P. T.; Nguy, A.; Minnetian, N.; Deng, Z.; Iavarone, A. T.; Offenbacher, A. R.; Klinman, J. P. Detecting and Characterizing the Kinetic Activation of Thermal Networks in Proteins: Thermal Transfer from a Distal, Solvent-Exposed Loop to the Active Site in Soybean Lipoxygenase. *J. Phys. Chem. B* **2019**, *123* (41), 8662–8674.

(36) Kostenko, A.; Ray, K.; Iavarone, A. T.; Offenbacher, A. R. Kinetic Characterization of the C-H Activation Step for the Lipoxygenase from the Pathogenic Fungus Magnaporthe Oryzae: Impact of N-Linked Glycosylation. *Biochemistry* **2019**, *58* (29).

(37) Ghai, R.; Falconer, R. J.; Collins, B. M. Applications of Isothermal Titration Calorimetry in Pure and Applied Research—Survey of the Literature from 2010. *J. Mol. Recognit.* **2012**, *25* (1), 32–52.

(38) Pascal, B. D.; Willis, S.; Lauer, J. L.; Landgraf, R. R.; West, G. M.; Marciano, D.; Novick, S.; Goswami, D.; Chalmers, M. J.; Griffin, P. R. HDX Workbench: Software for the Analysis of H/D Exchange MS Data. *J. Am. Soc. Mass Spectrom.* **2012**, *23* (9), 1512–1521.

(39) Offenbacher, A. R.; Hu, S.; Poss, E. M.; Carr, C. A. M.; Scouras, A. D.; Prigozhin, D. M.; Iavarone, A. T.; Palla, A.; Alber, T.; Fraser, J. S.; Klinman, J. P. Hydrogen-Deuterium Exchange of Lipoxygenase Uncovers a Relationship between Distal, Solvent Exposed Protein Motions and the Thermal Activation Barrier for Catalytic Proton-Coupled Electron Tunneling. *ACS Cent. Sci.* **2017**, *3* (6), 570–579.

(40) Goldberg, R. N.; Kishore, N.; Lennen, R. M. Thermodynamic Quantities for the Ionization Reactions of Buffers. *J. Phys. Chem. Ref. Data* **2002**, *31* (2), 231.

(41) Johnson, R. A.; Fulcher, L. M.; Vang, K.; Palmer, C. D.; Grossoehme, N. E.; Spuches, A.

M. In Depth, Thermodynamic Analysis of Ca2+ Binding to Human Cardiac Troponin C: Extracting Buffer-Independent Binding Parameters. *Biochim. Biophys. Acta - Proteins Proteomics* **2019**, *1867* (4), 359–366.

(42) Johnson, R. A.; Manley, O. M.; Spuches, A. M.; Grossoehme, N. E. Dissecting ITC Data of Metal Ions Binding to Ligands and Proteins. *Biochim. Biophys. Acta - Gen. Subj.* **2016**, *1860* (5), 892–901.

(43) Fox, J. M.; Zhao, M.; Fink, M. J.; Kang, K.; Whitesides, G. M. The Molecular Origin of Enthalpy/Entropy Compensation in Biomolecular Recognition. *https://doi.org/10.1146/annurev-biophys-070816-033743* **2018**, *47*, 223–250.

(44) Knapp, M. J.; Rickert, K.; Klinman, J. P. Temperature-Dependent Isotope Effects in Soybean Lipoxygenase-1: Correlating Hydrogen Tunneling with Protein Dynamics. *J. Am. Chem. Soc.* **2002**, *124* (15), 3865–3874.

(45) Lewis, E. R.; Johansen, E.; Holman, T. R. Large Competitive Kinetic Isotope Effects in Human 15-Lipoxygenase Catalysis Measured by a Novel HPLC Method. *J. Am. Chem. Soc.* **1999**, *121* (6), 1395–1396.

(46) Dainese, E.; Sabatucci, A.; Van Zadelhoff, G.; Angelucci, C. B.; Vachette, P.; Veldink, G. A.; Agrò, A. F.; Maccarrone, M. Structural Stability of Soybean Lipoxygenase-1 in Solution as Probed by Small Angle X-Ray Scattering. *J. Mol. Biol.* **2005**, *349* (1), 143–152.

(47) Lorber, B.; Fischer, F.; Bailly, M.; Roy, H.; Kern, D. Protein Analysis by Dynamic Light Scattering: Methods and Techniques for Students. *Biochem. Mol. Biol. Educ.* **2012**, *40* (6), 372–382.

(48) Aleem, A. M.; Jankun, J.; Dignam, J. D.; Walther, M.; Kühn, H.; Svergun, D. I.; Skrzypczak-Jankun, E. Human Platelet 12-Lipoxygenase, New Findings about Its Activity,

Membrane Binding and Low-Resolution Structure. *J. Mol. Biol.* **2008**, *376* (1), 193–209.

(49) Shang, W.; Ivanov, I.; Svergun, D. I.; Borbulevych, O. Y.; Aleem, A. M.; Stehling, S.; Jankun, J.; Kühn, H.; Skrzypczak-Jankun, E. Probing Dimerization and Structural Flexibility of Mammalian Lipoxygenases by Small-Angle X-Ray Scattering. *J. Mol. Biol.* **2011**, *409* (4), 654–668.

(50) Eek, P.; Põldemaa, K.; Kasvandik, S.; Järving, I.; Samel, N. A PDZ-like Domain Mediates the Dimerization of 11R-Lipoxygenase. *Biochim. Biophys. Acta - Mol. Cell Biol. Lipids* **2017**, *1862* (10), 1121–1128.

(51) Richieri, G. V.; Ogata, R. T.; Kleinfeld, A. M. Equilibrium Constants for the Binding of Fatty Acids with Fatty Acid-Binding Proteins from Adipocyte, Intestine, Heart, and Liver Measured with the Fluorescent Probe ADIFAB. *J. Biol. Chem.* **1994**, *269* (39), 23918–23930.

(52) Loch, J. I.; Bonarek, P.; Polit, A.; Riès, D.; Dziedzicka-Wasylewska, M.; Lewiński, K. Binding of 18-Carbon Unsaturated Fatty Acids to Bovine β-Lactoglobulin—Structural and Thermodynamic Studies. *Int. J. Biol. Macromol.* **2013**, *57*, 226–231.

(53) Matsuoka, S.; Sugiyama, S.; Matsuoka, D.; Hirose, M.; Lethu, S.; Ano, H.; Hara, T.; Ichihara, O.; Kimura, S. R.; Murakami, S.; Ishida, H.; Mizohata, E.; Inoue, T.; Murata, M. Water-Mediated Recognition of Simple Alkyl Chains by Heart-Type Fatty-Acid-Binding Protein. *Angew. Chemie - Int. Ed.* **2015**, *54* (5), 1508–1511.

(54) Rovoli, M.; Thireou, T.; Choiset, Y.; Haertlé, T.; Sawyer, L.; Eliopoulos, E.; Kontopidis, G. Thermodynamic, Crystallographic and Computational Studies of Non-Mammalian Fatty Acid Binding to Bovine β-Lactoglobulin. *Int. J. Biol. Macromol.* **2018**, *118*, 296–303.

(55) Straume, M.; Freire, E. Two-Dimensional Differential Scanning Calorimetry: Simultaneous

Resolution of Intrinsic Protein Structural Energetics and Ligand Binding Interactions by Global Linkage Analysis. *Anal. Biochem.* **1992**, *203* (2), 259–268.

(56) Martínez, J. C.; Filimonov, V. V.; Mateo, P. L.; Filimonov, V. V.; Schreiber, G.; Fersht, A. R. A Calorimetric Study of the Thermal Stability of Barstar and Its Interaction with Barnase. *Biochemistry* **1995**, *34* (15), 5224–5233.

(57) Celej, M. S.; Dassie, S. A.; González, M.; Bianconi, M. L.; Fidelio, G. D. Differential Scanning Calorimetry as a Tool to Estimate Binding Parameters in Multiligand Binding Proteins. *Anal. Biochem.* **2006**, *350* (2), 277–284.

(58) Majumdar, R.; Manikwar, P.; Hickey, J. M.; Samra, H. S.; Sathish, H. A.; Bishop, S. M.; Middaugh, C. R.; Volkin, D. B.; Weis, D. D. Effects of Salts from the Hofmeister Series on the Conformational Stability, Aggregation Propensity, and Local Flexibility of an IgG1 Monoclonal Antibody. *Biochemistry* **2013**, *52* (19), 3376–3389.

(59) Bhunia, A.; Ilyas, H.; Bhattacharjya, S. Salt Dependence Conformational Stability of the Dimeric SAM Domain of MAPKKK Ste11 from Budding Yeast: A Native-State H/D Exchange NMR Study. *Biochemistry* **2020**, *59* (31), 2849–2858.

(60) Minor, W.; Steczko, J.; Stec, B.; Otwinowski, Z.; Bolin, J. T.; Walter, R.; Axelrod, B. Crystal Structure of Soybean Lipoxygenase L-1 at 1.4 Å Resolution†,‡. *Biochemistry* **1996**, *35* (33), 10687–10701.

(61) Bradshaw, M. D.; Gaffney, B. J. Fluctuations of an Exposed π-Helix Involved in Lipoxygenase Substrate Recognition. *Biochemistry* **2014**, *53* (31), 5102–5110.

(62) Cooley, R. B.; Arp, D. J.; Karplus, P. A. Evolutionary Origin of a Secondary Structure: π-Helices as Cryptic but Widespread Insertional Variations of α-Helices That Enhance Protein Functionality. *J. Mol. Biol.* **2010**, *404* (2), 232–246.

(63) Ivanov, I.; Shang, W.; Toledo, L.; Masgrau, L.; Svergun, D. I.; Stehling, S.; Gómez, H.; Di Venere, A.; Mei, G.; Lluch, J. M.; Skrzypczak-Jankun, E.; González-Lafont, À.; Kühn, H. Ligand-Induced Formation of Transient Dimers of Mammalian 12/15-Lipoxygenase: A Key to Allosteric Behavior of This Class of Enzymes? *Proteins Struct. Funct. Bioinforma.* **2012**, *80* (3), 703–712.

(64) Hu, S.; Cattin-Ortolá, J.; Munos, J. W.; Klinman, J. P. Hydrostatic Pressure Studies Distinguish Global from Local Protein Motions in C−H Activation by Soybean Lipoxygenase-1. *Angew. Chemie* **2016**, *128* (32), 9507–9510.

(65) Aleem, A. M.; Tsai, W. C.; Tena, J.; Alvarez, G.; Deschamps, J.; Kalyanaraman, C.; Jacobson, M. P.; Holman, T. Probing the Electrostatic and Steric Requirements for Substrate Binding in Human Platelet-Type 12-Lipoxygenase. *Biochemistry* **2019**, *58* (6), 848–857.

Chapter 4

Hydrogen-deuterium exchange study of 15-lipoxygenase-1 and allosteric effector

Introduction

Lipoxygenases (LOXs) are a class of non-heme, metal-containing enzymes that are found in plants, animals, fungi, and bacteria.[1] LOXs catalyze the peroxidation of polyunsaturated fatty acids (PUFAs) into diverse hydroperoxide products. This reaction is a form of C-H activation, also called C-H bond cleavage, where a C-H bond is cleaved and replaced with a C-X bond, where X is carbon, nitrogen, or carbon.[2] In LOXs, the cofactor abstracts the hydrogen using proton-coupled electron transfer (PCET), and a carbon radical is formed on the PUFA chain. The carbon radical then reacts to molecular oxygen and forms a hydroperoxide product.[3] The proposed mechanism of this reaction is shown in Figure 4.1.

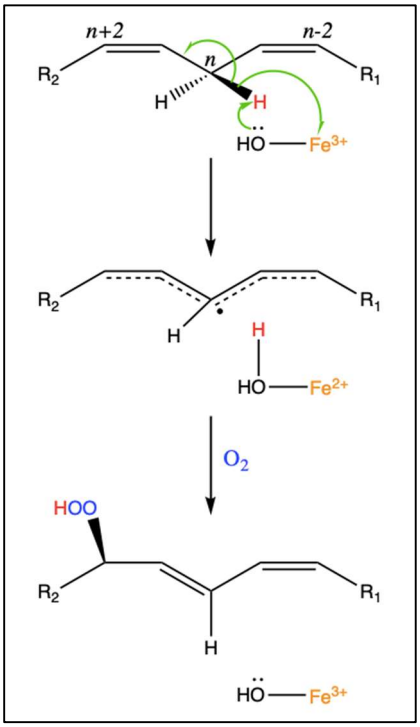

Figure 4.1 *Mechanism of C-H bond cleavage done by human 15-LOX-1.*

Though LOXs have low sequence homology between different species, LOXs maintain certain structural similarities that are evident across the different kingdoms. LOXs all maintain a catalytic domain that is predominately alpha-helical and contains a metal catalytic center. Additionally, all plant and animal LOXs have a secondary domain located at the N terminus called the Polycystin-1, Lipoxygenase, α-Toxin (PLAT) domain, and this domain is primarily composed of beta-sheets.[4] Within humans, 6 isoforms of LOX have been identified, and they are named based on the carbon number on arachidonic acid (AA) where the oxygenation is catalyzed, e.g., 5-LOX catalyzes the oxidation at the 5th carbon, (Figure 4.2).

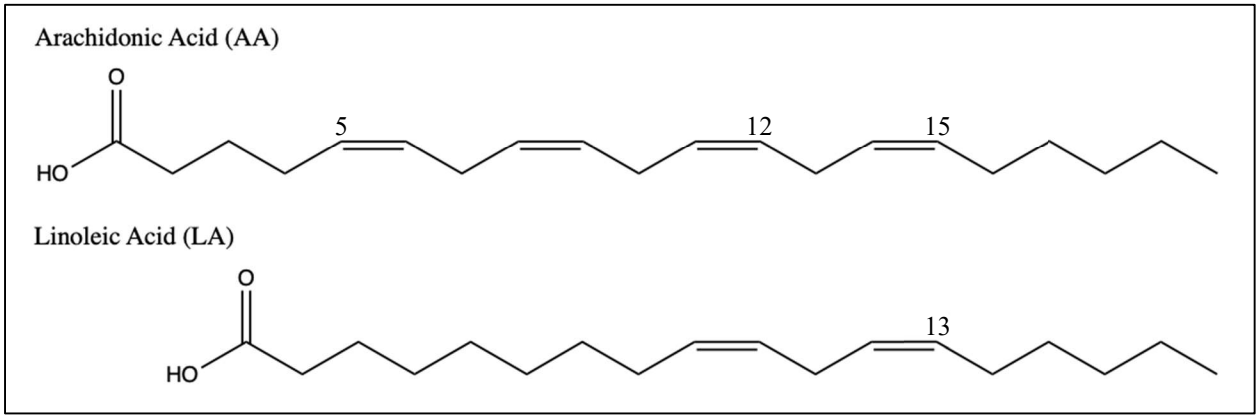

Figure 4.2 *Arachidonic acid (top) and linoleic acid (bottom), with relevant carbons labeled.*

There have been two isoforms identified that catalyze the oxidation of AA at the 15th carbon position, 15-LOX-1 and 15-LOX-2. The two isoforms only share a 37% sequence homology (Figure 4.3)[5] and are expressed in different cell types within the body. Each LOX isoform that is found in humans is tissue specific: 5-LOX is mainly expressed in leukocytes, 12-LOX is primarily found in platelets, 15-LOX-1 is expressed in reticulocytes, eosinophils, and macrophages, and 15-LOX-2 is found in skin cells, the cornea, the prostate, the lung, and esophageal cells.[6] There is also a difference in substrate specificity between the two 15-LOX isozymes (Table 4.1). Using steady-state kinetics, it was discovered that 15-LOX-2 displays a preference for AA, the more common

substrate found in animals, while 15-LOX-1 prefers linoleic acid (Figure 4.2), which is more commonly found in plants.[7]

Table 4.1 *Substrate specificity of 15-LOX isozymes*[a]

	AA	LA	AA/LA
15-LOX-1	2.0 ± 0.2	2.5 ± 0.2	0.80 ± 0.1
15-LOX-2	0.10 ± 0.01	0.013 ± 0.001	8.0 ± 1.0

[a]*Values displayed are* k_{cat}/K_M ($\mu M^{-1}s^{-1}$) *and were collected at 22 °C in 25 mM HEPES (pH 7.5). Reproduced from reference.*[7]

```
15-LOX-1   1    MGLYRIRVSTGASLYAGSNNQVQLWLVGQHGEAA------LGKRLWPARGKETELKVEVP   54
15-LOX-2   21   MAEFRVRVSTGEAFGAGTWDKVSVSIVGTRGESPPLPLDNLGKEF--TAGAEEDFQVTLP   78

15-LOX-1   55   EYLGPLLFVKLRKRHLLKD-------DAWFCNWISVQGPGAGDEVRFPCYRWVEGNGVLS   107
15-LOX-2   79   EDVGRVLLLRVHKAPPVLPLLGPLAPDAWFCRWFQLTPPRGG-HLLFPCYQWLEGAGTLV   137

15-LOX-1   108  LPEGTGRTVGEDPQGLFQKHREEELEERRKLYRWGNWKDGLILNMAGAKLYDLPVDERFL   167
15-LOX-2   138  LQEGTAKVSWADHHPVLQQQRQEELQARQEMYQWKAYNPGWPHCLDEKTVEDLELNIKYS   197

15-LOX-1   168  EDKRVDFEVSLAKGLADLAIKDSLNVLTCWKDLDDFNRIFWCGQSKLAERVRDSWKEDAL   227
15-LOX-2   198  TAKNANFYLQAGSAFAEMKIKGLLDRKGLWRSLNEMKRIFNFRRTPAAEHAFEHWQEDAF   257

15-LOX-1   228  FGYQFLNGANPVVLRRSAHLPARL---------VFPPGMEELQAQLEKELEGGTLFEADF   278
15-LOX-2   258  FASQFLNGLNPVLIRRCHYLPKNFPVTDAMVASVLGPG-----TSLQAELEKGSLFLVDH   312

15-LOX-1   279  SLLDGIKANVILCSQQHLAAPLVMLKLQPD-GKLLPMVIQLQLPRTGSPPPPLFLPTDPP   337
15-LOX-2   313  GILSGIQTNVINGKPQFSAAPMTLLYQSPGCGPLLPLAIQLS--QTPGPNSPIFLPTDDK   370

15-LOX-1   338  MAWLLAKCWVRSSDFQLHELQSHLLRGHLMAEVIVVATMRCLPSIHPIFKLIIPHLRYTL   397
15-LOX-2   371  WDWLLAKTWVRNAEFSFHEALTHLLHSHLLPEVFTLATLRQLPHCHPLFKLLIPHTRYTL   430

15-LOX-1   398  EINVRARTGLVSDMGIFDQIMSTGGGGHVQLLKQAGAFLTYSSFCPPDDLADRGLLGVKS   457
15-LOX-2   431  HINTLARELLIVPGQVVDRSTGIGIEGFSELIQRNMKQLNYSLLCLPEDIRTRGVEDIPG   490

15-LOX-1   458  SFYAQDALRLWEIIYRYVEGIVSLHYKTDVAVKDDPELQTWCREITEIGLQGAQDRGFPV   517
15-LOX-2   491  YYYRDDGMQIWGAVERFVSEIIGIYYPSDESVQDDRELQAWVREIFSKGFLNQESSGIPS   550

15-LOX-1   518  SLQARDQVCHFVTMCIFTCTGQHASVHLGQLDWYSWVPNAPCTMRLPPPTTKD-ATLETV   576
15-LOX-2   551  SLETREALVQYVTMVIFTCSAKHAAVSAGQFDSCAWMPNLPPSMQLPPPTSKGLATCEGF   610

15-LOX-1   577  MATLPNFHQASLQMSITWQLGRRQPVMVAVGQHEEEYFSGPEPKAVLKKFREELAALDKE   636
15-LOX-2   611  IATLPPVNATCDVILALWLLSKEPGDQRPLGTYPDEHFTEEAPRRSIATFQSRLAQISRG   670

15-LOX-1   637  IEIRNAKLDMPYEYLRPSVVENSVAI   662
15-LOX-2   671  IQERNQGLVLPYTYLDPPLIENSVSI   696
```

Figure 4.3 *Sequence alignment of human 15-LOX-1 (blue) and 15-LOX-2 (red) with overlapping amino acids highlighted in yellow. Modified from reference.*[5]

While they have their differences, both 15-LOX isoforms are implicated in various diseases, making them key targets for drug design and development. However, the exact role 15-LOXs have within the body is contradictory. There is evidence to support that 15-LOX-1 is both involved in tumor suppressing and carcinogenic activities.[8] Additionally, 15-LOX-2 has been shown to be highly expressed in atherosclerotic lesions, implicating its involvement in pathogenesis, as well as being implicated in the production of resolvins, which activate anti-inflammatory pathways within the body.[9] Isoform selective inhibitors have been discovered for 15-1 and 15-2. For example, the recent discovery of 15-LOX-2 inhibitor, 327069, has been shown to inhibit 15-LOX-2 activity with K_{ic} of 0.70 μM with little-to-no inhibition towards 15-LOX-1 up to 100 μM. (Table 4.2) The co-crystal structure of this inhibitor with 15-LOX2 shows that the inhibitor binds in the active site, adjacent to the catalytic center. The specificity of the isoform selective inhibitors highlights the structural differences between 15-LOX1 and 15-LOX-2.[10] The differences in the structure between these isoforms are based on the differences in the sequences. While there are multiple X-ray structures of 15-LOX-2, there is no X-ray structure of 15-LOX-1, there are only models of the structure that have been developed based on the amino acid sequence of the protein.

Table 4.2 *Inhibitory studies of allosteric inhibitor, 327069*

Disassociation Constants (μM)		IC_{50} (μM)	
K_{ic}	K_{iu}	15-LOX-2	15-LOX-1
0.70 ± 0.07	1.2 ± 0.9	0.34[a]	>50[b]

[a]A full IC_{50} value was obtained for 15-LOX-2, [b]while other values were estimated. Reproduced from reference.[10]

Due to the duplicitous nature of this enzyme, 15-LOX isoform selective inhibitors may not be the most effective therapeutic option. To solve this issue of altering 15-LOX activity in a beneficial way, a deeper understanding of the allosteric regulation of 15-LOXs is necessary. 15-LOX-1 has previously been implicated in having an allosteric binding site. Researchers synthesized oleyl sulfate (OS), shown in Figure 4.4A, to investigate the regulation of SLO and 15-LOX-1. OS was synthesized based on oleic acid (OA), which was originally thought to be a competitive inhibitor for SLO. However, steady-state kinetics studies performed with OA added to SLO and 15-LOX-1 displayed a hyperbolic increase in the $^{D}k_{cat}/K_M$, also called ΔKIE, and a hyperbolic decrease in the k_{cat}/K_M, which represents the overall catalytic efficiency. This data was the result of OA forming a ternary complex with the enzyme and the substrate. The formation of a ternary complex could either be due to OA aggregating with the substrate or OA binding at a second binding site on the enzyme. The regulation of the catalytic activity of an enzyme through a compound binding at a secondary binding site on the enzyme implicates allosteric regulation.

To determine if OA was simply aggregating with the substrate, a new version of OA was synthesized that was more soluble, called OS. The same results were observed with the addition of OS to the enzyme, a hyperbolic increase in the $^{D}k_{cat}/K_M$ (Figure 4.4B) and a hyperbolic decrease in the k_{cat}/K_M (Figure 4.4C). Since these studies were conducted at a lower OS concentration than the aggregation point, it eliminated aggregation as the cause of the formation of the ternary complex. This supports that OS was inhibiting the activity of SLO and 15-LOX-1 through the formation of a ternary complex by binding at a secondary binding site.[11] This was the first evidence of allosteric regulation of SLO or 15-LOX.

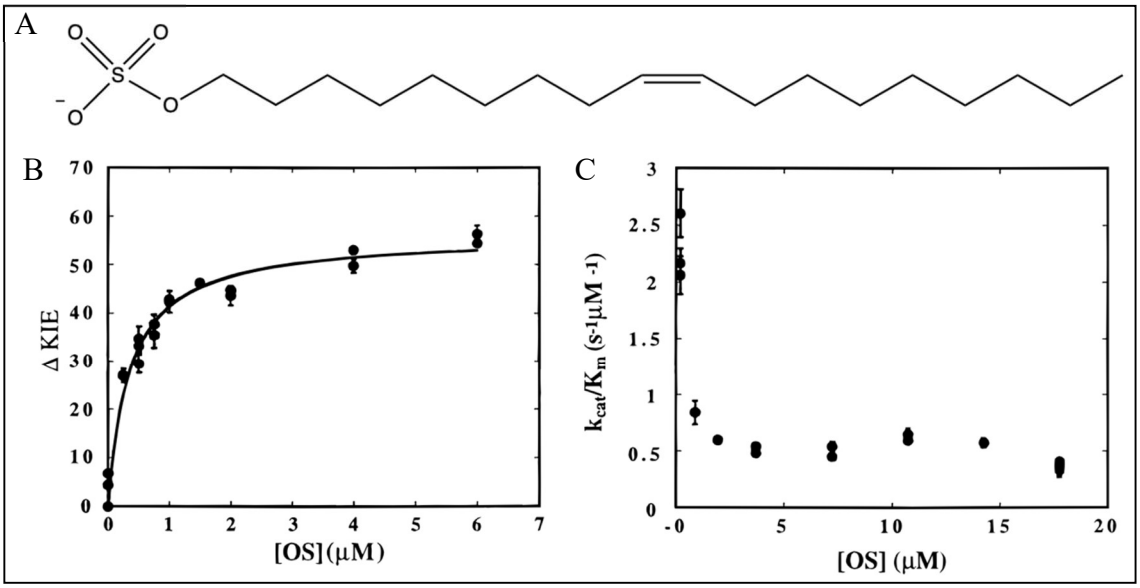

Figure 4.4 *Observed effect of oleyl sulfate (A) on* $^{D}k_{cat}/K_M$ *(B) and* k_{cat}/K_M *(C) for 15-LOX-1. Reproduced from reference.*[11]

Since the discovery of OS as an allosteric inhibitor, researchers have been searching for new allosteric effector molecules that regulate 15-LOX-1. Using molecular dynamics simulations and software, researchers identified clusters of residues that had correlated motions, several clusters were present in the active site (Figure 4.5A). Using this information, along with the program CAVITY, researchers were able to identify four possible binding pockets within 15-LOX-1, shown in Figure 4.5B. synthesize allosteric effector molecules that would optimally bind to the residues located within the pocket, shown in Figure 4.5C. An example of one such molecule is PKUMDL_MH_1001, structure shown in Figure 4.6A, which increased the activity of 15-LOX-1 by 85%.[12]

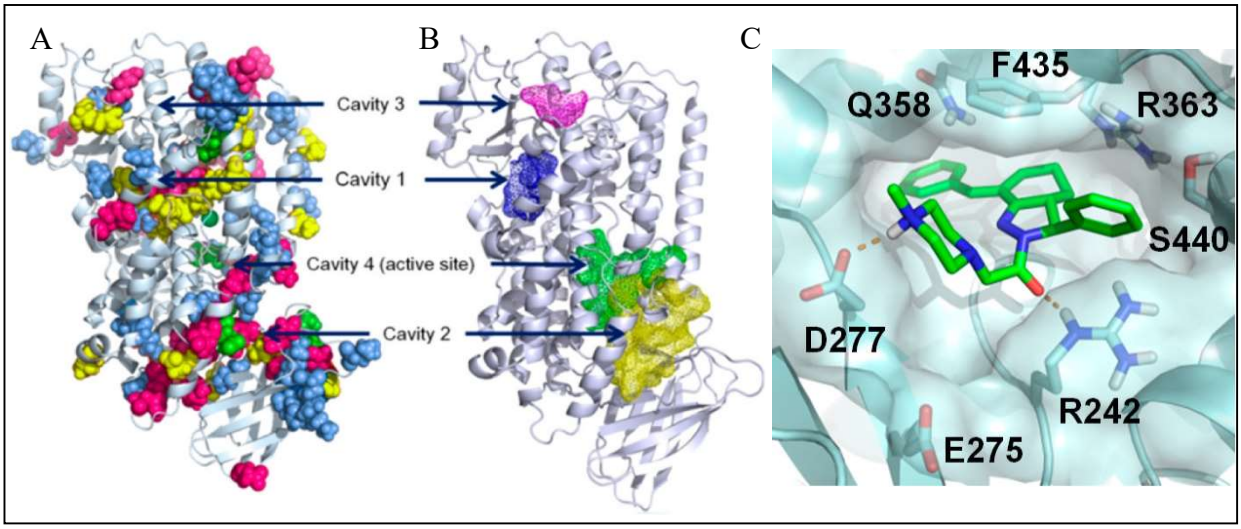

Figure 4.5 *Clusters of residues with correlated motions (A) and pockets identified with the program, CAVITY (B) shown on the structure of 15-LOX-1. Allosteric activator, PKUMDL_MH_1001, docked into the predicted allosteric binding site, Cavity 1, with residues predicted to interact with the molecule labeled. Reproduced from reference.*[12]

To probe the mechanism of activation utilized by PKUMDL_MH_1001, researchers used kinetic assays with the addition of the activator in varying concentrations ranging from 0 to 40 μM. When 0 μM of activator was added to the enzyme, the researchers observed that 15-LOX-1 activity was being inhibited by an increasing substrate concentration, shown as the red line in Figure 4.6B. However, they observed that this substrate inhibition was reduced with the addition of an increasing concentration of the activator, shown with the purple, lime, and blue lines in Figure 4.6B. This supported the theory that the activator, PKUMDL_MH_1001, was increasing the activity of 15-LOX-1 by reducing the binding affinity for a second substrate molecule, which would ordinarily inhibit the activity of the enzyme at high substrate concentration levels.[8]

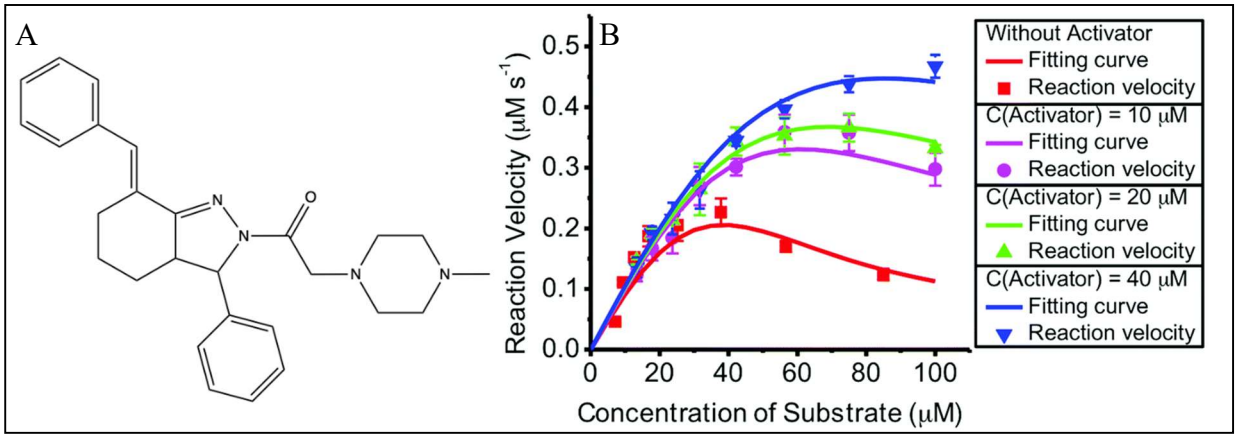

Figure 4.6 *Structure of allosteric activator, PKUMDL_MH_1001, (A) and kinetics assay of 15-LOX-1 with increasing concentrations of activator added (B). Reproduced from reference.*[8]

The predicted allosteric binding site of PKUMDL_MH_1001 has a unique location on the protein compared to SLO and 15-LOX-2. The predicted allosteric binding sites of 15-LOX-1 and 15-LOX-2 are compared in Figure 4.7. The results from HDX-MS studies of SLO incubated with OS support the conclusion that the allosteric effector was binding close to the N-terminal of SLO, which is located at the PLAT domain.[13] Similarly, docking studies of 15-LOX-2 indicate the allosteric effector is binding near the N-terminal, at the interface of the PLAT and catalytic domains.[14]

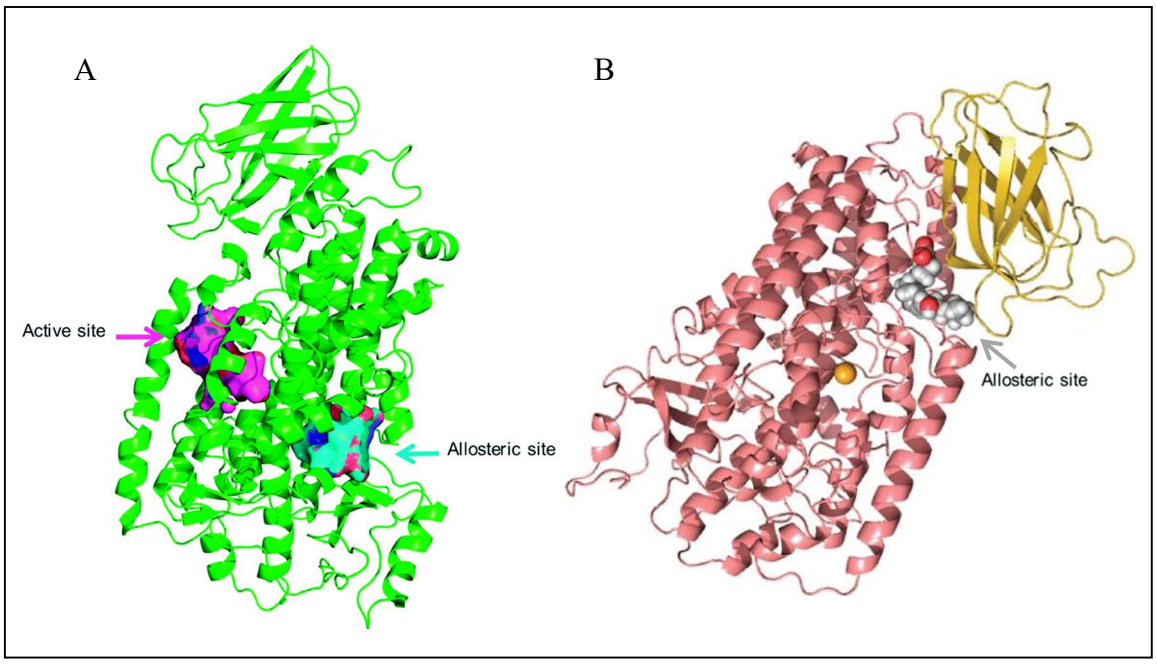

Figure 4.7 *Predicted allosteric binding sites on 15-LOX-1 (A)*[8] *and 15-LOX-2 (B). Reproduced from reference.*[14]

Presented herein, the dynamics of 15-LOX-1 were analyzed using HDX-MS and compared to previously obtained HDX data on 15-LOX-2 to highlight any dynamic differences among the isoforms. We also used a combination of biophysical techniques, differential scanning calorimetry and size exclusion chromatography, to provide evidence to support that the addition of the allosteric activator, PKUMDL_MH_1001, does not result in any large-scale conformational changes occurring to 15-LOX-1.

Methods

Purification

Wild-type (WT) 15-LOX-1 was obtained from the Holman group. The sample was concentrated to *ca* 2.5 mL then additionally purified using size exclusion chromatography (SEC). 15-LOX-1 was concentrated to ~50-100 μM, frozen in liquid N_2 and stored in aliquots at -80 °C. 15-LOX-1 concentration was determined spectroscopically, $\varepsilon_{280} = 119.6\ mM^{-1}\ cm^{-1}$.

Size Exclusion Chromatography (SEC)

The protein was purified and the oligomerization upon binding with the effector molecules was done using SEC with a Superdex^{TM} 200 increase 10/300 GL column on an ÄKTA^{TM} Prime FPLC. The buffer used for SEC-fast protein liquid chromatography (FPLC) was 50 mM HEPES (pH 7.5) with 0.15 M NaCl. When appropriate, the column was pre-equilibrated in buffer supplemented with 20 μM PKUMDL_MH_1001 (allosteric activator). The elution volume was monitored by a change in absorbance at 280 nm.

Differential Scanning Calorimetry (DSC)

DSC experiments were conducted on a TA-instruments Nano-DSC microcalorimeter. The 15-LOX-1 samples were prepared at 14 μM concentration in 50 mM HEPES (pH 7.5) with 0.15 M NaCl. When present, PKUMDL_MH_1001 (allosteric activator) was added in equal molar concentration. The DSC experiments were carried out in heat-only mode, from 30 – 90 °C at a rate of 1 °C min^{-1}. The pressure was kept at 3 atm during the course of the experiment. These experiments were performed in triplicate.

Hydrogen-Deuterium Exchange Mass Spectrometry (HDX-MS)

Aliquots of 15-LOX-1 (100 μM) were thawed and were diluted 10-fold (5 μL into 45 μL) in 10 mM HEPES (pD 7.4) with 0.15 M NaCl D_2O (99% D) buffer (corrected; $pD = pH_{read} + 0.4$). Samples were incubated randomly at 10 time points (0, 10, 20, 45, 60, 180, 600, 1800, 3600, and 7200 seconds) at 10 °C using a water bath. The HDX samples were prepared over the course of five days and the time points were randomized to reduce systematic error. Each time point was prepared and processed once. At the designated incubation time, all samples were then treated identically; the samples were rapidly cooled (5-6 seconds in a -20 °C bath) and acid quenched (to

pH 2.4, confirmed with pH electrode, with 0.32 M citric acid stock solution to 90 mM final concentration). The acid solution was supplemented with 20 mM DTT to maintain reducing conditions for reducing disulfide bonds. Procedures from this point were conducted near 4 °C. Prior to pepsin digestion, guanidine HCl (in citric acid, pH 2.4) was mixed with the samples to a final concentration of *ca.* 0.5 M. HDX samples of 15-LOX-1 were digested with pre-equilibrated (10 mM citrate buffer, pH 2.4), immobilized pepsin for 2.5 min. The peptide fragments were filtered, removing the pepsin, using spin cups (cellulose acetate) and by centrifugation for 10 seconds at 4 °C. Samples were flash frozen immediately in liquid N_2 and stored at -80 °C until data collection.

Deuterated, pepsin-digested 15-LOX-1 samples of were analyzed using an Agilent 1200 LC (Santa Clara, CA) that was connected in-line with the LTQ Orbitrap XL mass spectrometer (Thermo). The LC was equipped with a reversed-phase analytical column (Viva C8, 30 mm length × 1.0 mm inner diameter, 5 μm particles, Restek, Bellefonte, PA) and guard pre-column (C8, Restek). Solvent A was 99.9% water/0.1% formic acid and solvent B was 99.9% acetonitrile/0.1% formic acid (v/v). Each sample was thawed immediately prior to injection onto the column. The elution program consisted of a linear gradient from 5% to 10% B over 1 min, a linear gradient to 40% B over 5 min, a linear gradient to 100% B over 4 min, isocratic conditions at 100% B for 3 min, a linear gradient to 5% B over 0.5 min, and isocratic conditions at 5% B for 5.5 min, at a flow rate of 300 μL/min. The column compartment was maintained at 4 °C and lined with towels to absorb atmospheric moisture condensation. The column exit was connected to the ESI source of the mass spectrometer using PEEK tubing (0.005” inner diameter × 1/16” outer diameter, Agilent). Mass spectra were acquired in the positive ion mode over the range m/z = 350 to 1800 using the

Orbitrap mass analyzer, in profile format, with a mass resolution setting of 100,000 (at m/z = 400). Data acquisition was controlled using Xcalibur software (version 2.0.7, Thermo).

Mass spectral data acquired for HDX measurements were analyzed using the software, HDX Workbench.[15] The percent deuterium incorporation was calculated for each of these peptides, taking into account the number of amide linkages (excluding proline residues) and the calculated number of deuterons incorporated. The values were normalized for 100% D_2O and corrected for peptide-specific back-exchange (BE), HDX% = (observed, normalized extent of deuterium incorporation {in percent})/(1-{BE/100}).

Peptide specific back exchange (BE) was determined by fully exchanging the protein-derived peptides in 100% D_2O and then examining the reverse exchange (D to H). First, the peptides were generated from pepsin digestion of 15-LOX-1 in H_2O. The water was then removed using lyophilization. The peptide mixture was then dissolved in D_2O buffer (pD 9). The solution was incubated at 90 °C for 2 hours, then collected using centrifugation. The collection was sonicated, and acid quenched to pD 2.5. The samples were frozen using liquid N_2 and stored at -80 °C until data collection. The extent of the exchange was analyzed in the same manner as the other samples, described above. The BE values were calculated using HDX Workbench software, (Pascal 2012) BE (%) = 100% - (observed extent of deuterium incorporation (%)). BE values ranged from 28 to 87%, for an average value of 61%. The resulting data were plotted as deuterium exchange versus time using Igor Pro software (See Appendix B).

Results and Discussion

DSC and SEC Indicate a Lack of Large-Scale Conformational Change

DSC experiments were conducted to determine the effect of the allosteric activator, PKUMDL_MH_1001, on the structure and folding stability of 15-LOX-1. DSC has previously been used to characterize the binding parameters of ligands to proteins.[16–18] For 1:1 ligand:protein concentration ratios, a change in melting temperature, T_m, of 2-5 °C is often reported. Contrary to what is mentioned above, the addition of equal molar activator did not result in any significant difference in folding stability compared to the apo protein (Figure 4.8). This supports the conclusion that the activator does not induce any large-scale conformational changes to 15-LOX-1 to allosterically regulate the protein. The DSC data collected on 15-LOX-1 was also compared to data collected on 15-LOX-2, shown in Table 4.3. The observed melting temperature of 15-LOX-1 was slightly lower than 15-LOX-2, however the enthalpy of 15-LOX-1 was less than half of the enthalpy of 15-LOX-2. Since these enzymes have almost identical molecular weights, this data suggests that the 15-LOX-1 had a significantly lower stability than 15-LOX-2. Additional SEC experiments showed no shift in elution volume when the column was pre-equilibrated with the activator (Figure 4.9). The SEC data also displays a broadened peak, which was suggests impurities in the protein sample or different oligomerization states of the protein. However, the peak is broadened regardless of the presence of the activator, and therefore does not suggest any induced structural changes upon binding to the effector molecule.

Table 4.3 *DSC thermodynamic parameters of 15-LOXs*[a]

	MW (kDa)	T_m (°C)	ΔH (kJ/mol)
15-LOX-1	75.6	52	370
15-LOX-2	75.8	57.1 ± 0.2	800 ± 30

[a]*Conducted in 50 mM HEPES (pH 7.5) supplemented with 0.15 M NaCl.*

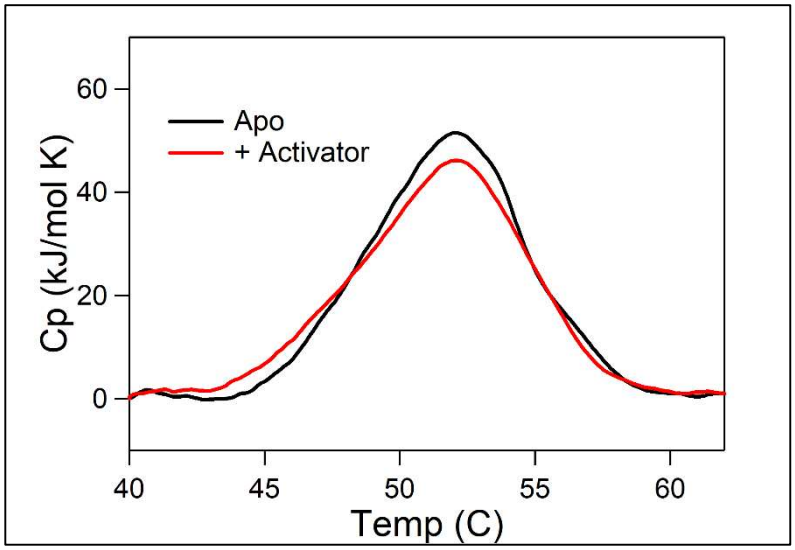

Figure 4.8 *DSC thermograms of 15-LOX-1 in 50 mM HEPES (pH 7.5) with 0.15 M NaCl in the absence (black) and presence (red) of equal molar PKUMDL_MH_1001 (allosteric activator).*

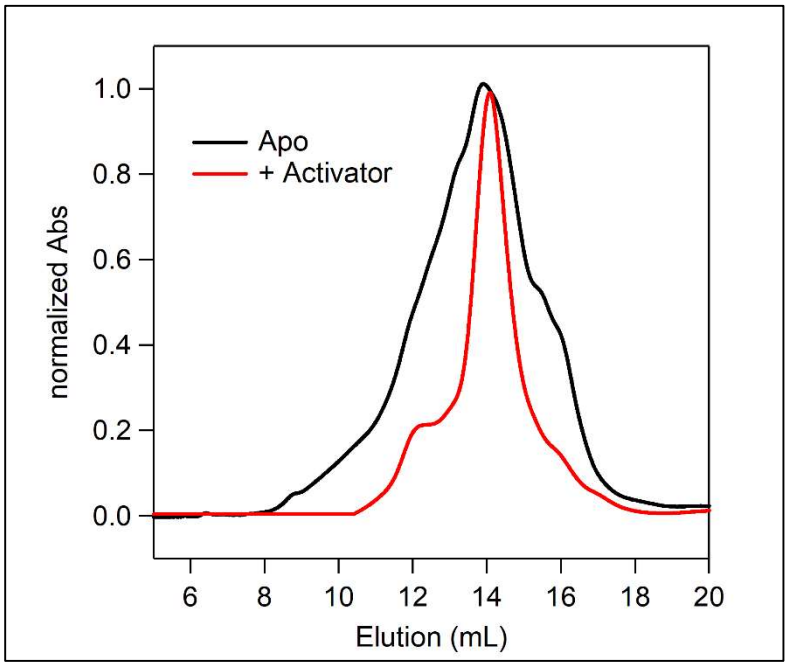

Figure 4.9 *SEC-FPLC traces of 15-LOX-1 in 50 mM HEPES (pH 7.5) with 0.15 M NaCl in the absence (black) and presence (red) of 10 μM PKUMDL_MH_1001 (allosteric activator). The peaks correspond to a monomeric form.*

Hydrogen-Deuterium Exchange Mass Spectrometry (HDX-MS)

To investigate the dynamics of 15-LOX-1 compared to 15-LOX-2, HDX-MS experiments were conducted. HDX-MS of 15-LOX-2 was previously characterized and is shown in Figure 4.10A-D,[10] and is compared to the new HDX data on 15-LOX-1 shown in Figure 4.10E-H. While the two 15-LOX isoforms share a sequence identity of 37%, how that translates to the protein dynamics has yet to be determined. From this list, 46 non-overlapping peptides that were analyzed for 15-LOX-1, which represent a coverage of 84% of the protein's sequence. As a function of time, most of these peptides showed higher rates of H/D exchange when compared to 15-LOX-2. This is especially noticeable in helix α2 and the PLAT domain, which both have a mostly low percent exchange at 10 seconds in 15-LOX-2, while in 15-LOX-1 these peptides are nearly completely exchanged at 10 seconds. The cumulative data supports the DSC results in Table 4.3, indicating that the 15-LOX-1 protein, in our hands, is considerably less stable than 15-LOX-2. These data provide a partial explanation for the inability to crystalize 15-LOX-1. Additional HDX-MS analysis of 15-LOX-1 was also performed in the presence of the allosteric activator, PKUMDL_MH_1001. There was no observable difference in the H/D exchange rate for any of the peptides upon the addition of the activator, this was likely the result of the lower stability of the protein, however, more investigation would need to be done to confirm this theory.

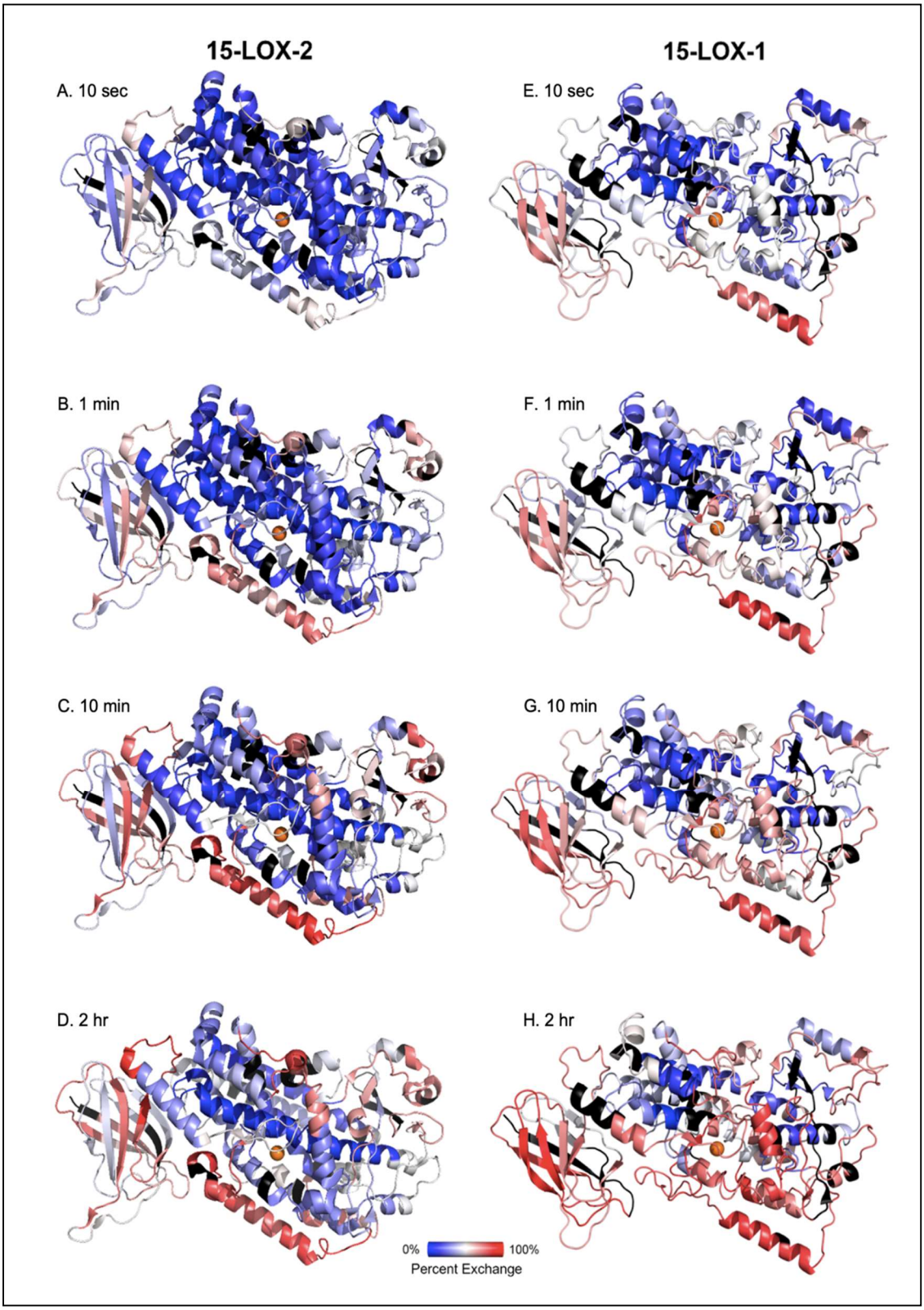

Figure 4.10 *HDX-MS properties of 15-LOX-2 (A-D)[10] compared to 15-LOX-1.*

References

(1) Brash, A. R. Lipoxygenases: Occurrence, Functions, Catalysis, and Acquisition of Substrate. *J. Biol. Chem.* **1999**, *274* (34), 23679–23682.

(2) Whittington, C.; Latham, J.; Offenbacher, A. R. Tunneling through the Barriers: Resolving the Origins of the Activation of C-H Bonds Catalyzed by Enzymes. In *ACS Symposium Series*; 2020; Vol. 1357.

(3) Hatcher, E.; Soudackov, A. V.; Hammes-Schiffer, S. Proton-Coupled Electron Transfer in Soybean Lipoxygenase. *J. Am. Chem. Soc.* **2004**, *126* (18), 5763–5775.

(4) Newcomer, M. E.; Brash, A. R. The Structural Basis for Specificity in Lipoxygenase Catalysis. *Protein Sci.* **2015**, *24* (3), 298–309.

(5) Agarwala, R.; Barrett, T.; Beck, J.; Benson, D. A.; Bollin, C.; Bolton, E.; Bourexis, D.; Brister, J. R.; Bryant, S. H.; Canese, K.; Charowhas, C.; Clark, K.; Dicuccio, M.; Dondoshansky, I.; Federhen, S.; Feolo, M.; Funk, K.; Geer, L. Y.; Gorelenkov, V.; Hoeppner, M.; Holmes, B.; Johnson, M.; Khotomlianski, V.; Kimchi, A.; Kimelman, M.; Kitts, P.; Klimke, W.; Krasnov, S.; Kuznetsov, A.; Landrum, M. J.; Landsman, D.; Lee, J. M.; Lipman, D. J.; Lu, Z.; Madden, T. L.; Madej, T.; Marchler-Bauer, A.; Karsch-Mizrachi, I.; Murphy, T.; Orris, R.; Ostell, J.; O'sullivan, C.; Panchenko, A.; Phan, L.; Preuss, D.; Pruitt, K. D.; Rodarmer, K.; Rubinstein, W.; Sayers, E.; Schneider, V.; Schuler, G. D.; Sherry, S. T.; Sirotkin, K.; Siyan, K.; Slotta, D.; Soboleva, A.; Soussov, V.; Starchenko, G.; Tatusova, T. A.; Todorov, K.; Trawick, B. W.; Vakatov, D.; Wang, Y.; Ward, M.; Wilbur, W. J.; Yaschenko, E.; Zbicz, K. Database Resources of the National Center for Biotechnology Information. *Nucleic Acids Res.* **2016**, *44* (Database issue), D7.

(6) Klil-Drori, A. J.; Ariel, A. 15-Lipoxygenases in Cancer: A Double-Edged Sword? *Prostaglandins Other Lipid Mediat.* **2013**, *106*, 16–22.

(7) Wecksler, A. T.; Kenyon, V.; Deschamps, J. D.; Holman, T. R. Substrate Specificity Changes for Human Reticulocyte and Epithelial 15-Lipoxygenases Reveal Allosteric Product Regulation. *Biochemistry* **2008**, *47* (28), 7364–7375.

(8) Meng, H.; Dai, Z.; Zhang, W.; Liu, Y.; Lai, L. Molecular Mechanism of 15-Lipoxygenase Allosteric Activation and Inhibition. *Phys. Chem. Chem. Phys.* **2018**, *20* (21), 14785–14795.

(9) Kuhn, H.; Banthiya, S.; Van Leyen, K. Mammalian Lipoxygenases and Their Biological Relevance. *Biochim. Biophys. Acta - Mol. Cell Biol. Lipids* **2015**, *1851* (4), 308–330.

(10) Tsai, W. C.; Gilbert, N. C.; Ohler, A.; Armstrong, M.; Perry, S.; Kalyanaraman, C.; Yasgar, A.; Rai, G.; Simeonov, A.; Jadhav, A.; Standley, M.; Lee, H. W.; Crews, P.; Iavarone, A. T.; Jacobson, M. P.; Neau, D. B.; Offenbacher, A. R.; Newcomer, M.; Holman, T. R. Kinetic and Structural Investigations of Novel Inhibitors of Human Epithelial 15-Lipoxygenase-2. *Bioorg. Med. Chem.* **2021**, *46*, 116349.

(11) Mogul, R.; Johansen, E.; Holman, T. R. Oleyl Sulfate Reveals Allosteric Inhibition of Soybean Lipoxygenase-1 and Human 15-Lipoxygenase. *Biochemistry* **2000**, *39* (16), 4801–4807.

(12) Meng, H.; McClendon, C. L.; Dai, Z.; Li, K.; Zhang, X.; He, S.; Shang, E.; Liu, Y.; Lai, L. Discovery of Novel 15-Lipoxygenase Activators to Shift the Human Arachidonic Acid Metabolic Network toward Inflammation Resolution. *J. Med. Chem.* **2016**, *59* (9), 4202–4209.

(13) Offenbacher, A. R.; Iavarone, A. T.; Klinman, J. P. Hydrogen-Deuterium Exchange

Reveals Long-Range Dynamical Allostery in Soybean Lipoxygenase. *J. Biol. Chem.* **2018**, *293* (4), 1138–1148.

(14) Wecksler, A. T.; Kenyon, V.; Garcia, N. K.; Deschamps, J. D.; Van Der Donk, W. A.; Holman, T. R. Kinetic and Structural Investigations of the Allosteric Site in Human Epithelial 15-Lipoxygenase-2. *Biochemistry* **2009**, *48* (36), 8721–8730.

(15) Pascal, B. D.; Willis, S.; Lauer, J. L.; Landgraf, R. R.; West, G. M.; Marciano, D.; Novick, S.; Goswami, D.; Chalmers, M. J.; Griffin, P. R. HDX Workbench: Software for the Analysis of H/D Exchange MS Data. *J. Am. Soc. Mass Spectrom.* **2012**, *23* (9), 1512–1521.

(16) Straume, M.; Freire, E. Two-Dimensional Differential Scanning Calorimetry: Simultaneous Resolution of Intrinsic Protein Structural Energetics and Ligand Binding Interactions by Global Linkage Analysis. *Anal. Biochem.* **1992**, *203* (2), 259–268.

(17) Martínez, J. C.; Filimonov, V. V.; Mateo, P. L.; Filimonov, V. V.; Schreiber, G.; Fersht, A. R. A Calorimetric Study of the Thermal Stability of Barstar and Its Interaction with Barnase. *Biochemistry* **1995**, *34* (15), 5224–5233.

(18) Celej, M. S.; Dassie, S. A.; González, M.; Bianconi, M. L.; Fidelio, G. D. Differential Scanning Calorimetry as a Tool to Estimate Binding Parameters in Multiligand Binding Proteins. *Anal. Biochem.* **2006**, *350* (2), 277–284.

Appendix A: HDX-MS traces of soybean lipoxygenase-1 in the presence of oleyl sulfate and 0.15 M NaCl when appropriate

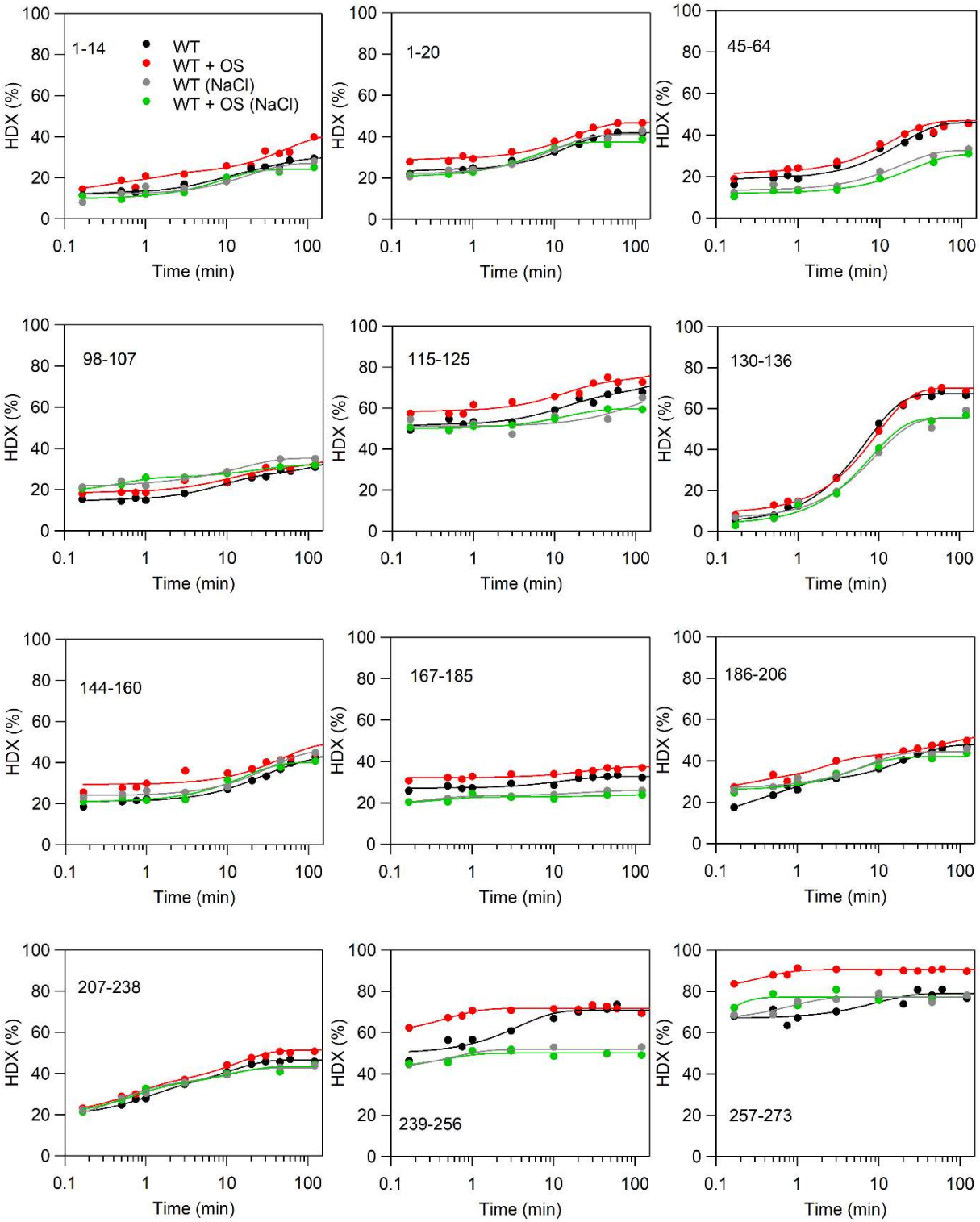

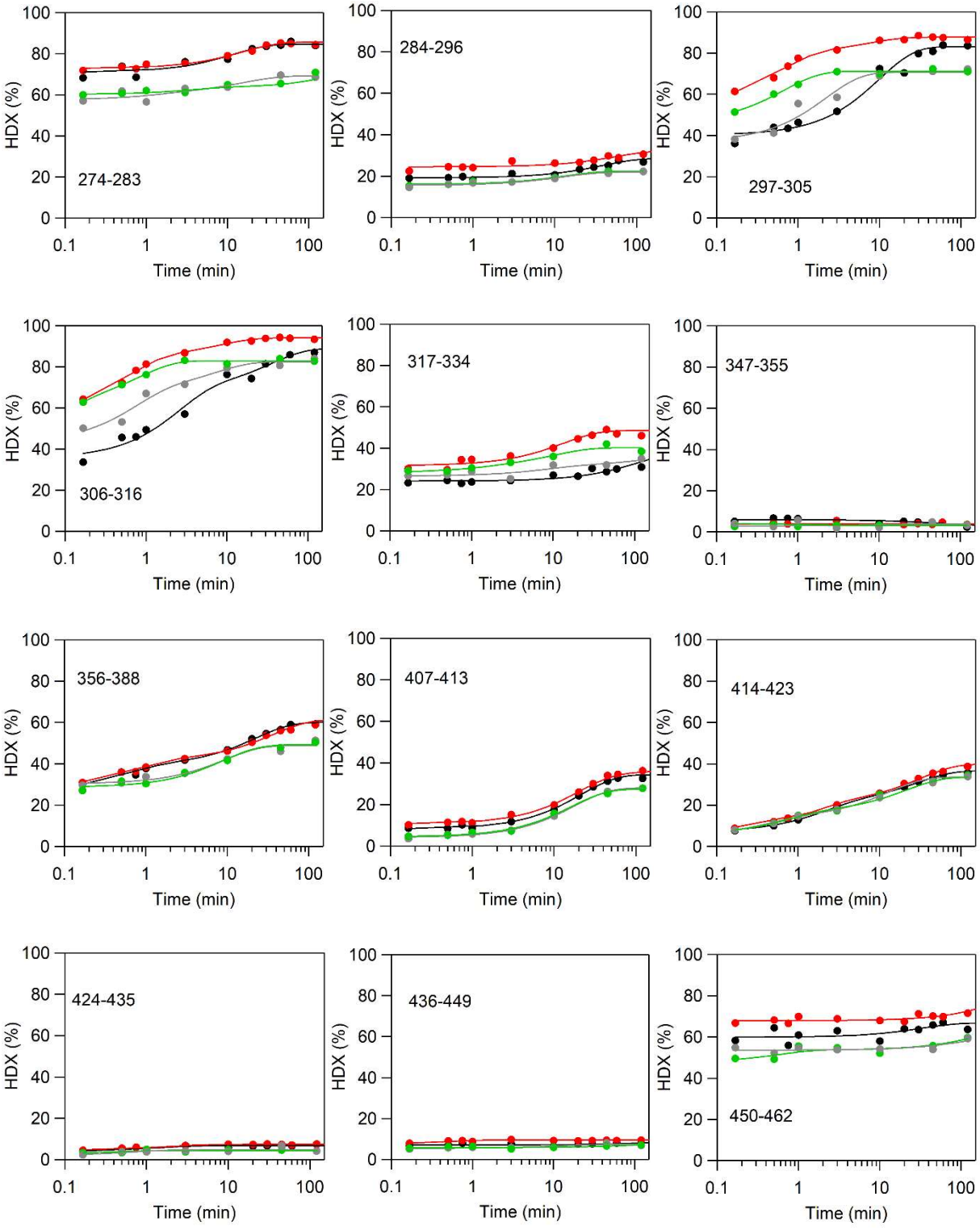
274-283
284-296
297-305
306-316
317-334
347-355
356-388
407-413
414-423
424-435
436-449
450-462
HDX (%)
Time (min)
0
20
40
60
80
100
0.1
1
10
100

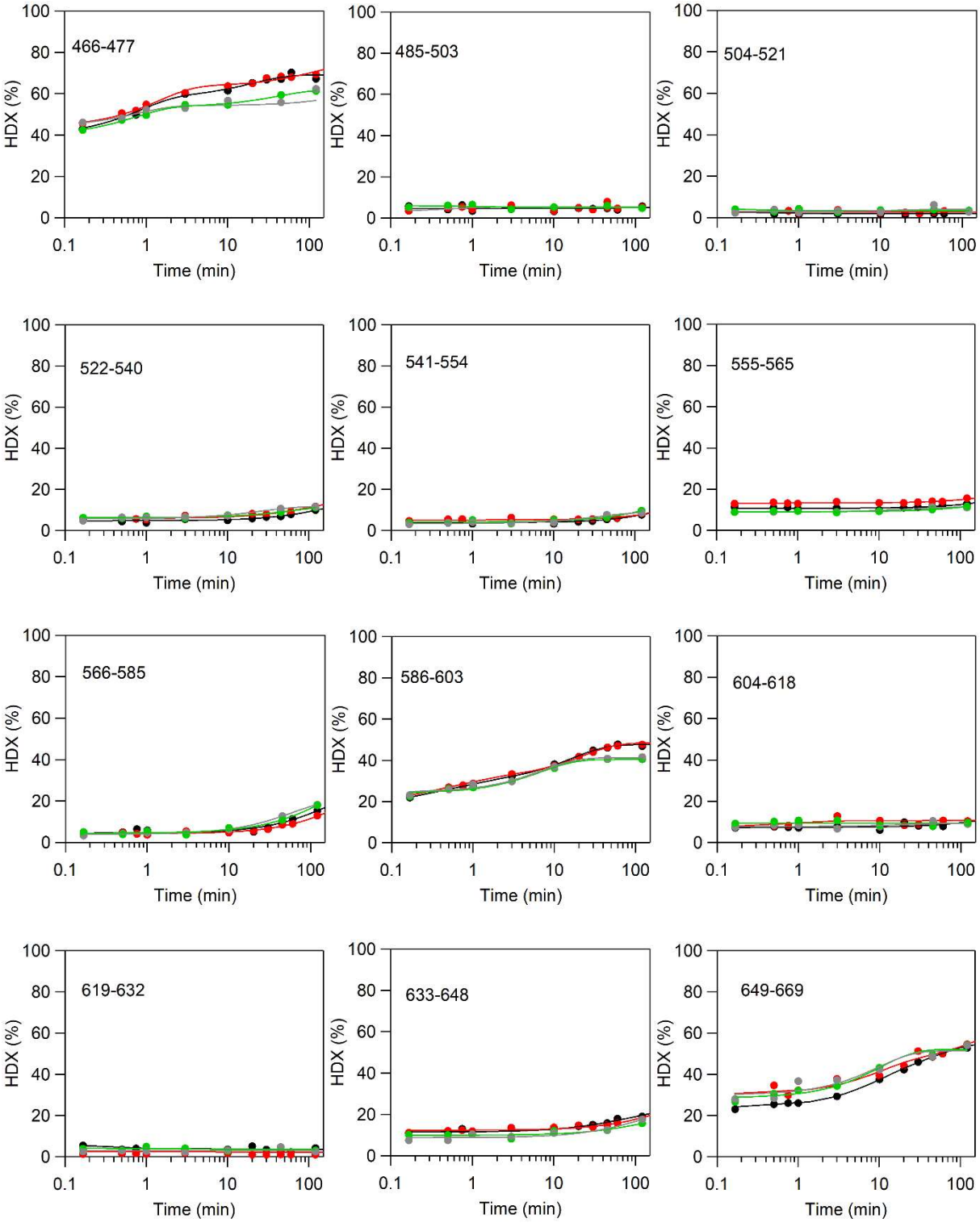
466-477
485-503
504-521
522-540
541-554
555-565
566-585
586-603
604-618
619-632
633-648
649-669
HDX (%)
Time (min)
0
20
40
60
80
100
0.1
1
10
100

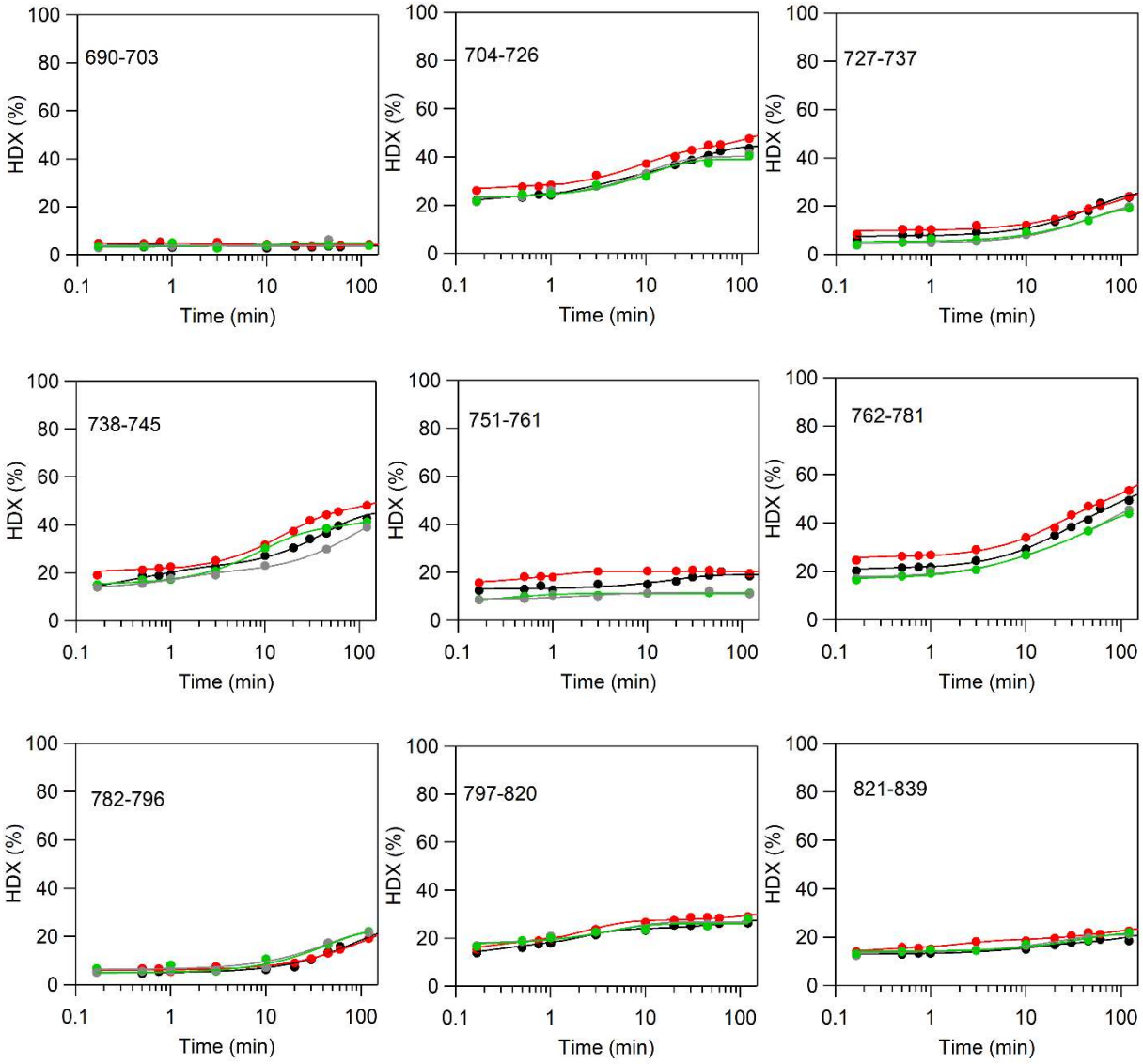
690-703
704-726
727-737
738-745
751-761
762-781
782-796
797-820
821-839
HDX (%)
Time (min)
0
20
40
60
80
100
0.1
1
10
100

Appendix B: HDX-MS traces of 15-lipoxygenase-1

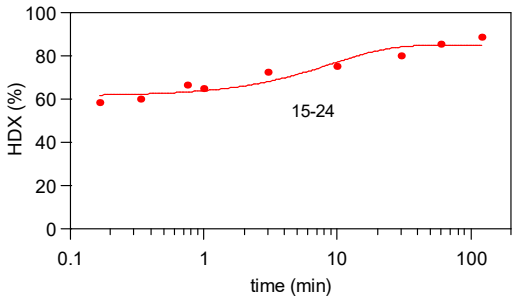

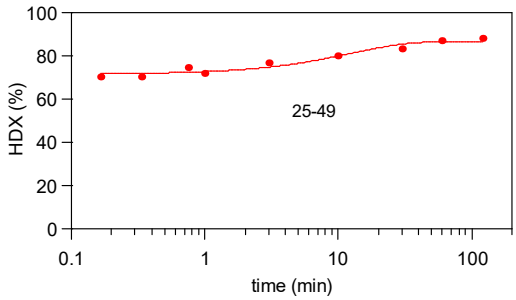

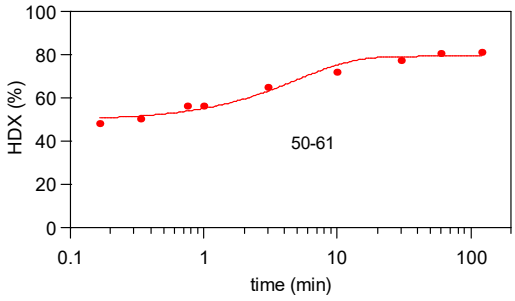

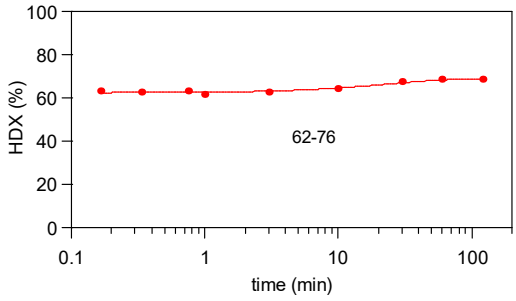

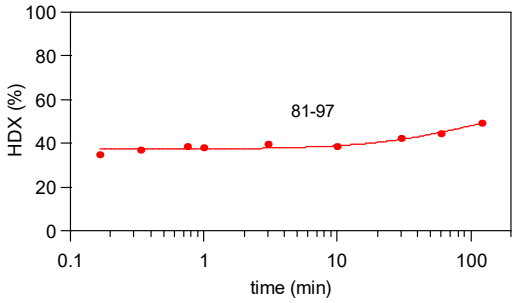

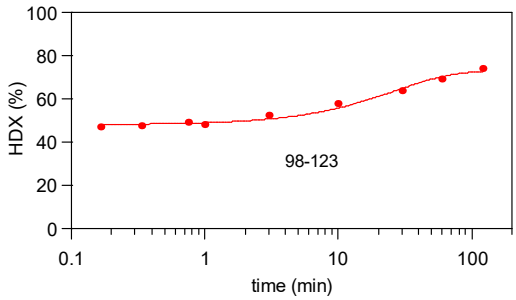

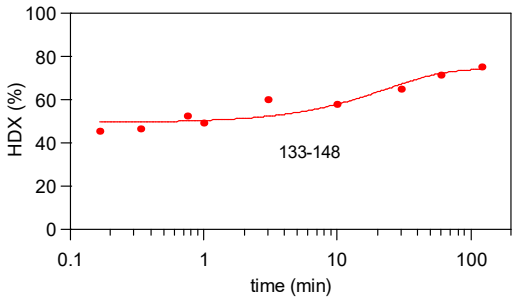

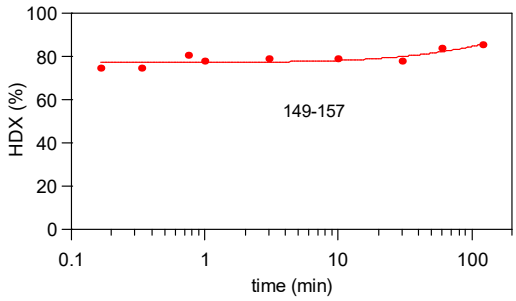

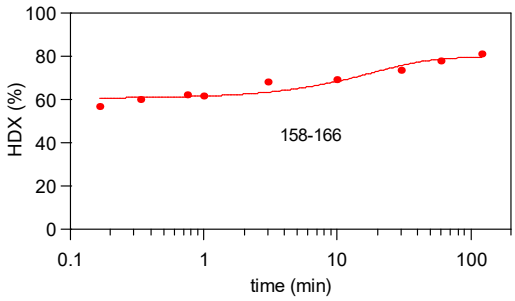
158-166
HDX (%)
time (min)

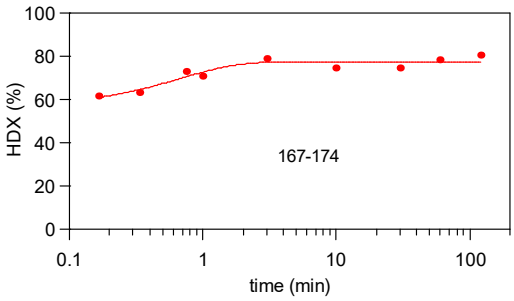
167-174
HDX (%)
time (min)

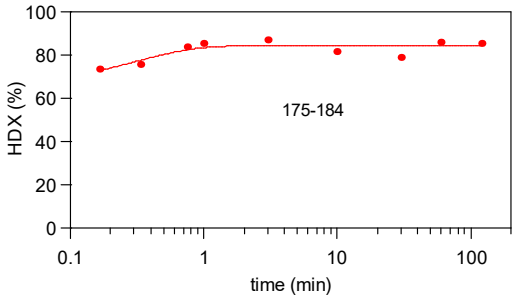
175-184
HDX (%)
time (min)

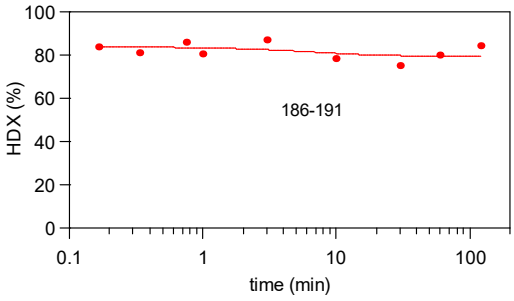
186-191
HDX (%)
time (min)

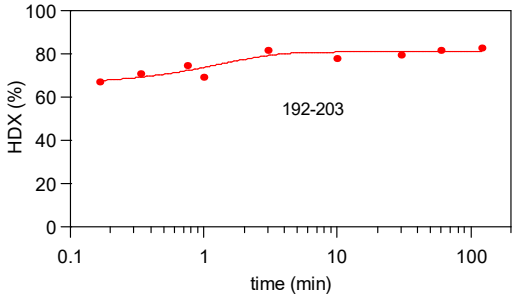
192-203
HDX (%)
time (min)

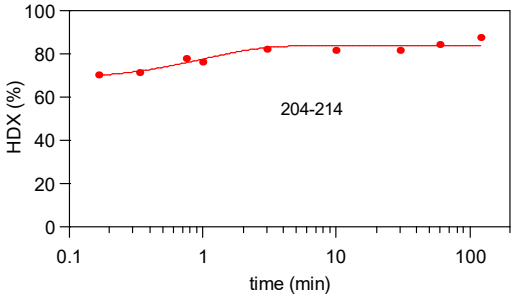
204-214
HDX (%)
time (min)

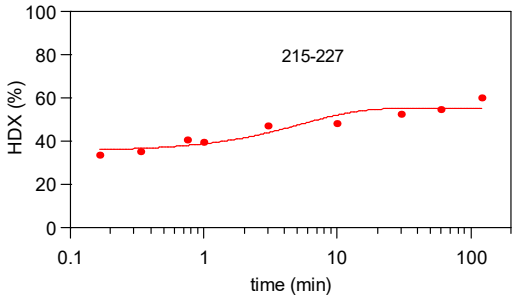
215-227
HDX (%)
time (min)

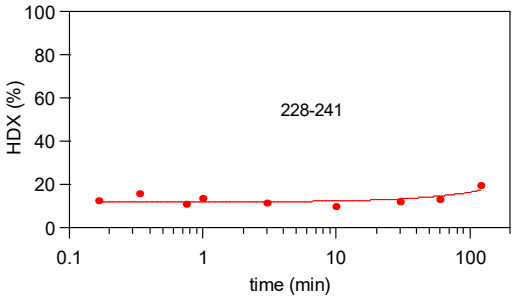
228-241
HDX (%)
time (min)

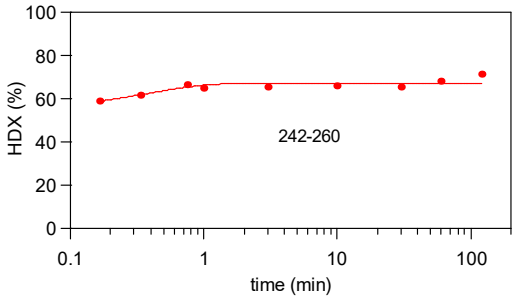
242-260
HDX (%)
time (min)

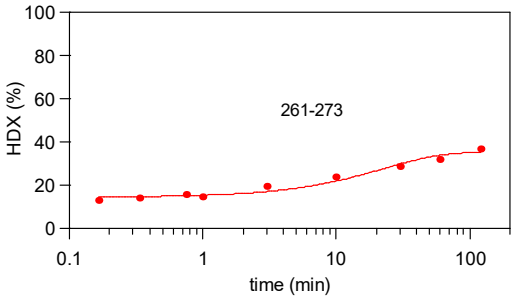
261-273
HDX (%)
time (min)

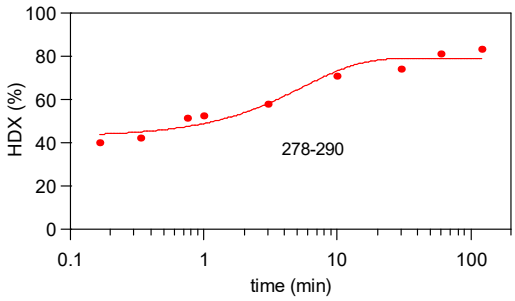
HDX (%)
time (min)
278-290

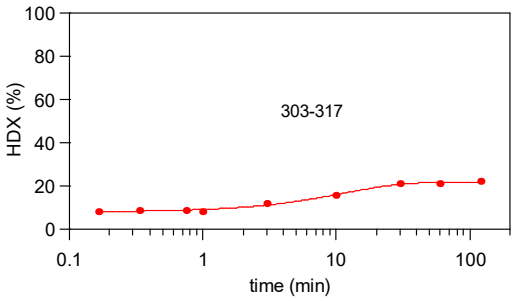
HDX (%)
time (min)
303-317

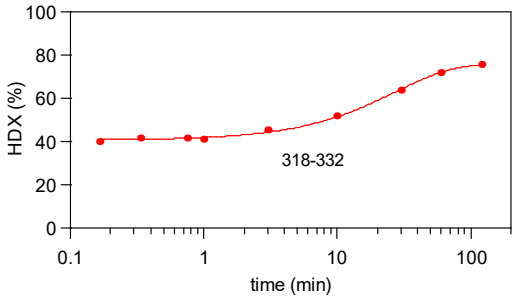
HDX (%)
time (min)
318-332

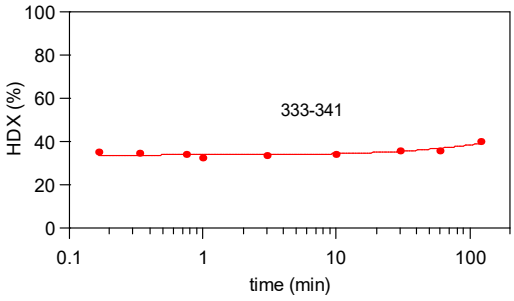
HDX (%)
time (min)
333-341

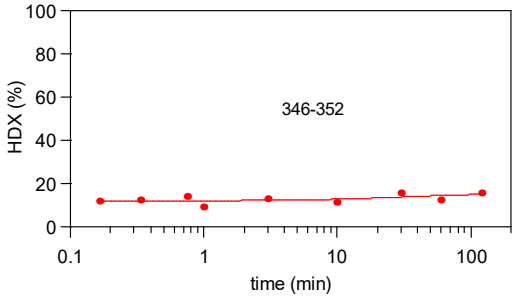
HDX (%)
time (min)
346-352

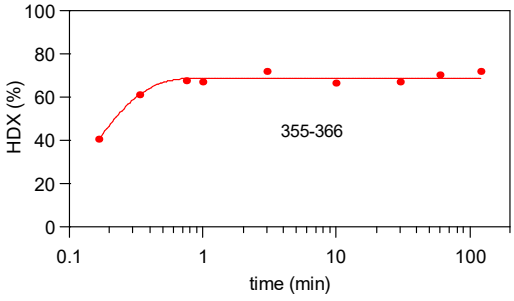
HDX (%)
time (min)
355-366

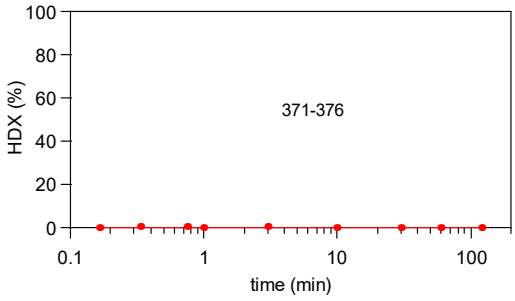
HDX (%)
time (min)
371-376

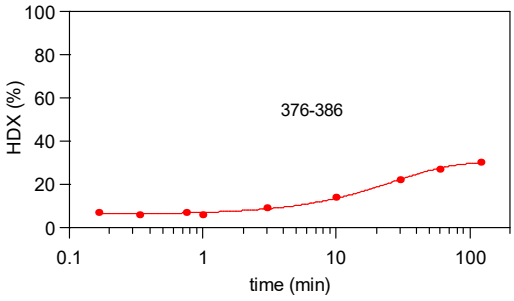
HDX (%)
time (min)
376-386

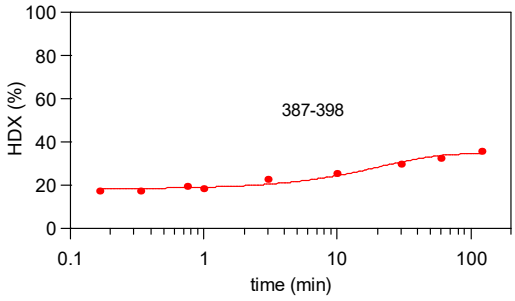
HDX (%)
time (min)
387-398

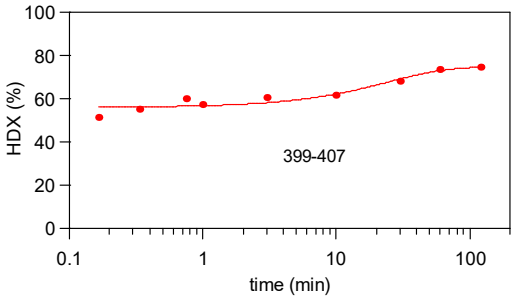
HDX (%)
time (min)
399-407

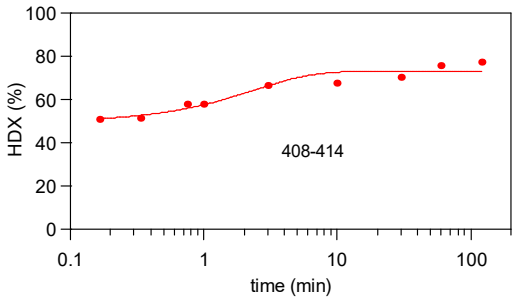
HDX (%)
time (min)
408-414

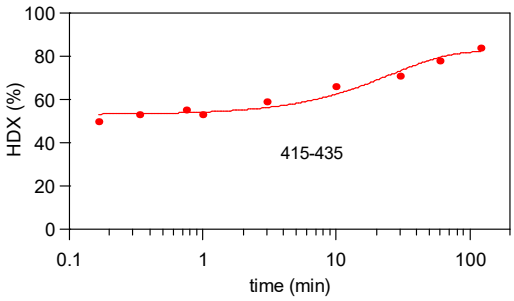
HDX (%)
time (min)
415-435

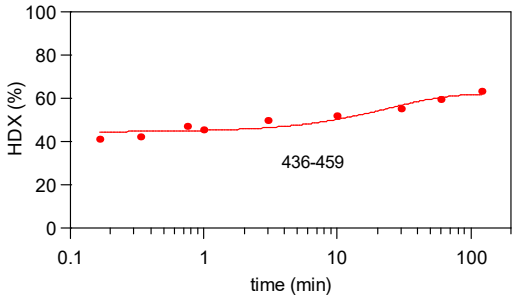
HDX (%)
time (min)
436-459

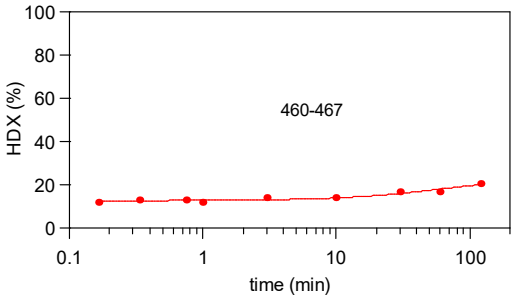
HDX (%)
time (min)
460-467

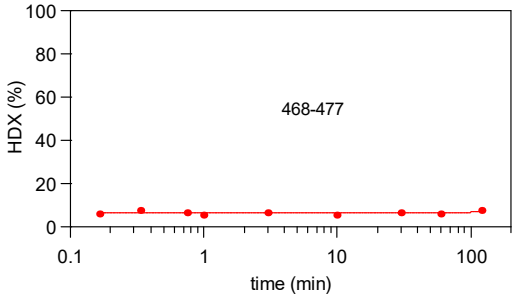
HDX (%)
time (min)
468-477

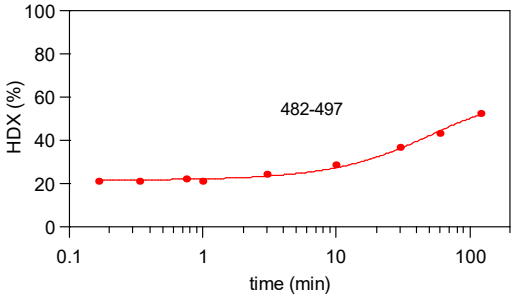
HDX (%)
time (min)
482-497

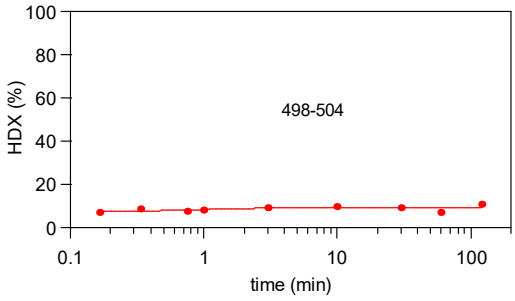
HDX (%)
time (min)
498-504

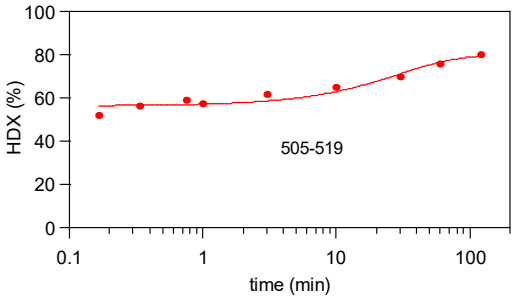
HDX (%)
time (min)
505-519

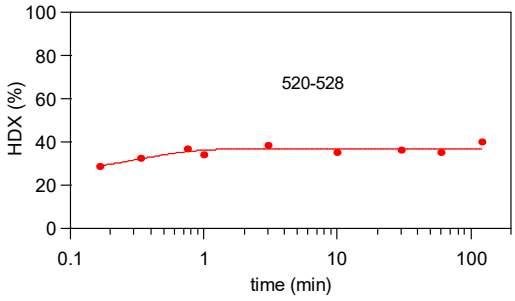
HDX (%)
time (min)
520-528

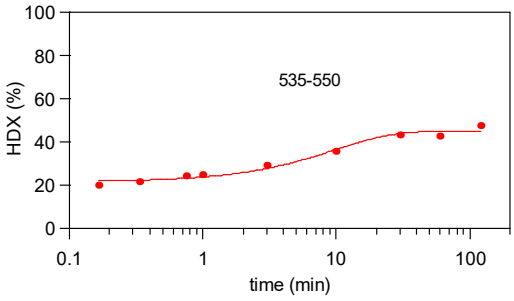
HDX (%)
time (min)
535-550

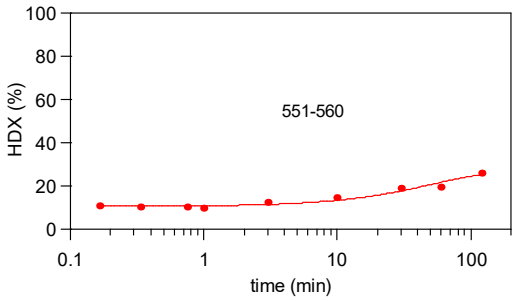
HDX (%)
551-560
time (min)

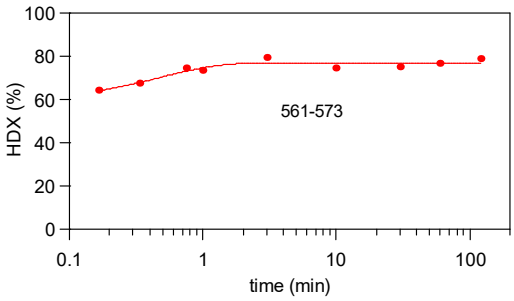
HDX (%)
561-573
time (min)

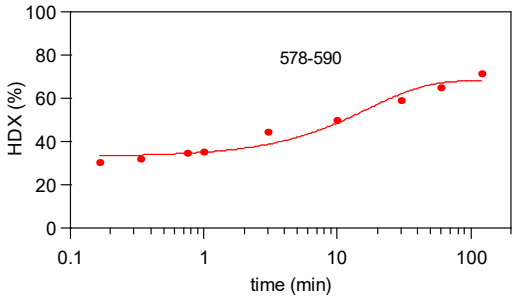
HDX (%)
578-590
time (min)

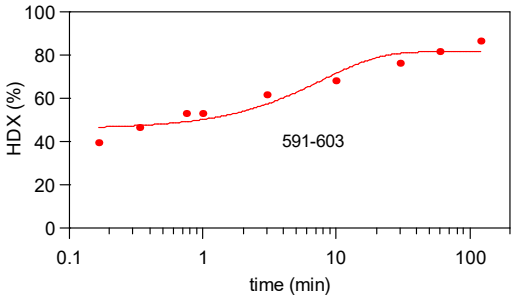
HDX (%)
591-603
time (min)

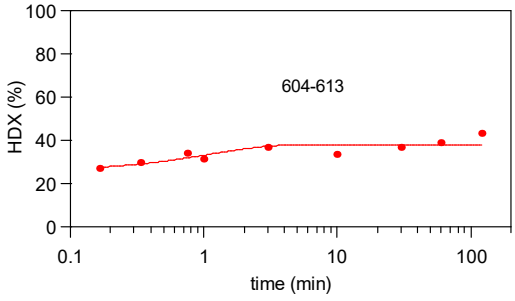
HDX (%)
604-613
time (min)

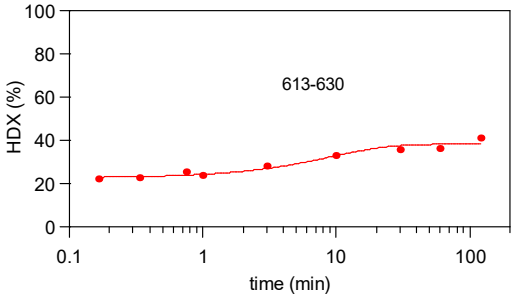
HDX (%)
613-630
time (min)

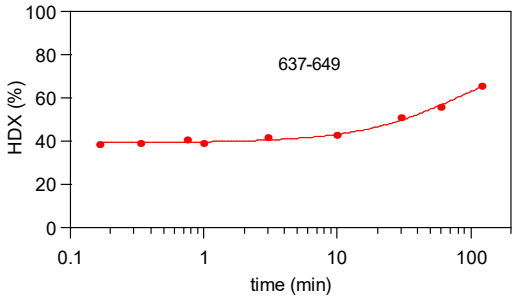
HDX (%)
637-649
time (min)

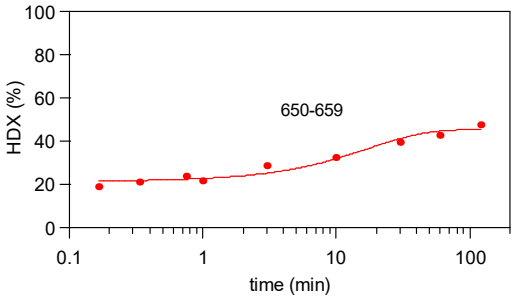
HDX (%)
650-659
time (min)